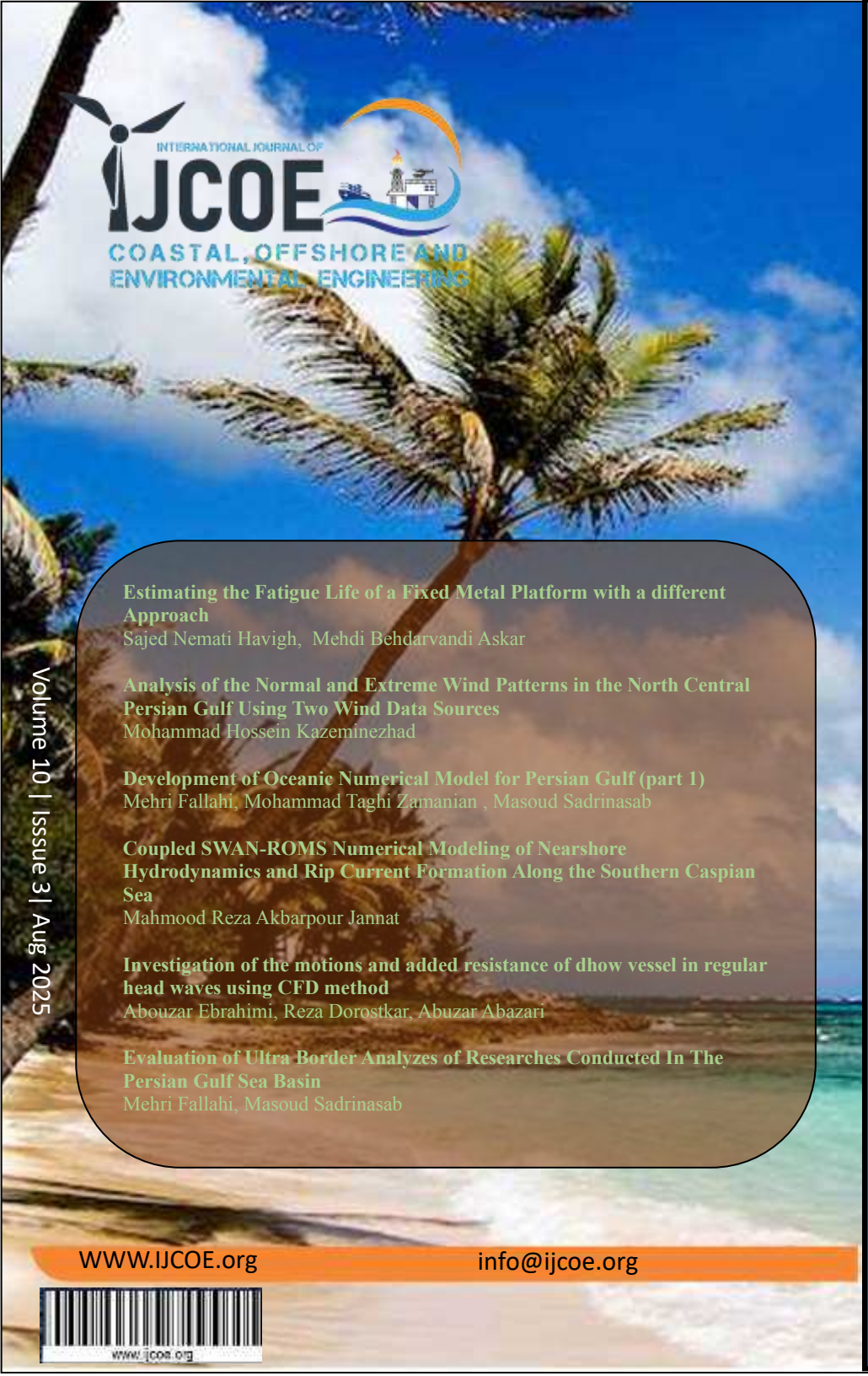

Volume 10 | Issue 3 | Aug 2025

WWW.IJCOE.org info@ijcoe.org

www.ijcoe.org

International Journal of Coastal, Offshore and Environmental Engineering (IJCOE) Vol.10/Issue 3/ Aug 2025

International Journal of Coastal, Offshore & Environmental Engineering
Since 2015

Volume 10 | Issue3 | Aug 2025

IJCOE

International Journal of Coastal, Offshore & Environmental Engineering
Since 2015
ISSN: 2980-8721 (online)

In The Name of God

Message from the Editor-in-Chief

The IJCOE journal office was established in 2015,and its first issue was published in 2016. TheIJCOE covers a wide range of research in thefields of oceanography & ocean technology, aswell as marine industries & marine engineering.The editorial board of IJCOE consists of nearly130 of the greatest scientists and researchersfrom over 30 countries worldwide, and thejournal's review board comprises 1,000 membersfrom all five continents. The membership andapplication process for joining the editorial andreview boards of this journal is ongoing. IJCOE isa research-academic quarterly journal that haspublication and distribution permissions fromthe Press Organization and permission topublish scientific-research articles from theMinistry of Science, Research, and Technology(MSRT) with an "A" rating. It also holds a "Q1"rating from the ISC institute with an impactfactor (IF) of approximately 0.43 and isconsidered a "core journal" (prestigious andoutstanding journal). IJCOE is an open-accessjournal and allows the download and receipt ofaccepted articles in full text for free. It respectsand adheres to copyright and COPE regulations.The journal's office operates 24/7, providingservices to researchers. In addition to publishinga regular quarterly journal, IJCOE has 16 specialissues on specific topics in preparation. It alsoprovides conditions for publishing specializedbooks, references, and handbooks. Moreover, itis ready to cooperate with the secretariats ofreputable international conferences to publishtheir selected and outstanding articles. IJCOEevaluates, appraises, and publishes books,articles, and the scientific achievements andfindings of esteemed researchers and scientistsworldwide who are innovating and conductingin-depth research in the "important and strategicfield of the maritime technology & Oceanengineering." It welcomes any form of jointcooperation with universities, research institutes,and related research centers at the national,regional, and international levels, and extends ahand for collaboration.

Classification of Editorial Board in IJCOE

- Editor-in-Chief
- Director-in-Chief
- Deputy Editor
- Executive Managers
- English Text Editor
- Technical Editor
- International Editorial Board
- National Editorial Board
- Editorial Board Associate
- Editorial Board Assistant
- Guest Editorial Board
- Advisory Board
- Administrative Coordinator
- Honorary Board Member
- Methodology Advisor

Author Benefits

- Open Access
- Rapid Publication
- Thorough Peer-Review
- No Copyright Constraints
- Coverage by Leading Indexing Services
- Discounts On Article Processing Charges (APC)
- No Space Constraints, No restriction on the maximum length of the papers, number of figures or colors

INTERNATIONAL JOURNAL OF IJCOE COASTAL, OFFSHORE & ENVIRONMENTAL ENGINEERING

Aims of IJCOE

Hydrodynamics

Marine equipment

Structural mechanics

Ocean environmental predictions

Stochastic calculations Experimental

Automatic Control of Marine Systems

Scope of IJCOE

Marine Hazards

Ocean Acoustics

Naval Architecture

Ocean Engineering

Coastal Engineering

Marine Meteorology

Marine Earth Sciences

Underwater Technology

Marine Renewable Energy

Polar & Arctic Engineering

Marine Renewable Energy

Marine Geography & Geodesy

Marine Environmental Engineering

Automatic Control of Marine Systems

Hydro Physics & Physical Oceanography

Type of papers

- Case Studies
- Book Reviews
- Review Article
- Letters to the Editor
- Methodology Papers
- Editorials and Commentaries
- Response or Rejoinder Papers
- Perspective or Opinion Papers
- Conceptual or Theoretical Papers
- Meta-Analysis and Systematic Reviews
- Short Communications or Brief Reports
- Research Articles (Original Research Papers)

Scientific Research Journal

Ministry of Science, Research And Technology (MSRT)

Jurnal Ranking 2023: A

Ministry Of Science, Research And Technology (ISC)

Citation Impact 2022: 0.429

Quartile 2022 : Q1

Core Collection

IJCOE is a Member of

Cantact Us

Office 1 | Research Institute of Meteorology and Atmospheric Science

Address | Tehran, Shahid Kharrazi Highway, Pajoohesh Blvd, Research Institute of Meteorology and Atmospheric Science, Sand and Dust Storm International Research Center (SDS-IRC), No. 13, 1st floor.

Phone | +982144787652

Postal code | 13611-14977

website | www.rimac.ac.ir

Office 2 | Iranian National Institute for Oceanography and Atmospheric Science

Address | Tehran, Dr. Fatemi Gharbi St., Shahid Etemadzade St., No. 3, third floor.

Phone | +982166944873

Postal code | 13389 – 14118

website | www.inio.ac.ir

Email | Info@ijcoe.org

Website | www.ijcoe.org

Follow Us

Volume & Issue:

Volume 10, Issue 3, Aug 2025

Number of Articles: 6

Content

IJCOE
COASTAL, OFFSHORE & ENVIRONMENTAL ENGINEERING

INTERNATIONAL JOURNAL OF
COASTAL & OFFSHORE ENGINEERING IJCOE Vol.10/No. 3/Summer 2025 (1-9)

Available online at: www. Ijcoe.org

Estimating the Fatigue Life of a Fixed Metal Platform with a different Approach

Sajed Nemati Havigh [1] Mehdi Behdarvandi Askar[2*]

[1] *Graduated of Marine Structures, Department of Offshore Structures, Faculty of Marine Engineering, Khorramshahr University of Marine Science and Technology*

[2]*Assistant Professor, Department of Offshore Structures, Faculty of Marine Engineering, Khorramshahr University of Marine Science and Technology* (Corresponding author) sazehenteghal@yahoo.com*

ARTICLE INFO

Article History:
Received : 22 OCT 2024
Accepted : 17 SEP 2025

Keywords:
Fatigue, Jacket, concentration, S-N curves, ABAQUS Aqua

ABSTRACT

Offshore platforms are among the important structures in the energy industry and play a significant role in the economies of countries. One of the most important factors in the sudden failure, as well as the reduction of the strength of the offshore platforms, in the long run, is the fatigue phenomenon in connections and members of the structure. Acceptable consistency in comparison to each other.The present study reviews the conventional methods of fatigue analysis of marine structures and seeks to introduce an effective way to estimate the fatigue life. Since the natural period of is an important factor for analysing of structures, it has also been investigated. Even though the recommendation of the regulations in all of states, is the use of the spectral method in fatigue analysis, but this method, despite its high accuracy, requires more time and cost compared to the deterministic analysis.

1. Introduction

The offshore area is considered as one of the most important areas in the oil and gas industry for all countries worldwide. Such both countries that exploit the energy reservoirs and the consumer countries are inextricably intertwined with this industry. The technology of monitoring and drilling and the design and construction of structures in the seas and oceans are among the most important sectors of the offshore oil industry, which provides the possibility of access to more resources. The design and analysis of marine platforms is one of the most complicated engineering tasks with respect to the complexities that exist in determining the loadings applied to platforms in marine environments, which indeed definitely no precise standard schema has yet been provided for the design of these structures, and continuously with the advancement of related sciences and engineering tools, we are witnessing changes and updates to various regulations in this field. Since the sea environment is a fully dynamic environment and the loadings caused by waves, winds, and subsurface currents are permanent dynamic loads that are applied to the structure and cause fatigue and frailty in various components especially in the structural connections, the design of the structures for this phenomenon has become necessary and in recent decades has attracted the attention of the researchers in this industry. Fatigue is one of the most important topics that is of particular importance in the design of all structures exposed to continuous cyclic loads. Fixed platforms of template type are also among these dynamic (dynamic behavior) structures.

Because of the nature of most marine environmental loads are repetitive and syclical, the structures which placed into those are subject to cyclic loading. Waves, winds and earthquakes with a hydrodynamic candition, are the main loads that will be applied to the structure [1]. In the present study, different methods of fatigue analysis have been studied and compared to finally introduce a useful and low cost method. In the mid-nineteenth century, researchers turned their attention to the phenomenon of fatigue in materials. Meanwhile Mr. Wohler's studies led to (S-N)[1] curves [2]. The S-N curves are widely used to stimating of fatigue life [3].

1.1 Some of the Previous Researches

The topic of fatigue in engineering sciences is one of the topics with a short history so that It has not been fully analyzed and understood to this day. Generally, the knowledge of the stability of engineering structures against the massive loadings due to

[1] stress-cycle curves

earthquakes or floods is of particular importance in the civil engineering sector. What differentiates the phenomenon of fatigue and loadings applied to the structure from the phenomena such as earthquakes is that a phenomenon such as an earthquake, quite tangibly affects the structure, but the loads that lead to a fracture in the structure due to fatigue are applied to the structure subtly and with stresses or strains less than the breaking point in the long run and in a continuous and cyclic form. The tragedy of an oil platform in the North Sea, 123 crew members were killed Alexander L.Kielland, Norwegian oil platform. One of the main members connected to the pantons overaly failed and detached from the structuer and led it to compelletly collapse (Almar-Naess, 1985)as shown in Fig 1.

Figure 1: oil platform in the North Sea called Alexander

The sedco135 semi-submersible drilling rig, which started its activity in the Gulf of Mexico in 1965, suffered failure due to fatigue in one of its braces after two years in 1967.

One of the most widely used offshore structures is the fixed platform of template type or jacket, which is a steel structure with braces and a deck, and with bases fixed by numerous piles to the seabed. Fatigue cracks are the main cause of the breakdown in fixed platforms of template type (Stacey, 2007). Also, in studies carried out previously, the determination of fatigue damage due to ocean waves was developed using mathematical expressions (Nolte, K. G., and Hansford, J. E.,1976). This study clarified the relationship between the wave height and the range and distribution of the stress with respect to the interaction between the range of the stress and the number of cycles for the occurrence of failure and the probability of the event of the dispersion of wave heights.

The scientific debates taken place indicated that the most important issues related to the fatigue in offshore metalstructures were calculations related to the determination of fatigue stress and fatigue life (Almar-Naess, A., 1985). In the topic related to the stress concentration factor (SCF) in connections, simplifications, and reviewing previous research studies in the area of stress concentration and fatigue mechanics in tubular connections, failure analysis and reliability analysis in the connections were performed (Dover, WD and Madhava Rao, AG, 1996). (Etube et al., 1999) presented a model of the response of a steel jack-up platform for fatigue calculations. By analyzing a mathematical model to achieve the transfer function of the dynamic response of a conventional jack-up platform, they found that a complex interaction between the structure and the soil at the base of the platform could be modeled satisfactorily using spring and solid foundation. (Ramachandra Mutthy et al., 1994) and (Gandhi et al., 2000a) and (Gandhi et al., 2000b) performed studies on fatigue phenomena on hardened tubular metal connections and the effects of corrosion and fatigue behavior. (Vugts, J. H., 2005) discussed the study of the fatigue failure and the impact of the incoming wave on the structure. This scholar conducted his studies on a symmetrical circular structure (a vertical cylinder) and presented the results in numerical. Form based on a spectral analysis, (Shangfeng et al., 2007) performed fatigue calculations on a metal template platform located in the South China Sea. (They carried this out) by examining the transfer function of the stresses of a connection, which was the first systematic method for providing assistance and preliminary instruction for (obtaining) the dynamic response of the structure, and (emphasized the fact) that a proper choice of frequency and bandwidth has a significant effect on the structural response. A metal template platform located in the Bohai Gulf, which has also a conically shaped structure as an icebreaker, was optimized by (Li et al., 2008), and the results indicated that the fatigue life of the platform can be increased, and also the weight of the platform can be reduced. (Marco et al., 2007) presented an effective nonlinear dynamic approach for calculating the fatigue failure due to waves in offshore structures, and they also identified its industrial applications for increasing the fatigue life. In this study, due to the symmetry of the connection members, only one half of the member was analyzed.

(Khalafi et al., 2014) conducted a study on a metal template platform and studied the fatigue life of its connections. They also carried out studies to determine the minimum safety factor for each connection and they presented all their results in the form of diagrams and tables. Among the important results of this research we can mention the following that: the impact of sea currents on the fatigue life of the connections under study is about 10% and can be neglected, and also predictably the connections are considerably under the influence of the waves in the wave splash zone and are sensitive to breakdown and failure. This research also confirmed that the simplified fatigue analysis method could have negative effects on the accuracy of fatigue calculations. This is particularly the case for platforms that the impact of dynamic specifications is significant

in them and the abovementioned method does not take into account the natural period of the structure.

2. Hydrodynamic Forces and affects of the Waves

During the splash of sea waves to the structures exposed to water, forces are applied to the structures that are caused by the acceleration and velocity of water droplets, determining these forces depends on such factors as the state of the sea and the type of the structure itself. With regard to the type of the structure being floating or fixed, and/or bulky or with a small surface, different situations arise in determining the forces. The environments forces applied to the platforms include wind, marine currents, waves, ice, earthquake, hydrostatic variations, as well as the effect of floating forces on the members due to variations on the surface as the impact of tides (API). The share of the wind force is less than 40% of the hydrodynamic forces (DNV), which in the analysis of fatigue in the jacket structure its effects are neglected because the wind force is applied to the upper levels of the platform and outside the water.

In general, the status of a marine environment is summarized in its waves; including the waves with certain height and periods, and the waves caused by wind or tectonic movements of the seabed or tsunami and other factors that are involved in the status of the sea. In this research, because of the small diameter of the members of the structure compared to the wavelength, the Morrison equation, and Airy linear wave theory were used.

2.1 Fatigue in Offshore Platforms

The wave loading is the major force applied to the marine platforms. The wave loading, due to being cyclic, causes fatigue in members and structural connections. The structural connections have a high sensitivity to fatigue failure due to the concentration of stress and welding defects in these areas.

3. Materials and Methods

3.1 Fatigue Analysis Methods

There is tow common methodes for fatigue life analysis in offshore structures, deterministic and spectral. Due to the API-RP 2A and some released researchs, connection areas are subject to stresse concentration phenomena and these areas are so important for stability of structures. Hence, it's necessary to evaluation of fatigue analysis on the connections that are subject to cyclic stresses. The APA regulation recommend that the spectral analysis is accurate at all. Of course, for structures that their natuaral period is less than 3 and maximum height to 122 m for water depth about 100m, and in lack of the precise analysis for any justsifiable reason, the API recommendes a simplified procedure according to the part of C.5.2 [3].

3.1.1 Deterministic Method

For the deterministic analysis, we need to select a number of waves with specific properties (height and period) from wave scatter diagram. The wave selection method is according to the highest rate of repeatation of the wave in the wave scatter diagram. These selected waves categorized with each other and then applied separately to the structure. Nominal stresses in the Structure include members and connections by applying the appropriate stress concentration factor (SCF) for every separate element is converted to the hotspot stress. After finding the hotspot stress range and according to the occurrences of each wave and using S-N curves and Palmgren-Miner law (equation 5) separately for each selected wave, the fatigue damage index is obtained for selected waves. Eventually, overall fatigue damage and usful life of the platform is obtained from sume of each wave's damege on the structure.In general, this approach based on the time domain theory with using seprate waves and sum of their effects on the structure. According to the DNV recommendation, the hotspot stresses calculate at least on 8 points of around of each connection (at every 45 degrees).

3.1.2 Spectral method

Contrary to the deterministic method, spectral approach use wave spectrum instead of the separate waves. The dynamic response of structure is one of the main principles of this method. Therefore, the effects of the all of waves participate in the calculation of the fatigue life of structure.

The waves are modeled and instead of applyin geach wave separately (with specific features) to the structure, the wave spectrum is used for it and then by a transfer function is converted to the hotspot stress spectrum on the cicumferential points of the connection. This method is in frequncy domain analysis that is assumed for a certain period, the force is proportional to the wave height. Therefore, to creat a transfer fanction the nonlinear term of drag forc in the Morrison equation shoud be linear by a proposed way of the regulation such as using of steepness of the continuous wave. In the dynamic analysis in deep waters under the influence of large storm waves, the dominant wave force consists of the drag force that is nonlinear, therefore, for a proper's response, these structures should be dynamically analyzed in the time domain [4].

The hotspot stress rang (HSSR) is the same as the stress on the toe of a connection. The stress concentration factor (SCF) introdueced as follows in Eq.(1):

$$SCF = \frac{HSSR\ at\ the\ Location}{Range\ of\ Nominal\ brace\ stress} \quad (1)$$

The (HSSR) is calculated at the 8 points around the joints. The API regulation proposes the Efthymiou equations for non reinforced tubular joints and Lloyd equations for reinforced tubular joints. The regulation recommends minimum values of stress concentration for all of tubular joint parts (main and subsidiary members) the value 2, for the intrnally reinforced joints the value of 2.5, for the extrrnally reinforced joints the value of 6.

Most of joints are used in offshore structures are the multi-planner joints. Therefor we need to compute separatly SCF for each joint. The Maximum value will used in the final calculations for each joint. Geometric parameters of a tubular joint can be seen in the figure below at Figure 2.

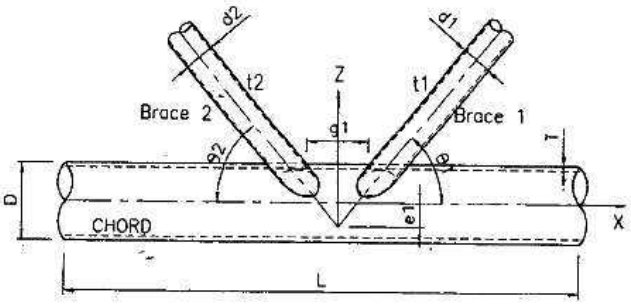

Figure (2): Geometric Parameters of Tubular Connection (DNV) [5]

Where is, D: diameter of main member, t: sub_member tickness , T: main member tickness
L: length of the members
Θ: angle between the two members
g: distance between two braces at the toe of the weld

The 8 peripheral spots of a joint for calculating of hotspot stress are displayed in figure 3. Axial load (N), in-plane bending moment (IPB), out of plane bending moment (OPB) can be seen in the figure 3, a and b.

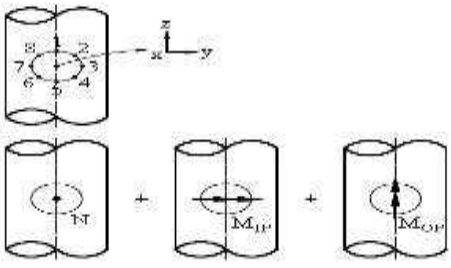

Figure (3): Forces Applied to a joint (DNV) [5], **(a).**

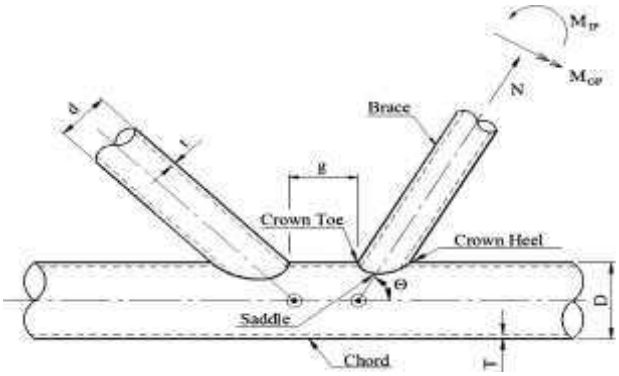

Figure (3): Forces Applied to a joint (DNV) [5], **(b).**

The DNV regulation proposes the following equqtion Eq.(2), for calculating hotspot stress and then used in the S-N curves [5].

$$HSSR = DAF\ (\frac{F_{ax}}{A} SCF_{axi} + \frac{F_{ipb}}{Z} SCF_{ipb}\ Sin\theta_i + \frac{F_{opb}}{Z} SCF_{OPB} Cos\theta_i) \quad (2)$$

Where in Eq.(2) DAF: dynamic magnification coefficient, Z: modulle of the cross-section, $SCFipb$: SCF of in-plane bending moment, $SCFOPB$: SCF of out of plane bending moment, θ: angle between spots.

3.1.3 Stress-cycle Diagrams

The API regulation offer the following diagram according to Eq.(3), for x and x' modes,Figure 4.

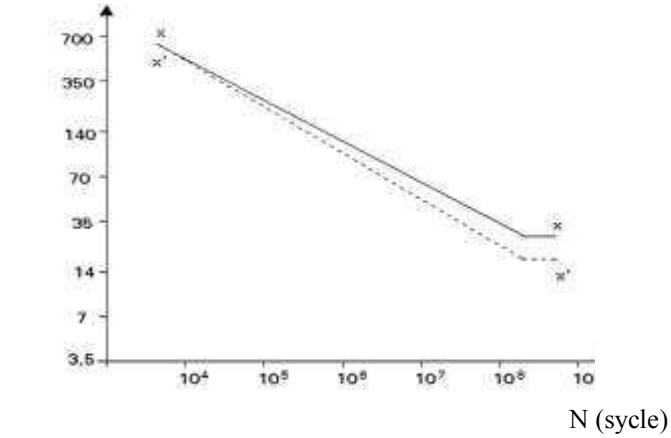

Figure (4) - S-N Curves in the API [3]

$$N(s) = 2 \times 10^6 \times (\frac{\Delta\sigma}{\Delta\sigma_{ref}})^{-m} \quad (3)$$

Where in Eq.(3), N(s): Number of cycles allowed, $\Delta\sigma$: the current stress , $\Delta\sigma ref$: experimental standard stress and m: diagram slope, according the following table:

Table (1) - Characteristic values of the equation of the S-N curves

Application	$\Delta\sigma ref$ in two million cycles mpa	m	curve
Two sides with flat weld profile and control with x-ray	100	4/38	X
Susceptible weld with rugged sides	79	3/74	X'

The X is for the situation that the weld of joint is controlled and the thickness of subsidiary member is less than 25 mm.the following Eq.(4), can be used for modification of thickness effects.

$$S = S_o\left(\frac{t_{ref}}{t}\right)^{0.25} \quad (4)$$

S_o: allowed stress obtained from S-N Curves, S: allowed stress, t: thickness of the subsidiary member t_{ref}:16 mm for X' curve and 25 mm for X.

About unchecked welded joints, X' one is used. However, it must comply with the standard AWS profile and it is used where the subsidiary tubular joint is less than 16 mm. to modification of thickness effects, the equation 4 can also used [3].

3.2 fatigue life estimating methods

3.2.1 Palmgren–Miner theory

Several methods have been investigated by scientists in relation to the estimation of the ultimate lifetime of structures and components. However, Miner' rule is still one of the most widely used lifetime estimation equation. Although it is worth mentioning that Miner's rule has been scientifically criticized many times over the course of the period that it was published and used up until to this date. Not taking into account the loading history can be mentioned as one of the flaws of the Miner's rule, which has a tangible impact on the results of the lifetime estimates. This cumulative rule proceeds to determine the "cycles until failure" from the stress-cycle curve for the various sea states and the stresses caused by it. According to the number of waves under study, with the accumulation of the damages resulted from each wave, the total damage is obtained. In the process, the impact of the previous wave on the structure is not considered, and it is based on the assumption that each wave crashes into an intact and healthy structure. Despite the fact that the structure has been attacked before confronting the next wave and has taken impacts from the previous wave. Despite this fact, Miner's rule is still one of the most widely used theories of lifetime estimation in the above cycle, due to the ease of use, and because it is an empirical rule and is also consistent with the stress-cycle curve and provides acceptable solutions. The procedure of this method has been shown summarily in Figure 7. The mathematical equation of this theory, along with the introduction of its parameters, have been described in the previous sections where it was necessary, and for the sake of brevity, only the general Eq.(5), is given here[8].

$$D = \sum \frac{n_i}{N_i} \leq 1 \quad (5)$$

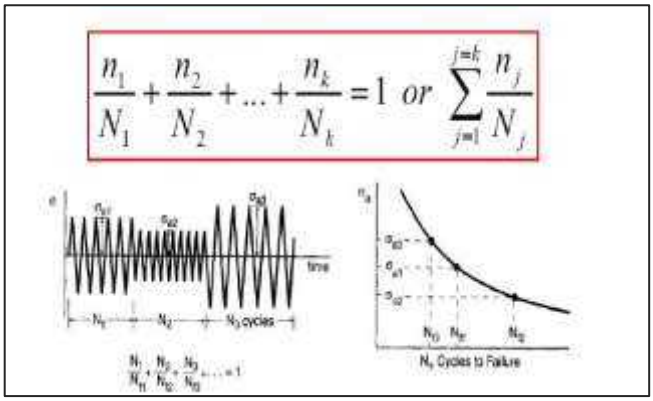

Figure (5) - The general process of Palmgren-Miner

The Palmgren-Miner cumulative method is generally used in the estimation of fatigue life, but because in the calculations it does not take into consideration the history of stresses, it has some deficiencies, therefore, we can achieve a more accurate and realistic estimate by correcting these deficiencies. In the proposed method, by taking into account the impacts of the loading, it has been attempted to obtain a more accurate estimate of the structural lifetime. There are three main steps in this method that we will deal with them:

- Reviewing the history of stress
- Using the entire range of S-N curves
- Using the sequential method

The stress history is obtained by structural analysis during various states of the wave phase for nodes in the structure. The conversion of the partial range of curve to the full range is based on the curve modeling technique that was performed by Kohout and Vechet. A general overview of this curve conversion is presented in Figure 6.

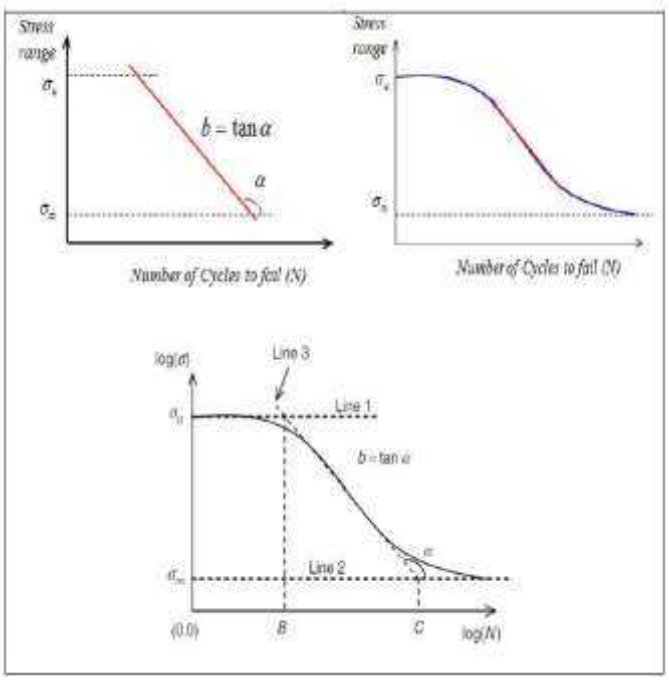

Figure (6) – The display of the general steps of the expansion of Wöhler curve

As can be seen, the graph is given in the logarithmic form, which it has also been given similar to this in all regulations. In Figure (6), line number 1 crosses the equivalent point of the final stress of **σu**, and line number 2crosses the equivalent point of the compressive strength of **σ∞**. The infinite compressive strength is, in fact, a stress at which it can acceptably be said that a structure with infinite cycles of this stress does not still reach the failure. Also, line 3 shows the tangent line in the range that is used in the regulations for the calculable range of limited cycles of the stress. Also, points B and C represent the range of the tangent line 3 on the horizontal axis with lines 1 and 2, and also "a" is the Basquin index. The full range of the S-N curve is presented by the two models of Basquin and Kohout, which can be presented by equations (6)-A and (6)-B:

$$\sigma = \sigma_{\infty}\left(\frac{N+B}{N+C}\right)^{b} \qquad (6)\text{-A}$$

$$\sigma = aN^{b} \qquad (6)\text{-B}$$

Where b is the slope of the tangent line.

In the regulations, these curves are usually provided with two slopes, which are generally considered to be 3 and 5. The limit of the compressive strength is considered to be 1 MPa. The curves used for connections and tubular members are known as T-Curves. In Figure 7, the final curve is displayed. It should be noted that the basic equation of the S-N curves is obtained from the logarithmic equation in the general form of:

$$\log N = \log a - m\log \Delta\sigma \qquad (7)$$

where in Eq.(7), m: negative slope of S-N curve, N:estimated cycle rate of the curve for the stress range, log a: parameter of the horizontal logarithmic axis N.

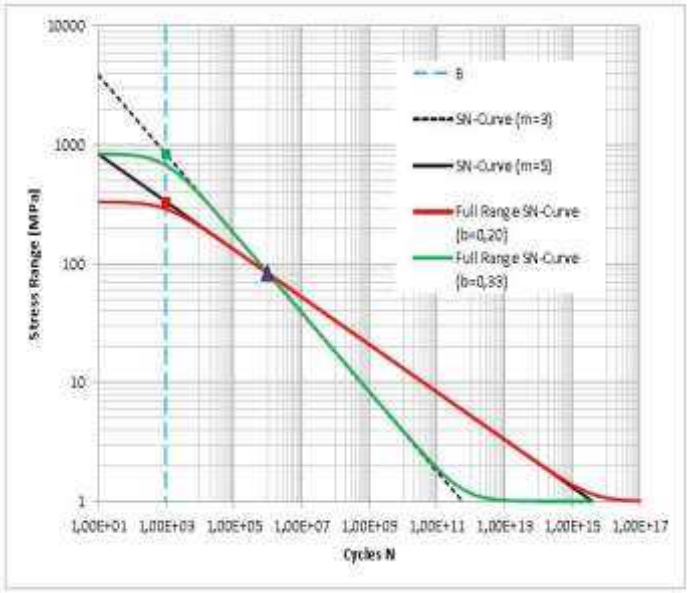

Figure (7) - The general range of the curve known as T-CURVE

In Fig. 9, the curves related to slopes 3 and 5 can be seen. The red curve with a slope of 0.2 and the green curve with a slope of 0.33 have been given, which these curves can be extracted from equation (14). With regard to the ranges covered by the curves, the curve with a slope of 0.2 is suitable for this research. because the stresses in the research are in the high-cycle range.

3.2.2 Sequential Law

The basis of this rule is based on the assumption that: If the physical state of damage is the same, then fatige life estimation should depend on the load condition only [9]. The procedure of this method is that first, by definition, the initial damage index Di at the level one of the stress of σi, which is obtained from the curve by reading the corresponding (N_i) and according to Eq.(17), is obtained. Then, this damage is transferred to the next level of the stress $\sigma_{(i+1)}$. This process continues until the value of the equivalent stress reaches to the final stress and the damage index approaches to one millimeter. During this process, the cycle values of each stress range are also involved, which are taken into account as ni in the equations. The value of the remaining cycle for the failure in

each step is obtained from the subtraction of Ni - ni, which again for this cycle the equivalent stress is obtained from the curve as well. The curve in Figure 8, clearly illustrates this procedure. The parametric equations of this procedure are given below.

$$` D_i = \frac{\sigma_{(i)eq} - \sigma_i}{\sigma_u - \sigma_i} \qquad (8)$$

$$D_i = \frac{\sigma_{(i)eq} - \sigma_i}{\sigma_u - \sigma_i} = \frac{\acute{\sigma}_{(i+1)eq} - \sigma_{i+1}}{\sigma_u - \sigma_{i+1}} \quad (9)$$

Where is the equivalent stress of the remaining cycle of $\acute{\sigma}_{(i+1)eq}$ of the level i that is transferred to the next level and results in the permitted cycle of $\acute{N}_{(i+1)R}$, and this same trend continues.

$$\acute{\sigma}_{(i+1)eq} = D_i(\sigma_u - \sigma_{i+1}) + \sigma_{i+1} \quad (10)$$

$$N_{(i+1)R} = \acute{N}_{(i+1)R} - n_{i+1} \quad (11)$$

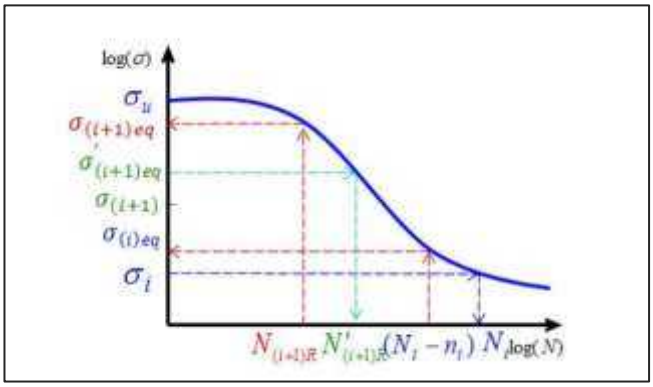

Figure (8) – The functional procedure in sequential law method in S-N curve[9]

The verification of this theory has been done with the aid of the studies of the scientists active in this field. These studies have been performed experimentally and numerically, which the results of these studies can be seen in the form of diagrams. These studies have been performed with different slopes that are in the form of a comparison with Palmgren-Miner law and the experimental results have been plotted as some diagrams. These studies have been carried out based on the full range (extended) curves of S-N curves. In the experiments performed, 45c and 16Mn steels, and also the values of B and C, and compressive strength limit, and a specific slope in the selected equation, that is based on equation 6, have been used. These graphs can be seen in Figures 9 and 10. From the general analysis of these diagrams, it can be seen that in determining the fatigue life, the "sequential law" has performed much better and more precise than Palmgren-Miner law. This can be found out from the results obtained from the sequential law being close to the experimental results given in the diagrams.

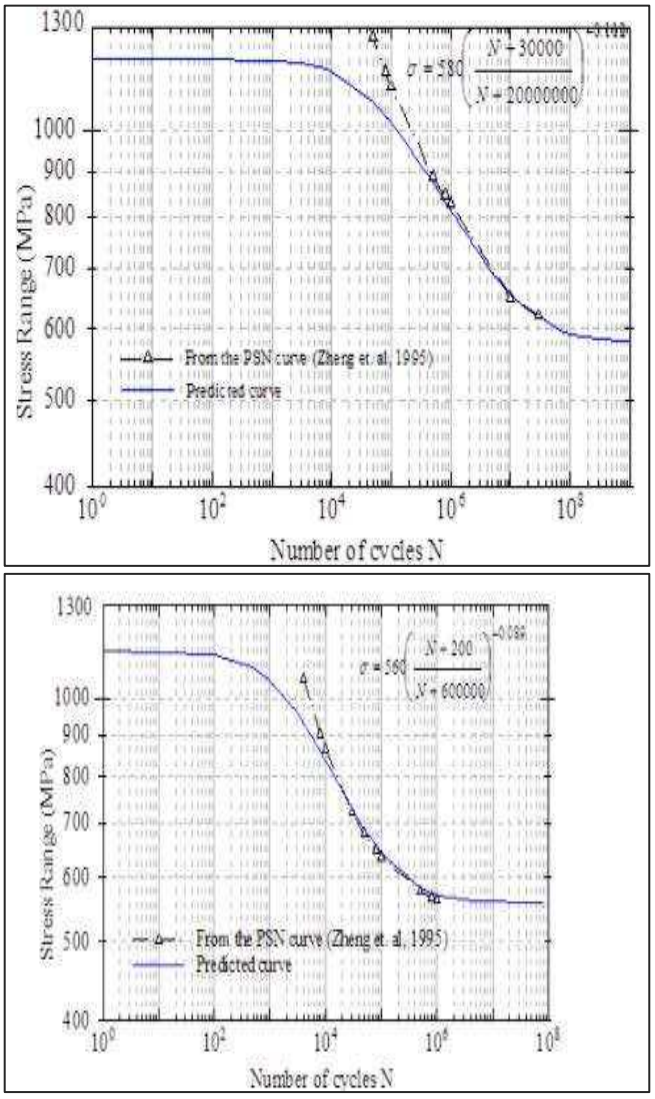

Figure (9) – The verification of sequential rule by experimental results (Zheng et al, 1995)

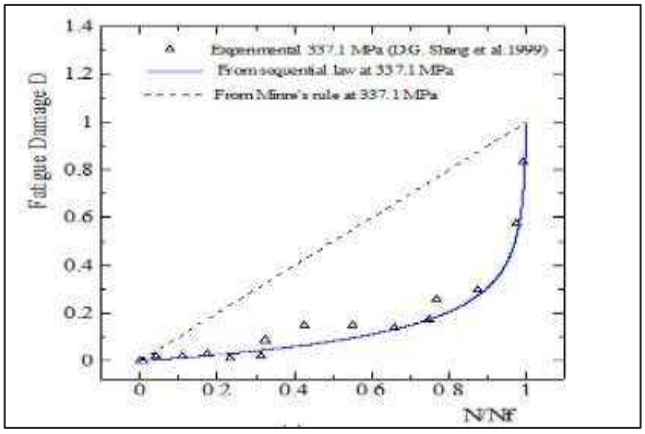

Figure (10), a – The comparison of sequential rule with experimental and Miner's rule results (Shang et al., 1999)

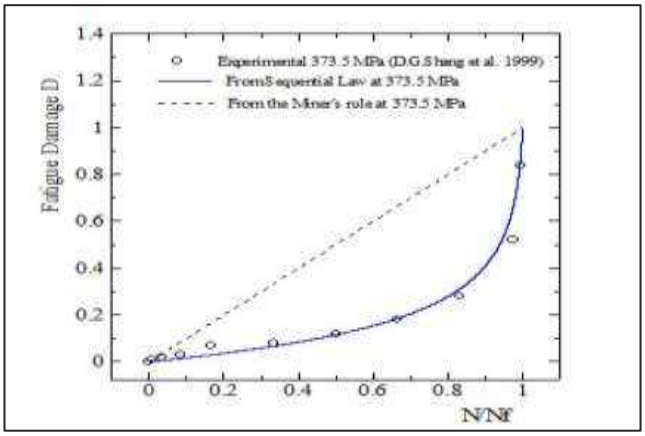

Figure (10), b – The comparison of sequential rule with experimental and Miner's rule results (Shang et al., 1999)

3.3 The Studied Sample Case

The studied platform is one of the sample jackets located in the Persian Gulf that has been modeled by ABAQUS finite element software. Depending on the gemetrical design parameters and the istalled depth of the fixed offshore platforms and environmentall and hydrodynamic condition in the Persian Gulf, a jacket platform is modeld similar to the SPD15 according to a plan of Iran Oil Copany. The depth and overall height of the modeled platform are 66.6 and 73.85 meters, respectively. It modeled in 3D and formable by the wire module of the Abaqus. the members of the modeled offshore structure provided by pipe profile and Beam elements (in 3D) with the ability to take into account the rotation, displacement and bending at the end of each element. The platform is meshed by B32 element ans fixed leg on the see bottom.The natural period of this model is less than 3 second that makes it possibe to use deterministic and static analysis in the modeling [10].

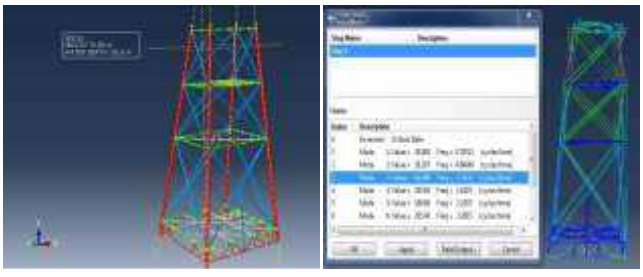

Figure 11 – The platform modeled by ABAQUS

In the software, applying the wave and current loading is done by Aqua coding where first, a wave with the specifications of a period of 11 seconds and a height of 12.2 meters is applied to the structure. In the fatigue analysis of the platform, the one-year dispersion table belonging to the Persian Gulf has been used, in such a way that, the waves with a higher number of incident events were selected and used (Table 2). In this research, according to thereports used in offshore engineering operations of the National Iranian Oil and Gas Company, the northwest direction was selected as the direction of the dominant wave, and for the purpose of finding the direction of the dominant wave, the changes of the angle of the incident wave with the structure were neglected.

Table (2) – The dispersion of the selected waves.

	Height	Cycle range	Number of event
Wave1	۳/۹۰	۰/٤ - ۰/۰	۱٦۱۳۲۳۱
Wave 2	٤/۹۰	۰/٥ – ۰/۹	٥۸۷۳۳۱
Wave 3	٤/۳۰	۱/۰ – ۱/٤	۱۷۹۷۰۹

From the location of the structure, it can be deduced that the structure has been positioned directly against the dominant waves because the north of the platform is along the northwestern geographical direction of the earth. According to DNV and API regulations, in the platforms with natural frequencies less than 3 seconds, the dynamic magnification coefficient (DAF) can be neglected, because it does not have much effect in increasing the applied static stresses. And often in these cases, the value of 1 is used for this coefficient. The method of the calculation of this coefficient is given by Eq.(12).

$$(12) DAF = \frac{1}{\sqrt{\left[1-(\frac{T_P}{T_W})^2\right]^2+\left[(2\beta\frac{T_P}{T_W})^2\right]^2}}$$

Where in Eq.(12), T = Natural period of the structure, T_W = Period of the wave, β = Attenuation coefficient

The modeling done for the fatigue analysis has been assessed for a connection at the base of the platform, Figure 12. For the verification of the model, the platform has been analyzed without wave loadings and under the weight of the structure, and the inconsistency of the results indicates the operating of the loading in the software.

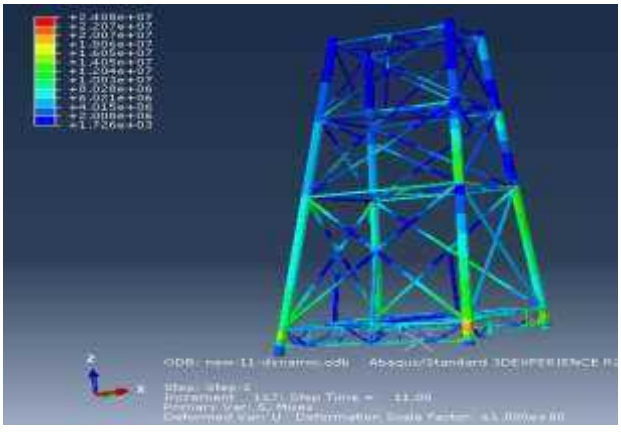

Figure (12): under loading platform

4.Discussion and Results

Since the analysis of marine offshore structures is of great importance with regard to the sea conditions and environmental loadings, determining the type of analysis and recognizing the importance of the conditions governing the environment has a significant role in the analysis of these structures. The quasi-static analysis is one of the most appropriate analyzes in jacket structures because the dynamic loads of the sea do not occur at a high speed and a short time like explosions. Nevertheless, pure static loads are not dominant in the sea either. Therefore, the quasi-static analysis is the most appropriate type of analysis in this type of structure. The API regulation requires a dynamic analysis at depths of more than 120 meters for all marine structures. In this research, with regard to the stress analysis performed, and taking into account the stress concentration coefficients and the use of stress-cycle diagrams for the selected type K connections, such results were obtained. According to the analyses obtained from dynamic, static, and quasi-static methods, the difference of about 33.1% in determining the maximum stress indicates the accuracy of thestatic and quasi-static analyses at depths below 100 meters and a natural period of less than 3 seconds, which confirms the regulations as well. Platform connections are one of the most sensitive structural points where stresses and concentration of stresses occur due to geometric imperfections and changes in cross-sections and welds. Therefore, in the present study, connections were observed as critical structural points that there is a need to analyze, study, and improve the performance of the structures in these points. Miner and sequential law are among the laws used for estimating the lifetime of these connections, which have been used in this research. The life of the present critical connection, which due to the depth of the area, is considered as an un-inspectable connection, was obtained to be selected about 37 and 33 years for the braces from the Miner and sequential laws, respectively. The difference of about 12% in the results indicates the importance of the methods used for estimating the lifetime of the structures.

Applying effects of the every wave on a structure and incorporating it on stracture situation that is subject to next wave can be leds us to accurate estimate for structure fatigue life. Regarding these results, the sequential law has a significant degree of accuracy in estimating fatigue life compared to the Miner law, which is also recommended for engineering tasks.

References:

1- Tabeshpour, M. R., Komachi, Y., Golafshani, A. A., (2012), *Assesment and Rehabilitation of Jacket Pelatforms*, ISBN: 978-953-53-0123-9.

2- ALMAR-NAESS, A., (1985), *Fatigue Handbook– Offshore Steel Structure*, Tapir, Trondheim, Norge, 520p.

3- American Petroleum Institute, (2002), *API RP 2A – WSD, Recommended Practice for Planning Design and Constructing Fixed Offshore Platforms, Working Stress Design*, 21st Edition.

4- Anastogtopoulos, S. A., (1982), *Dynamic Response of Offshore Structures to Extrem Waves Including Fluid-Structur Interaction. Eng structures*, Vol.4, pp 179-185.

5- Det Norske Veritas, October 2001, *DNV, Recommended Practice RP- C203, Fatigue Strength Analysis Offshore Steel Structures*.

6- Morison. J.R. & et al, (1950), *The force exerted by surface waves on piles*, American Institute of Mining &Metallurgical Engineerings, Vol. 189, PP.147-154.

7- Weicheng, C. Xiaoping, H. Fang, W., (2014), *Towards a Unified Fatigue Life Prediction Method for Marine Structure, Springer, Heidelberg*, New York, Dordrecht London, 281 p.

8- Wöhler's experiments on the strength of metals (1867) Engineering vol. 4pp160-161

9- Mesmacque, G., Garcia, S., Amrouche, A., Rubio-Gonzalez, C., (2005), *Sequential Law in Multiaxial Fatigue, a New Damage Indicator*, International Journal of Fatigue.,Volume 27, Issue 4, Pages 461-467.

10- Nemati Havigh. S., Behdarvani Askar. M., *The Process of Fatigue Analysis on Fixed Metal Offshore Platforms*, *Marine Science*, Vol. 7 No. 1, 2017, pp. 10-16. doi: 10.5923/j.ms.20170701.02.

INTERNATIONAL JOURNAL OF
COASTAL, OFFSHORE & ENVIRONMENTAL ENGINEERING IJCOE Vol.10/No. 3/ Summer 2025 (10-17)

Available online at: www. Ijcoe.org

Analysis of the Normal and Extreme Wind Patterns in the North Central Persian Gulf Using Two Wind Data Sources

Mohammad Hossein Kazeminezhad[1*]

[1] *Associate Professor, Ocean Engineering and Technology Department, Iranian National Institute for Oceanography and Atmospheric Science; mkazeminezhad@inio.ac.ir*

ARTICLE INFO

Article History:
Received : 22 OCT 2024
Accepted : 29 OCT2025

Keywords:
CFSR
Extreme Value Analysis
ERA5
Statistical Analysis
Peak Over Threshold

ABSTRACT

This study examines wind data from the North Central Persian Gulf, focusing on both normal and extreme wind patterns. The region's wind climate is influenced by dominant systems like the Shamal and Kaus winds, which significantly affect marine and offshore operations. To assess these wind conditions, two widely used reanalysis datasets including ERA5 and CFSR were analyzed for the period 1979-2023 at three locations in the Persian Gulf. A performance evaluation of ERA5 and CFSR data was conducted using Advanced Scatterometer (ASCAT) observations. Results revealed that while both datasets accurately represent general wind patterns, CFSR tends to better capture extreme wind speeds, though it exhibits greater scatter than ERA5. ERA5, on the other hand, underestimates high wind speeds, particularly at extreme values.

Wind roses were generated to analyze the prevailing wind directions, highlighting the predominance of northwesterly and westerly winds across all stations. These findings align with the region's exposure to the Shamal wind system. A frequency analysis showed that most winds occur at lower speeds (<6 m/s), with stronger winds (>9 m/s) more frequent in the northwest and west directions.

For extreme value analysis (EVA), the Peaks-Over-Threshold (POT) method was employed, using the 95th percentile to capture extreme events. Various probabilistic distribution models were fitted, with the Weibull distribution providing the best fit for both datasets. The results indicate that CFSR predicts consistently higher extreme wind speeds across all return periods compared to ERA5, which has implications for the design and safety of offshore structures in the Persian Gulf.

1. Introduction

The meteorological conditions, particularly the wind field, play a pivotal role in influencing the design of marine structures, encompassing both coastal and offshore installations. Accurate wind data is essential for understanding both normal and extreme wind conditions, which directly affect the structural integrity and operational safety of these installations. The Persian Gulf, a significant body of water in the Middle East, is influenced by various wind regimes that impact its marine and coastal environment.

This study focuses on the North Central region of the Persian Gulf, aiming to analyze and compare wind data from two prominent reanalysis datasets: ECMWF ReAnalysis 5 (ERA5) [1] and Climate Forecast System Reanalysis (CFSR) [2]. These datasets provide comprehensive historical weather data and are widely used in meteorological and climatological research. By evaluating normal and extreme wind patterns using these datasets, this study seeks to identify the most suitable wind data source for offshore studies in the Persian Gulf.

The Persian Gulf's wind patterns are influenced by extra-tropical wind regimes, primarily characterized by northwesterly winds in the northern part, which transition to westerly and southwesterly winds in the

southern and eastern regions [3]. Notably, several distinct wind systems, such as the Shamal and Kaus winds, significantly affect the region's climatic conditions.

The Shamal wind is one of the most significant wind systems in the Persian Gulf region. It is characterized by its strong, cool, and dry nature, predominantly blowing from the north or northwest. The Shamal wind occurs in both winter and summer, although its characteristics and impacts vary with the season. The winter Shamal, occurring from November to March, is most intense, often reaching gale force and causing sharp temperature drops and visibility issues due to dust storms [3, 4]. The summer Shamal, occurring from May to early July, is generally less intense but still affects marine and coastal activities.

The Kaus wind is another important wind system in the Persian Gulf, known for its moderate to gale-force intensity. This wind predominantly blows from the south to southeast and is most frequent between December and April. The Kaus wind often precedes the onset of Shamal winds and can reach gale force, particularly on the northeastern, Iranian side of the Persian Gulf. It brings warm and humid air from the southeast and can last from several hours to several days, impacting offshore operations [5, 6].

Reanalysis datasets such as ERA5 and CFSR have been extensively used in atmospheric and oceanographic studies. ERA5, produced by the European Centre for Medium-Range Weather Forecasts (ECMWF), provides high-resolution global climate data and has been validated against numerous observational datasets [1]. CFSR, developed by the National Centers for Environmental Prediction (NCEP), also offers comprehensive atmospheric data and is widely used in climatic and hydrological studies [2].

Several studies have focused on the climatology and meteorology of the Persian Gulf, highlighting the significance of its wind patterns. Hamzeh et al. [4] examined the seasonal variability of Shamal winds and their impact on the marine environment. Reynolds [3] provided an in-depth analysis of the Shamal wind system and its effects on the Persian Gulf region. Membery [5] and Purnell [6] discussed the characteristics of the Kaus wind and its influence on weather patterns.

In this paper, we first compile and analyze wind data from ERA5 and CFSR to determine their accuracy and reliability in representing wind conditions in the Persian Gulf. We perform extreme value analyses to estimate wind speeds for various return periods. This comprehensive analysis will help in understanding the general wind patterns and identifying the optimal wind data source for offshore design and safety assessments. By examining the wind roses at three locations in the North Central Persian Gulf, we aim to provide a detailed depiction of the dominant wind patterns. This information is crucial for the design and operation of offshore structures, ensuring their resilience against both typical and extreme wind conditions. Ultimately, this study will contribute to enhancing the safety and efficiency of marine operations in the North Central Persian Gulf by providing robust wind data analysis and recommendations.

2. Datasets

In this study two reanalysis wind datasets for the period of 1979-2023 were used to investigate the normal and extreme wind condition in the Persian Gulf. Wind analysis was conducted in 3 locations illustrated in Figure 1. As mentioned before two reanalysis wind data including ERA5 and CFSR are considered. ECMWF ReAnalysis 5 (ERA5) is the latest climate reanalysis produced by ECMWF, providing hourly data on many atmospheric, land-surface and sea-state parameters together with estimates of uncertainty. A first segment of the ERA5 dataset became completely available from January 2019 for public use (1979 to within 3 months of real time). The second segment extends the data from 1940-present. ERA5 provides hourly estimates of a large number of atmospheric, land and oceanic climate variables. The data cover the Earth on a 30 km grid and resolve the atmosphere using 137 levels from the surface up to a height of 80 km.

The Climate Forecast System Reanalysis (CFSR) atmospheric model was established by the National Centre for Environmental Prediction (NCEP). CFSR was designed as a global, high-resolution, coupled atmosphere-ocean-land surface-sea ice system to provide the best estimate of the state of these coupled domains. This model uses synoptic data for initialization. GFS (Global Forecast System) is the atmospheric model included in CFSR's modeling complex.

CFSR data covers the period from 1979 to 2010 (31-years) and since then, the operational re-forecast dataset, denoted CFSv2, is applied. Since CFSv2 is an operational dataset, regular updates of the dataset are possible. The underlying model in CFSv2 is the same as in CFSR, except that the spatial resolution of the grid decreased from 0.3° to 0.2°. The resolution of the atmospheric pressure is 0.5° for the entire period. Hereafter, 'CFSR' will refer to the combined CFSR and CFSv2 datasets.

Since the measured data in the studied area is limited, the ASCAT [7] data is used for initial evaluation of both wind resources. The Advanced Scatterometer (ASCAT) is a state-of-the-art European instrument deployed on the MetOp satellites, which plays a vital role in acquiring essential data for weather forecasting and climate research. Managed by NOAA/NESDIS, ASCAT wind products utilize measurements from the MetOp satellites, comprising MetOp-A (launched on October 19, 2006), MetOp-B (launched on September 17, 2012), and MetOp-C (launched on November 7,

2018). These satellites operate in a lower polar orbit at an altitude of 817 kilometers.

Specifically, ASCAT A-L2-25 km, ASCAT B-L2-25 km, and ASCAT C-L2-25 km data were utilized from the time of satellite launch up to the year 2023. This dataset comprises Level 2 ocean surface wind vector retrievals from ASCAT instruments onboard the MetOp-A, MetOp-B, and MetOp-C satellites, with a

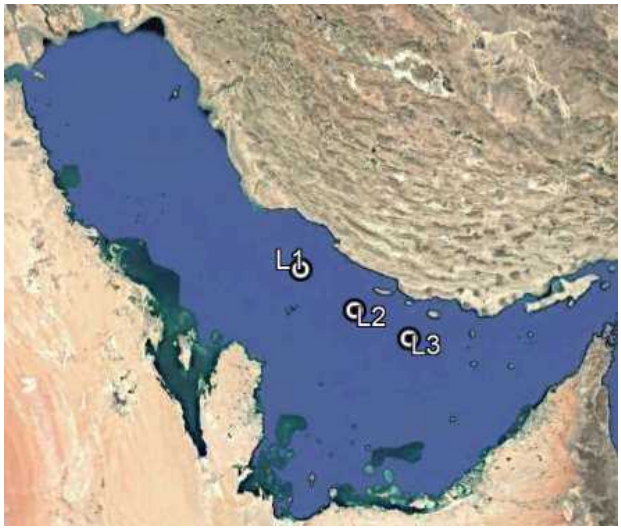

Figure 1. Study Area and selected locations (L1, L2, L3) for data analysing

sampling resolution of 25 km. ASCAT employs radar technology to measure the electromagnetic backscatter from the wind-affected ocean surface, providing valuable insights into wind speed and direction. This data aids in understanding and forecasting weather patterns and contributes to climate research efforts. The scatterometer's measurement principle capitalizes on the phenomenon where winds induce small-scale disturbances on the sea surface, altering its radar backscattering properties in distinct ways. These properties, well-documented and understood, depend on both the wind speed over the sea and the wind direction relative to the observation point of the sea surface.

3. Performance Evaluation of Wind Data

A critical challenge in coastal and offshore research within the Persian Gulf is selecting reliable wind data, given the limited availability of long-term, spatially comprehensive measurements. This study leverages ASCAT observational data to evaluate the performance of ERA5 and CFSR wind datasets. The objective is to assess the accuracy of ERA5 and CFSR wind speeds by comparing them against ASCAT measurements at three key stations: L1, L2, and L3. Figures 2 and 3 illustrate frequency scatter plots comparing CFSR and ERA5 wind speeds with ASCAT data at these locations.

At station L1, a total of 3,623 data points were identified as suitable for comparison between ASCAT wind speeds and those from CFSR and ERA5. The analysis reveals that wind speed scatter between CFSR and ASCAT is larger than that between ERA5 and ASCAT, as indicated by the Scatter Index (SI). However, CFSR exhibits a lower bias compared to ERA5. The scatter plots demonstrate a systematic underestimation of high wind speeds in the ERA5 data, a trend not observed in the CFSR dataset.

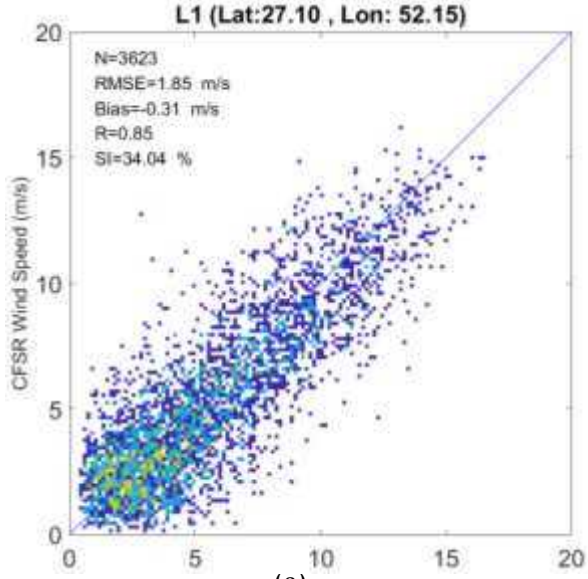

(a)

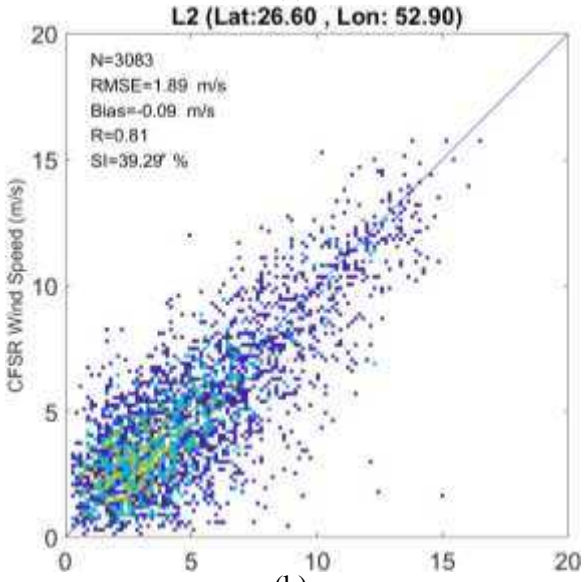

(b)

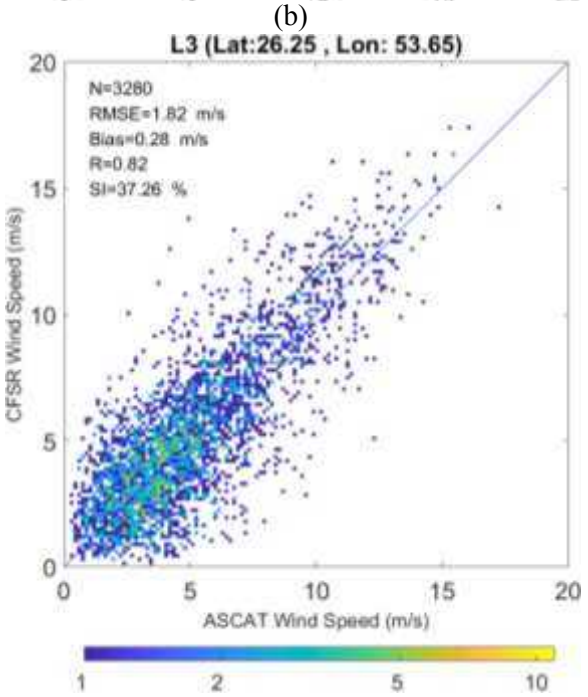

(c)

Figure 2. Comparison of ASCAT data with CFSR wind speed data at (a) L1, (b) L2 and (c) L3 stations

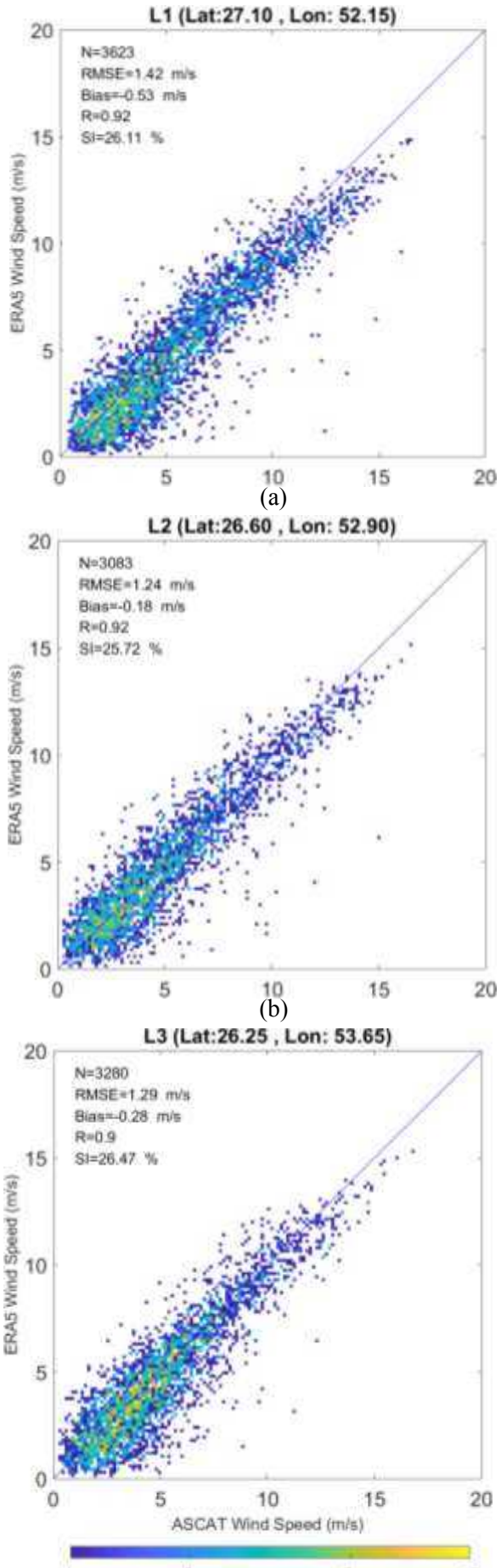

(c)

Figure 3. Comparison of ASCAT data with ERA5 wind data at (a) L1, (b) L2 and (c) L3 stations

The wind speed trends at stations L2 and L3 align with those observed at L1, with ERA5 consistently underestimating higher wind speeds, while CFSR maintains a better representation of extreme conditions. Despite the greater scatter observed in CFSR, it provides a more accurate estimation of extreme wind speeds, whereas ERA5, with lower scatter, offers a closer fit to overall wind patterns but underestimates higher wind speeds. These results suggest that both ERA5 and CFSR datasets are effective in capturing general wind patterns in the study area, though their utility in extreme wind speed analysis differs, with CFSR being more suitable for high wind speed events.

4. Normal Wind Pattern

This section presents an analysis of wind conditions at three stations (L1, L2, and L3) in the central-north Persian Gulf, based on wind data from ERA5 and CFSR datasets. The wind speed and direction are categorized into different ranges to assess the frequency distribution across the stations, focusing on wind speeds ranging from calm (<3 m/s) to extreme (>18 m/s) across the eight cardinal directions.

Initially, to examine the general wind patterns, wind roses derived from the CFSR and ERA5 datasets were investigated for stations L1, L2, and L3. Figure 4 displays the annual wind rose based on CFSR data. The analysis reveals that northwesterly and westerly winds predominantly prevail across all stations, with east and southeast winds also being significant. These patterns are attributed to the Shamal and Kaus winds in the Persian Gulf. At station L1, the maximum recorded wind speed was 19.8 m/s, coming from 319°. Similarly, at stations L2 and L3, the strongest winds were 19.6 and 20.5 m/s, respectively, originating from 311° and 298°.

Figure 5 displays the annual wind roses at stations based on ERA5 data. The wind patterns observed at stations L1, L2, and L3 based on ERA5 data demonstrate a high degree of consistency. Predominantly, the prevailing wind direction is from the northwest, with notable secondary frequencies from the southeast at L1 and L2, and from the east at L3. Detailed analysis shows that at station L1, the highest recorded wind speed was 16.9 m/s, coming from 312°. At stations L2 and L3, the strongest winds were 17.3 and 17.2 m/s, respectively, blowing from 311° and 303°.

A comprehensive analysis of the percentage occurrence of wind speed and direction at different stations, are

presented in Tables 1–6. The data presented in these tables, derived from the CFSR dataset, reveals that most winds occur in the lower wind speed range (0–6 m/s). Specifically, at station L1, approximately 62.28% of total wind occurrences fall within this range, while at stations L2 and L3, this percentage increases to 67.31% and 68.45%, respectively. The proportion of winds at higher speeds (>9 m/s) is notably higher in the

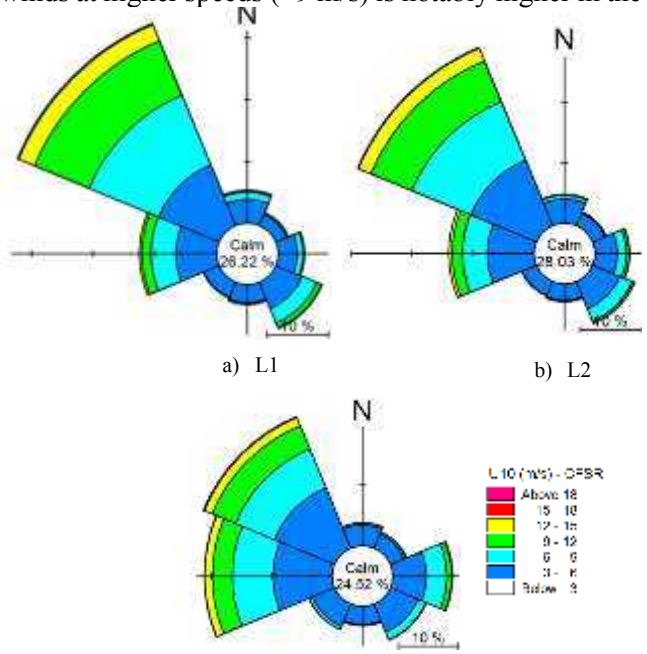

a) L1 b) L2

c) L3

Figure 4. Annual wind rose based on CFSR wind data at a) L1, b) L2 and c) L3

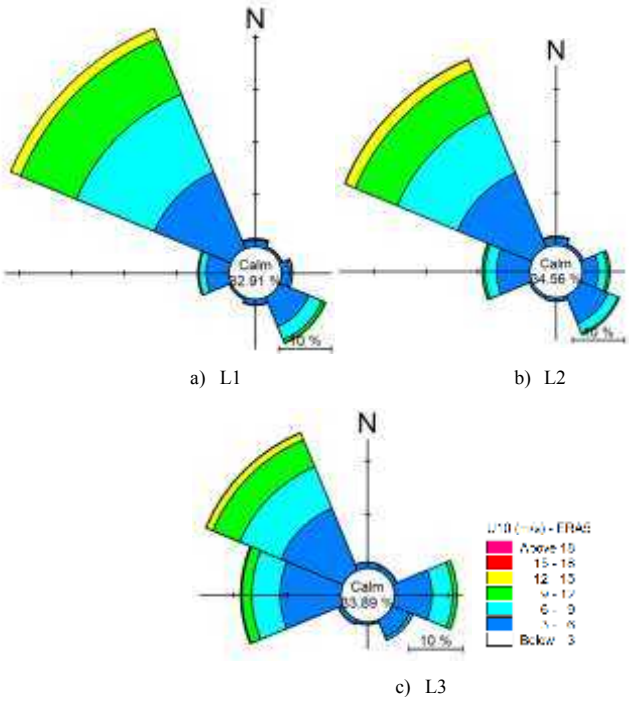

a) L1 b) L2

c) L3

Figure 5. Annual wind rose based on ERA5 wind data at a) L1, b) L2 and c) L3

northwesterly (NW) and westerly (W) directions, reflecting the dominance of these directions for stronger winds in the Persian Gulf.

Similar to CFSR, the ERA5 data also shows a dominance of winds in the lower wind speed ranges. In ERA5, the percentage of 0–6 m/s winds are slightly higher compared to CFSR, accounting for 63.81% of the total winds at L1, 68.64% at L2, and 71.55% at L3. Stronger winds (≥9 m/s) are more frequent in the NW direction, particularly at L1 and L3, where wind speeds

Table 1. Percentage occurrence of wind speed-direction at L1 based on CFSR data

Direction	Wind Speed (m/s) - CFSR - L1							
	0-3	3-6	6-9	9-12	12-15	15-18	>18	Sum.
N	3.764	3.818	1.223	0.220	0.030	0.001	0.000	**9.055**
NE	3.029	1.865	0.331	0.039	0.002	0.000	0.000	**5.266**
E	3.083	3.093	0.939	0.200	0.037	0.003	0.000	**7.356**
SE	2.914	4.582	2.572	0.758	0.163	0.019	0.002	**11.009**
S	2.564	2.892	0.262	0.028	0.003	0.000	0.000	**5.749**
SW	2.739	2.646	0.140	0.006	0.001	0.000	0.000	**5.532**
W	3.566	6.622	3.991	1.570	0.322	0.004	0.000	**16.075**
NW	4.566	10.579	12.267	9.484	2.853	0.208	0.002	**39.958**
Sum.	**26.224**	**36.096**	**21.726**	**12.305**	**3.410**	**0.236**	**0.004**	**100.00**

Table 2. Percentage occurrence of wind speed-direction at L2 based on CFSR data

Direction	Wind Speed (m/s) - CFSR - L2							
	0-3	3-6	6-9	9-12	12-15	15-18	>18	Sum.
N	4.270	4.001	0.648	0.102	0.018	0.001	0.000	**9.042**
NE	3.301	2.177	0.271	0.027	0.001	0.000	0.000	**5.777**
E	3.015	3.683	1.526	0.426	0.093	0.010	0.001	**8.753**
SE	2.697	4.878	2.159	0.448	0.066	0.011	0.000	**10.259**
S	2.602	2.776	0.161	0.013	0.001	0.000	0.000	**5.553**
SW	3.020	2.528	0.088	0.006	0.000	0.000	0.000	**5.642**
W	3.939	7.671	4.074	1.739	0.498	0.024	0.000	**17.946**
NW	5.182	11.628	10.481	7.327	2.236	0.172	0.002	**37.028**
Sum.	**28.026**	**39.343**	**19.408**	**10.089**	**2.913**	**0.218**	**0.003**	**100.00**

Table 3. Percentage occurrence of wind speed-direction at L3 based on CFSR data

Direction	Wind Speed (m/s) - CFSR - L3							
	0-3	3-6	6-9	9-12	12-15	15-18	>18	Sum.
N	3.340	3.456	0.268	0.045	0.007	0.001	0.000	**7.117**
NE	2.699	2.506	0.363	0.049	0.003	0.000	0.000	**5.620**
E	2.709	5.559	3.404	0.794	0.125	0.009	0.000	**12.601**
SE	2.599	4.991	1.339	0.104	0.004	0.001	0.000	**9.038**
S	2.464	2.974	0.193	0.008	0.001	0.000	0.000	**5.640**
SW	2.765	3.975	0.583	0.021	0.001	0.001	0.000	**7.346**
W	3.633	9.764	6.733	3.343	1.211	0.116	0.000	**24.800**
NW	4.310	10.745	6.984	4.149	1.457	0.189	0.006	**27.840**
Sum.	**24.518**	**43.969**	**19.868**	**8.514**	**2.809**	**0.316**	**0.006**	**100.00**

Table 4. Percentage occurrence of wind speed-direction at L1 based on ERA5 data

Direction	Wind Speed (m/s) - ERA5 - L1							
	0-3	3-6	6-9	9-12	12-15	15-18	>18	Sum.
N	3.467	1.291	0.291	0.043	0.004	0.000	0.000	**5.097**
NE	2.162	0.442	0.098	0.004	0.000	0.000	0.000	**2.705**
E	2.930	1.512	0.501	0.127	0.008	0.000	0.000	**5.077**
SE	4.779	6.052	2.748	0.690	0.076	0.001	0.000	**14.346**
S	3.449	1.002	0.131	0.022	0.000	0.000	0.000	**4.605**
SW	2.835	0.369	0.039	0.006	0.001	0.000	0.000	**3.250**
W	5.557	4.422	1.328	0.265	0.004	0.000	0.000	**11.576**
NW	7.732	15.809	16.174	11.529	2.078	0.023	0.000	**53.345**
Sum.	**32.911**	**30.899**	**21.310**	**12.685**	**2.171**	**0.025**	**0.000**	**100.00**

Table 5. Percentage occurrence of wind speed-direction at L2 based on ERA5 data

Direction	Wind Speed (m/s) - ERA5 - L2							
	0-3	3-6	6-9	9-12	12-15	15-18	>18	Sum.
N	4.231	1.575	0.170	0.031	0.001	0.000	0.000	**6.008**
NE	2.672	0.596	0.090	0.007	0.000	0.000	0.000	**3.365**
E	3.530	3.136	1.621	0.533	0.044	0.002	0.000	**8.866**
SE	4.630	5.747	2.049	0.352	0.020	0.000	0.000	**12.797**
S	2.892	0.649	0.072	0.013	0.000	0.000	0.000	**3.627**
SW	2.829	0.533	0.038	0.006	0.000	0.000	0.000	**3.406**
W	5.860	6.416	2.169	0.555	0.026	0.000	0.000	**15.025**
NW	7.911	15.439	12.593	8.818	2.104	0.040	0.000	**46.906**
Sum.	**34.555**	**34.090**	**18.802**	**10.316**	**2.195**	**0.042**	**0.000**	**100.00**

Table 6. Percentage occurrence of wind speed-direction at L3 based on ERA5 data

Direction	Wind Speed (m/s) - ERA5 - L3							
	0-3	3-6	6-9	9-12	12-15	15-18	>18	Sum.
N	3.273	1.052	0.080	0.012	0.001	0.000	0.000	**4.418**
NE	2.758	0.830	0.136	0.014	0.002	0.000	0.000	**3.740**
E	4.446	6.999	3.837	0.846	0.051	0.002	0.000	**16.180**
SE	4.334	3.553	0.579	0.065	0.001	0.000	0.000	**8.532**
S	2.692	0.478	0.052	0.016	0.001	0.000	0.000	**3.239**
SW	3.225	0.894	0.058	0.007	0.001	0.000	0.000	**4.185**
W	6.613	11.348	5.299	1.831	0.263	0.001	0.000	**25.354**
NW	6.545	12.518	8.354	5.474	1.415	0.045	0.000	**34.352**
Sum.	**33.885**	**37.672**	**18.394**	**8.265**	**1.735**	**0.049**	**0.000**	**100.00**

reach higher values more frequently compared to other directions.

At L1, both datasets indicate that northwesterly (NW) winds are dominant. The NW winds account for 39.96% of the wind occurrences in CFSR and 53.34% in ERA5. Winds from the west (W) direction are the second most frequent, contributing 16.08% (CFSR) and 11.58% (ERA5) of the total wind occurrences. Notably, winds from the NW direction are often associated with higher wind speeds in both datasets, suggesting that strong winds in the region are primarily driven by NW winds.

At L2 and L3, the wind patterns are largely similar to L1, with northwesterly (NW) winds being the most frequent, followed by westerly (W) winds. However, the frequency of NW winds at these two stations is slightly lower than at L1, though still prominent. This consistency across the stations suggests that all three locations are influenced by the same large-scale weather systems, such as the Shamal winds, which primarily blow from the northwest, but with a slightly reduced frequency as we move from L1 to L3.

In addition to the dominant northwesterly and westerly winds, which exhibit high occurrence frequencies, winds from the southeast and east directions also show relatively high frequencies and are associated with strong wind speeds in both datasets across all three stations. These winds are linked to the Kaus winds in the Persian Gulf, which, while less frequent than the Shamal winds, can reach intensities equal to or even exceeding those of the Shamal.

Comparing the wind speed distributions between CFSR and ERA5 at the three stations reveals certain differences. CFSR generally reports slightly stronger winds than ERA5, particularly in the higher wind speed categories (≥9 m/s). For example, at L1, the frequency of winds above 9 m/s in the NW direction is 27.73% in CFSR compared to 22.54% in ERA5. Based on the comparative analyses presented in Section 2, CFSR wind data, particularly within the higher wind speed categories, demonstrate a greater degree of reliability.

5. Extreme Wind Pattern

Random phenomena like wind speed cannot be precisely predicted, but statistical and probabilistic methods, such as Extreme Value Analysis (EVA), enable the estimation of their probability of occurrence and return periods. EVA is widely used across various fields, including coastal/ocean engineering and meteorology, to assess extreme events such as floods, waves, and wind.

The process of EVA involves fitting probabilistic distribution functions to observed data, allowing the determination of parameters for design purposes over extended periods. Generally, for EVA, three main approaches are typically used:

1. Cumulative Distribution Function (CDF) Method: This method fits the entire dataset to a distribution function and extrapolates to estimate wind speed for given design periods. However, the Coastal Engineering Manual [8] advises against using this method for wind speed analysis due to the difficulty in ensuring statistical independency and homogeneity of the data.
2. Annual Maximum Series (AMS): This approach focuses on selecting the maximum wind speed for each year. While it satisfies the requirement of independency, it may overlook significant storm events.
3. Peaks-Over-Threshold (POT): Also known as the partial duration series (PDS), this method selects wind speeds exceeding a certain threshold, ensuring that all major events are captured [9]. The POT method is favored in wind extreme value analysis for its ability to handle independent data more effectively.

Both AMS and POT methods are widely accepted for analyzing extreme wind events, with POT providing a more comprehensive approach for wind and wave extremes.

In this study, the Peaks-Over-Threshold (POT) method was used to select the data required for extreme value analysis. The 95th percentile criterion was applied for both ERA5 and CFSR datasets to determine the appropriate threshold. In this regard, the Weibull, Gumbel, Exponential, Generalized Pareto, and Log-Normal probabilistic distributions were employed, and the best-fitting distribution for the data was selected. The analyses showed that the Weibull distribution had the best fit for both datasets. Therefore, all the presented results are based on this statistical distribution.

Tables 7 and 8 present the extreme wind speeds (in m/s) for different return periods at three stations (L1, L2, and L3), based on CFSR and ERA5 datasets, respectively.

Table 7 shows the extreme values derived from the CFSR data, where the wind speed for a 1-year return period ranges between 16.6 and 16.9 m/s across the three stations. For a 10-year return period, wind speeds increase to a range of 18.9 to 19.5 m/s, while for a 100-year return period, values further rise to between 20.9 and 21.8 m/s.

Table 8 illustrates the extreme values based on the ERA5 data, with wind speeds for a 1-year return period varying from 14.5 to 14.8 m/s. For a 10-year return period, wind speeds range from 16.1 to 16.9 m/s, and for a 100-year return period, they rise to between 17.5 and 18.8 m/s.

The comparison of extreme wind speeds derived from the ERA5 and CFSR datasets (Tables 7 and 8) reveals notable differences that could impact the design of offshore and coastal structures. The CFSR dataset consistently shows higher wind speed estimates across all return periods. For instance, for the 1-year return period, CFSR estimates range from 16.6 to 16.9 m/s, while ERA5 ranges from 14.5 to 14.8 m/s. This discrepancy increases with longer return periods, with CFSR values for the 100-year return period ranging from 20.9 to 21.8 m/s, whereas ERA5 estimates are between 17.5 and 18.8 m/s.

These differences can significantly affect the structural design of offshore and coastal infrastructure, as wind speed directly influences design loads. Structures designed using the CFSR dataset, which predicts higher wind speeds, would incorporate larger safety margins, resulting in more robust designs capable of withstanding extreme wind events. In contrast, using ERA5 data, which tends to yield lower wind speed estimates, might result in under-design, especially in rare, high-wind scenarios like those associated with a 100-year return period.

This variation in estimated extreme wind speeds suggests that the choice of dataset can influence the safety and cost of structural designs. In regions prone to severe wind events, using the CFSR dataset might offer a more conservative and safer approach, as it appears to better capture extreme wind conditions. ERA5, on the other hand, might underestimate these extremes due to its reanalysis methodology, which can smooth out rare, high-intensity events.

Previous studies have highlighted similar trends. For example, Çalışır et al. [10] found that Both CFSR and ERA5 underestimate wind speeds. ERA5 performs better than the CFSR in lower wind speeds and worse in higher wind speeds. However, ERA5 winds have less bias and are more scattered than the CFSR winds against the satellite data. Simulated wave heights driven by CFSR winds performs better than the one driven by ERA5 winds against both buoy and satellite data. Gandoin and Garza [11] also noted that ERA5's smoothing effect in open ocean area could lead to an underestimation of extreme events, whereas CFSR data often captures more detailed and accurate depictions of such phenomena. These findings reinforce the importance of dataset selection when performing extreme value analysis for wind speed in engineering design.

Table 7. Extreme values of wind speed (m/s) based on CFSR data for different return period

Return Period (year)	Stations		
	L1	L2	L3
1	16.7	16.6	16.9
10	18.9	19.0	19.5
100	20.9	21.1	21.8

Table 8. Extreme values of wind speed (m/s) based on ERA5 data for different return period

Return Period (year)	Stations		
	L1	L2	L3
1	14.5	14.7	14.8
10	16.1	16.5	16.9
100	17.5	18.0	18.8

6. Conclusions

This study provides a comprehensive analysis of normal and extreme wind conditions in the North Central Persian Gulf using two widely recognized reanalysis datasets: ERA5 and CFSR. Through the evaluation of wind patterns, extreme value analysis, and validation against ASCAT observational data, several key insights were obtained.

CFSR demonstrated superior performance in capturing extreme wind events, making it a more suitable dataset for estimating high wind speeds necessary for offshore design and safety assessments. However, ERA5 proved to offer a more consistent representation of general wind patterns with lower scatter, although it tends to underestimate extreme wind speeds. The predominance of northwesterly winds, associated with the Shamal system, was observed across all study locations, with stronger winds more frequently occurring in the northwest and west directions.

The Peaks-Over-Threshold (POT) method, applied for extreme value analysis, confirmed that the Weibull distribution is the best fit for both datasets, further highlighting that CFSR consistently predicts higher extreme wind speeds across various return periods compared to ERA5. These findings carry significant implications for the design and safety of offshore structures in the region, emphasizing the need to carefully select the appropriate wind dataset based on specific project requirements.

In conclusion, this study contributes to enhancing the understanding of wind patterns and extreme wind behavior in the Persian Gulf. The results underscore the

importance of selecting reliable wind data sources, particularly in regions like the Persian Gulf where extreme weather events pose a substantial risk to offshore infrastructure. The insights gained from this study can guide future research and practical applications in marine and coastal engineering, helping ensure the resilience and safety of offshore operations.

8. References

[1] Hersbach, H., Bell, B., Berrisford, P., Hirahara, S., Horányi, A., Munoz-Sabater, J., ... & Thépaut, J. N. (2020), *The ERA5 global reanalysis.* Quarterly Journal of the Royal Meteorological Society, Vol. 146(730), p. 1999-2049.

[2] Saha, S., Moorthi, S., Pan, H. L., Wu, X., Wang, J., Nadiga, S., ... & Behringer, D. (2010). *The NCEP climate forecast system reanalysis.* Bulletin of the American Meteorological Society, Vol. 91(8), p. 1015-1058.

[3] Reynolds, R. M. (1993). *Physical oceanography of the Gulf, Strait of Hormuz, and the Gulf of Oman—Results from the Mt Mitchell expedition.* Marine Pollution Bulletin, Vol. 27, p.35-59.

[4] Hamzeh, P., Khosravi, H., & Sarbazi, H. (2014), *Seasonal variability of Shamal wind and its impact on the marine environment of the Persian Gulf.* Journal of Marine Science and Technology, Vol. 22(4), p.567-579.

[5] Membery, D. A. (1983), *The winter Shamal in the Persian Gulf.* Weather, Vol. 38(10), p.375-380.

[6] Purnell, H. (1998). *Climatology of the Kaus wind in the Persian Gulf region.* Meteorological Applications, Vol. 5(4), p.385-392.

[7] Figa-Saldaña, J., Wilson, J. J. W., Attema, E., Gelsthorpe, R., Drinkwater, M. R., Stoffelen, A. (2002). The advanced scatterometer (ASCAT) on the meteorological operational (MetOp) platform: A follow on for European wind scatterometers. Canadian Journal of Remote Sensing, 28(3), 404-412.

[8] Cem

[9] Kamphuis, J.W., (2010), Introduction to Coastal Engineering and Management, 2nd Edition, Advanced Series on Ocean Engineering: Volume 30, World Scientific.

[10] Çalışır, E., Soran, M. B., & Akpınar, A. (2021). Quality of the ERA5 and CFSR winds and their contribution to wave modelling performance in a semi-closed sea. Journal of Operational Oceanography, 16(2), 106–130.

[11] Gandoin, R., Garza, J., (2024) Underestimation of strong wind speeds offshore in ERA5. Wind Energy Science, Discussions.

INTERNATIONAL JOURNAL OF
COASTAL, OFFSHORE & MEDIUMAL ENGINEERING IJCOE Vol.10/No. 3/ Summer 2025 (18-29)

Available online at: www. Ijcoe.org

Development of Oceanic Numerical Model for Persian Gulf (part 1)

Mehri Fallahi[1], Mohammad Taghi Zamanian [2], Masoud Sadrinasab[3*]

1,PhD Physical Oceanography, Khorramshahr University of Marine Science and Technology, Khorramshahr and Instructor of Physics Lab, Department of Agricultural Machinery Engineering, University of Tehran, Tehran, Iran, mehri_fallahi@ut.ac.ir

۲,Invited Professor, Khorramshahr Marine Science and Technology University, Khorramshahr, Iran. zamanianmohammadtaghi@gmail.com

**۳,Associate Professor, Department of Environment Engineering, School of Graduate Environment, university of Tehran , Tehran, Iran. masoud.sadri@ut.ac.ir*

ARTICLE INFO

Article History:
Received : 20 APR 2025
Accepted : 29 SEP 2025

Keywords:
Persian Gulf
numerical model
primitive equations
sigma vertical coordinate
forced tide.

ABSTRACT

In this study, a three-dimensional numerical model (PersianGulfOceanicModel (ZSF974)) based on the primitive equations, in the Earth's Spherical Coordinates System with a sigma vertical coordinate, has been developed with the aim of predicting and calculating oceanographic parameters in the marine medium of the Persian Gulf. The finite difference method has been used for the numerical solution of the model equations. For discretization, the Lax–Wendroff scheme was applied to the advection terms, the DuFort–Frankel scheme to the diffusion terms, and the Matsuno scheme was used to eliminate instabilities arising from certain calculations within the program. The mesh used is the modified Arakawa C grid. This model, in addition to accommodating any type of non-level bottom, has the capability to vary resolution in both horizontal and vertical directions. The superiority of the process implemented in its design, the proper application of Nihoul's theory (1977) regarding the effect of surface stress induced by wind in the lower layers has enhanced the accuracy of the model's outputs. In this study is presented the process of designing the base model and the dimensions of its validation through models in laboratorial mediums. In all laboratorial oceanic mediums, the stationary state, the effect of neglecting the Coriolis force and earth's curvature, as well as the effect of applying a constant force have been investigated. Hypothetical (and approximate real) data and forced tide, have been used as the program's input. The results of the model's execution are consistent with ocean physics principles and the findings of previous researchers and can represent the overall behavior of an oceanic medium. This model can be used as a base model to examine the overall behavior of an oceanic medium. It also has the capability to be developed for implementation and conclusion in a real-world medium.

1. Introduction

The role of the oceans in climate regulation is fundamental. The strategic importance of the seas and oceans in transportation, fishing, energy supply, extraction of vast sub-sea mineral resources, and their contribution to national defense capabilities, as well as their role in maintaining biodiversity, is evident to everyone. One of the ways to proper use from the sea is to be aware of the dangers of working at sea by predicting sea conditions. This forecasting helps us maximize our benefits from the sea and minimize the damages that may occur to us or non-human resources as a result of marine activities.

The complex and deep interrelationship between the parameters and non-linear terms in the governing equations; are the reasons that analytical solutions for governing equations is impossible nowadays. Therefore, numerical solutions are the most important and suitable approach for obtaining results from governing equations for getting oceanic states and predicting oceanic parameters in oceanic mediums.

The goal of ocean modeling is to understand the interaction processes between the atmosphere and the ocean, as well as ocean's state. The use of these predictions provides the foundation for aiding in the climate prediction of the relevant oceanic medium [1]. Among the oceanic numerical models, the primitive equation models can be the most comprehensive one. These models, due to their three-dimensional nature, offer high resolution in the vertical direction. In numerical models, oceanic mediums are divided into multiple layers in the vertical direction. Mmulti-layering means that at least one oceanic parameter will have a different value with the same parameter value in the other layer. On the other hand, in a single-layer or two-layer oceanic medium, phenomena such as double diffusion and internal wave cannot be well recognized. [1].

In numerical solutions, it is necessary to validate or calibrate these results. For this purpose, developing a theoretical ocean model can be highly beneficial. Theoretical models are defined by having some of the characteristics of a real oceanic medium. The model created in this form will contain accuracy of the response to a part of the final model and this model itself can serve as one of the foundations for the real models.

Researchers have designed various numerical models for different purposes that have been used in various research fields. In 1992, Khaleghi Zavare developed a non-linear barotropic model for the Persian Gulf. This model is based on the integration of shallow water equations in the vertical direction and is sensitive to the earth's rotation and the effects of bathymetric variations. The model was designed to determine the response to the Persian Gulf from wind and tidal forces through numerical simulation [2]. In 1994, Zamanian used a two-layer model to study the currents of the Persian Gulf. This model was designed on the primitive equations in Cartesian Coordinates System with a sigma vertical coordinate. This model, in addition to determining the current fields caused by wind and tides, predicts temperature, salinity in two layers, vertical velocity at a given level, and sea surface height at the grid points [3]. James (1998), a three-dimensional numerical model used to simulate the development of disturbances on shelf-sea coastal currents and fronts [4]. Kampf and Sadri-Nasab (2006) used a three-dimensional hydrodynamic simulator (COHERENS) to model the water circulation and water mass properties of the Persian Gulf – a large inverted estuary. These findings indicate that the Persian Gulf experiences a distinct seasonal cycle [5]. Ibrayev et al. (2010) used a three-dimensional primitive equation model including sea ice thermodynamics and air-sea interaction to study seasonal circulation and water mass variability in the Caspian Sea under the influence of realistic mass, momentum and heat fluxes [6]. Mehrfar et al., 2020, employed COHERENS simulator as a three-dimensional hydrodynamic model to address the coastal currents in the western Persian Gulf. The obtained results suggested that a consequence of the influence of salinity flux, especially on the Iranian coasts, the speed of currents increases [7]. Heidari et al. (2018) designed a five-layer ocean numerical model based on primitive equations and the Earth's Spherical Coordinates System with a sigma coordinate. This research was conducted with the aim of predicting and calculating the currents caused by wind and oceanic parameter in the Caspian Sea [8]. Yining et al., 2024, proposed an ocean SWH (Significant Wave Height) prediction model, RIME-CNN-BiLSTM, for predicting 1, 6, 12, and 24 h SWH at three buoy observing stations in the Gulf of Mexico [9]. Deldar (2024) simulated wind waves in the Strait of Hormuz using the D3Delft three-dimensional simulation processor flow module hydrostatically and non-hydrostatically, where is prone to the formation of lee waves due to its many shallow channels. The results indicate the presence of lee waves in the Strait of Hormuz [10].

Fallahi et al. (2019) designed a "Five-Layer Numerical Ocean Model of the Persian Gulf." The aim of this study was to predict physical parameters in the Persian Gulf [11]. In the course of refining and enhancing the model, a laboratory-scale oceanic basin was configured to resemble the Persian Gulf. A two-year simulation revealed that the basin is dominated by semidiurnal tidal forcing, which prevails over wind stress and density gradient forces [22]. The consistency of the results with ocean physics principles and previous research findings provided a solid basis for further development of the model.

The Persian Gulf (Figure 1) is located in the south of Iran, with latitudes ranging from 24° N to 30°30' N, and longitudes from 48° E to 56°25' E from the Greenwich meridian.

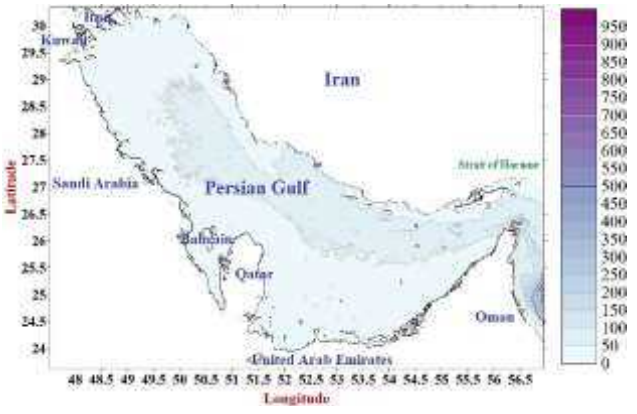

Figure 1- Location and bathymetry of the Persian Gulf

Since the Persian Gulf holds a vast maritime boundary for Iran, it has of significant medium and important for, economic, tourism, and strategic activities. Moreover, due to its unique geographical location, the Persian

Gulf holds special strategic and economic value in the western part of Asia. Therefore, any research or study for this basin is considered crucial and strategic in terms of planning.

Since numerical modeling can be a powerful research tool. The PersianGulfOceanicModel(ZSF974) was designed as a foundational model with the aim of predicting oceanographic parameters and sea state in this oceanic medium.

This model is not only enables the examination of complex dynamic processes but also plays a crucial role in marine resource management, provides prerequisite for knowing Persian Gulf's climate, and the enhancement of warning systems for atmospheric and oceanic phenomena.

The method employed in model's design allowing applicable to any hypothetical or real basin, whether closed or open. Another advantage of this model, is comparing to similar models designed by previous researchers, And the superior algorithm used in its design, which ensures that predictions and calculations are carried out correctly, is taking into account the proper relationships between the mathematical equations used in it. Furthermore, the correct application of Nihoul's theory regarding the effect of wind-induced surface stress on the lower layers in multi-layer mediums has made the model's outputs more accurate. [12]

This study presents the setup process of the "PersianGulfOceanicModel (ZSF974)" oceanic numerical model [11]. The technical notes for the design and development of the Base Oceanic Model (BOM) have been used to design and develop this model [1].

Therefore, the "PersianGulfOcean(ZSF974)" model is an development and expanded version of the "BOM" model to simulate real ocean mediums. The study was conducted in two stages: for laboratorial basins and real oceanic basins. This article presents the technical points of designing these models, and the aspects of "PersianGulfOceanicModel (ZSF974)" validation in laboratory mediums.

2. Method and Theoretical Framework

In design of this kind of oceanic models, in addition to there is utilizing and applying the governing physical principles of the atmosphere and ocean, such as Newton's laws, the conservation of mass, the conservation of salinity, and the conservation of thermal energy, the first and second laws of thermodynamics and the equation of state for seawater.

In order for the proposed model to accommodate any non-level bottom as the actual topography of oceanic mediums during the operational stage, the Sigma vertical coordinate (σ) has been utilized. In this study, the vertical coordinate is considered in the form introduced by Zamanian (2006) [1]:

$$\sigma = \frac{p - p_A}{p_b - p_A} \tag{1}$$

where σ presents the normalized vertical coordinate, p_b denotes the bottom pressure at any point in the oceanic medium, p_a refers to the atmospheric pressure over the oceanic medium and p stands for pressure at any point in the ocean medium. In this system, $\sigma = 0$ corresponds to the ocean surface, and $\sigma = 1$ presents the ocean bottom. The values $0 < \sigma < 1$ correspond to the intermediate levels.

The unit vectors in The Earth's Spherical Coordinates System with the sigma vertical coordinate can be defined as: $\mathbb{e}_\lambda$ in the direction of increasing λ, the longitude, $\mathbb{e}_\phi$ in the direction of increasing ϕ, the latitude and $\mathbb{e}_\sigma$ in the direction of increasing σ, downward. Also $\mathbb{e}_\sigma$ is a variant unit vector. The lengths components in this system are as follows:

$$\begin{cases} \delta s_\lambda = r \cos\phi \, \delta\lambda \\ \delta s_\phi = r \, \delta\phi \\ \delta s_\sigma = \dfrac{p_b - p_A}{\rho \, g} \, \delta\sigma \end{cases} \tag{2}$$

where $\delta_{s\lambda}$ is a portion length in longitude direction, r is the radial distance of the length component from the earth's center, ϕ is latitude, $\delta\lambda$ stands for increment of longitude, $\delta_{s\phi}$ refers to a portion length in latitude direction, $\delta\phi$ denotes to increment of latitude, $\delta_{s\sigma}$ represents a portion length in vertical direction, p_b indicates the bottom pressure, p_A stands for atmospheric pressure, ρ is the density, and g is the gravitational acceleration of the earth. The velocity vector in this system also write as follows:

$$\mathbb{u} = u \, \mathbb{e}_\lambda + v \, \mathbb{e}_\phi + w \, \mathbb{e}_\sigma \tag{3}$$

where the components of velocity are:

$$\begin{cases} u = r \cos\phi \, \dfrac{D\lambda}{Dt} \\ v = r \, \dfrac{D\phi}{Dt} \\ w = \dfrac{p_b - p_A}{\rho \, g} \, \dfrac{D\sigma}{Dt} \end{cases} \tag{4}$$

Using equations (2), (3) and (4), the total rate of change of a variable in this system gives by:

$$\frac{D\ldots}{Dt} = \frac{\partial\ldots}{\partial t} + \frac{u}{r\cos\phi}\frac{\partial\ldots}{\partial\lambda} + \frac{v}{r}\frac{\partial\ldots}{\partial\phi} + \dot{\sigma}\frac{\partial\ldots}{\partial\sigma} \tag{5}$$

In which $\frac{D\ldots}{Dt}$ is the total derivative, $\frac{\partial\ldots}{\partial t}$ represents the local rate of change, $\frac{u}{r\cos\phi}\frac{\partial\ldots}{\partial\lambda}$ denotes the eastward advection, $\frac{v}{r}\frac{\partial\ldots}{\partial\phi}$ represents the northward advection,

and $\dot{\sigma}\frac{\partial \dots}{\partial \sigma}$ refers to the representative of vertical advection or convection [1].

Based on the before-mentioned points, the model equations in the Earth's Spherical Coordinates System with the sigma vertical coordinate can be rewritten. These equations include, the eastward motion equation, the northward motion equation, the thermal conductivity equation, the temperature equation, the specific volume equation, the salinity equation, and the equation related to the first and second laws of thermodynamics.

To complete the design of the model, additional equations are required. These equations, referred to as the completion equations, are as follows: the hydrostatic equation, the equation for calculating geopotential, the equation for calculating bottom pressure tendency, the equation for the representative vertical velocity ($\dot{\sigma}$), and the equation for calculating the radial distance of each point from the earth's center. It is essential that all equations were written in the Earth's Spherical Coordinates System with the sigma vertical coordinate.

When the wind blows over an oceanic medium, the wind momentum is transferred to the ocean' surface due to the friction between the atmosphere and ocean. As a result, the wind speed decreases, and ocean's surface currents are generated.

Surface stress approximately depends on wind speed in the form of a quadratic. This stress is the aerodynamic force per unit area that is exerted by the wind on the sea surface [13].

$$\boldsymbol{\tau}_s = c_d\, \rho_a\, (|\mathbb{v}_{\boldsymbol{a}}| - |\mathbb{v}_{\boldsymbol{s}}|)\, (\mathbb{v}_a - \mathbb{v}_s)\ \mathrm{Nm}^{-2} \qquad (6)$$

where $\boldsymbol{\tau}_s$ is the surface stress, c_d is aerodynamic drag coefficient known as the aerodynamic drag coefficient, ρ_a is the air density, $\mathbb{v}_{\boldsymbol{a}}$ is the wind speed at the 10-meter level above the sea surface, and $\mathbb{v}_{\boldsymbol{s}}$ is the oceanic current velocity at the surface.

According to Wu (1985), aerodynamic drag coefficient, which is dimensionless, is given by:

$$c_d = (0.8 + 0.065\, U_{10}) \times 10^{-3} \qquad (7)$$

where c_d stands for aerodynamic drag coefficient and U_{10} denotes the wind speed at a 10-meter height. For bottom stress, the formulation proposed by Nihoul (1977) has been used. [12]

$$\boldsymbol{\tau_b} = -m\, \boldsymbol{\tau_s} + C_D \rho_w\ |\mathbb{v}|\ \mathbb{v} \qquad (8)$$

Where $\boldsymbol{\tau_b}$ is the bottom stress, $m = 0.7$ is the dimensionless coefficient for surface stress, $\boldsymbol{\tau_s}$ is the surface stress, $C_D = 0.00211$ is the dimensionless drag coefficient for hydrodynamics, ρ_w is the water density, $|\mathbb{v}|$ is the magnitude of the integrated current, and $\mathbb{v}$ is the vector of the integrated current.

In general, the stress tensor in the Earth's Spherical Coordinates System with the sigma vertical coordinate is given as follows [1]:

$$\boldsymbol{\tau} = \begin{bmatrix} \tau_{\lambda\lambda} & \tau_{\lambda\phi} & \tau_{\lambda\sigma} \\ \tau_{\phi\lambda} & \tau_{\phi\phi} & \tau_{\phi\sigma} \\ \tau_{\sigma\lambda} & \tau_{\sigma\phi} & \tau_{\sigma\sigma} \end{bmatrix} \qquad (9)$$

In this context, each term represents the stress associated with velocity changes in different directions of the coordinate system [1].

As an example, $\tau_{\lambda\sigma}$ represents the stress associated with the changes of the vertical velocity indicator, $\dot{\sigma}$, in the longitudinal direction; $\tau_{\sigma\phi}$ represents the stress associated with the changes of the latitudinal velocity in the vertical direction and $\tau_{\sigma\sigma}$ represents the stress associated with the changes in the vertical velocity indicator, $\dot{\sigma}$, in σ direction.

The structure of a multilayer ocean model in Earth's Spherical Coordinates System with the sigma vertical coordinate is introduced as shown in Figure 2.

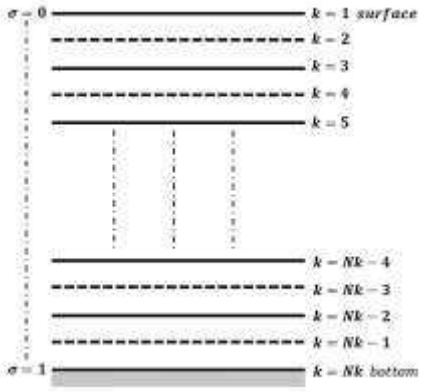

Figure 2- Vertical alignment scheme of a multilayer oceanic medium

Figure 2 shows the schematic of the vertical orientation of an n-layer (level: $Nk = 2n + 1$) oceanic medium. The counter of the levels is k.

a) Odd numbers of k correspond to the boundaries of the layers, while even numbers are assigned to the inter-layer regions.

b) $k = 1$ represents the first level or the ocean surface, which is indicated by $\sigma = 0$ in the vertical coordinate system.

c) $k = Nk$ represents the last level or the ocean floor, which is indicated by $\sigma = 1$ in the vertical coordinate system.

In this study, the Modified Arakawa C-grid [14] has been employed for gridding the oceanic medium.

To perform the initial steps for predicting the future state of the target medium, the model equations must be solved. In this study, a numerical method is used to solve the governing equations. Accordingly, the model equations are discretized based on an appropriate numerical method and scheme, and then a computer program has been developed in C# based on the discretized equations.

Geometric conditions, slope and elevation of the bed, and initial data can be entered into the calculations.
Determining an appropriate time step for the stability of the program is an important and notable aspect in any numerical modeling. Finite difference numerical method is used to solve and discretize the equations. For this purpose, the two-step Lax-Wendroff scheme is used for advection terms, the Dufort-Frankel scheme for diffusion terms, and the remaining derivatives are discretized using the central difference method. Furthermore, the Matsuno scheme [15] is used to mitigate the instability caused by certain computations in the program.
The Dufort-Frankel scheme is an explicit scheme and is always stable, while the stability condition for the Lax-Wendroff two-step scheme needs the C.F.L (*Courant, Friedrichs and Lewy stability condition*) condition [16], defines the stability condition differently for the Cartesian Coordinate System, which in the Earth's Spherical Coordinates System with a sigma vertical coordinate becomes:

$$\Delta t \leq min\left(\frac{r\,cos\,\phi\;\Delta\lambda}{u}, \frac{r\,\Delta\phi}{v}, \frac{\Delta\sigma}{\dot{\sigma}}\right) \qquad (10)$$

The initial execution begins with motion starting from rest. In this regard, assuming no forces are present, the local changes in the potentials whose gradients induce motion must be zero.
Regarding the boundary conditions, since water cannot pass through the surface and the bottom [3] closed boundaries are considered as rigid and no-slip condition is applied in this study. Therefore, the tangential and vertical velocity components at the boundaries are equal to zero, i.e.:

$$\mathbb{v}(\lambda, \phi, \sigma, t).\mathbf{n} = 0 \text{ and } \mathbb{v}(\lambda, \phi, \sigma, t).\mathbf{t} = 0 \qquad (11)$$

In the above equation, $\boldsymbol{t}$ and $\boldsymbol{n}$ are the unit vectors tangential and normal to the rigid boundary, respectively. Since no flow passes through the bottom of the medium, it follows that:

$$\sigma = 1 \quad \Rightarrow \quad u = v = \dot{\sigma} = 0 \qquad (12)$$

The dynamic boundary condition for the open boundary is considered as follows:

$$\frac{\partial p}{\partial \lambda} = \frac{\partial p}{\partial \phi} = \frac{\partial \Phi}{\partial \lambda} = \frac{\partial \Phi}{\partial \phi} = \frac{\partial p_b}{\partial \lambda} = \frac{\partial p_b}{\partial \phi} = 0 \qquad (13)$$

And kinematic boundary condition imposes:

$$u = \acute{u}, v = \acute{v}, \dot{\sigma} = \acute{\dot{\sigma}}, \rho = \acute{\rho}, \eta = \acute{\eta}, T = \acute{T}, s = \acute{s} \qquad (14)$$

And:

$$\left(\frac{D\,...}{Dt}\right)_{(\sigma=0)} = \left(\frac{D\,...}{Dt}\right)_{(\sigma=1)} = 0 \qquad (15)$$

where in (14) parameters without prime are belong to original oceanic medium and parameters with prime are out of original oceanic medium after open boundary
One of the assumptions used in the development of the Basic Oceanic Model is neglecting the term $-\vec{\Omega} \times (\vec{\Omega} \times \vec{r})$ in comparison to the other terms of the equation of motion in the Earth's Spherical Coordinates System with a sigma vertical coordinate.
Applying specific conditions to the program and comparing its outputs with theoretical physical principles can also serve as an appropriate validation for the designed model. Calibration during the model execution for experimental basins identifies the model's weaknesses and leads to its improvement.
For model's implementation in laboratorial oceanic basins (even real medium), hypothetical (and approximate real) data are used as input to the program. The tidal force is considered as a sinusoidal function with a hypothetical amplitude. However, tidal force have been made to incorporate water level variations in the Strait of Hormuz (which is the open boundary of the real medium). The water level variations in the Strait of Hormuz have been extracted from the hydrography information database of the National Cartographic Center of Iran [17].

3. Results and Discussion

Up to this point, the design process of the fundamental oceanic numerical model, PersianGulfOceanicModel (ZSF974), has been explained. The following sections present the results of the model's implementation in laboratorial oceanic basins, along with the validation aspects of these models. Finally, necessary strategies for improving the model and achieving an efficient version for real oceanic applications are provided.
The model design requirements necessitate the replication of fundamental experiments previously conducted by other researchers for model evaluation and validation, using the laboratory models of this study. The response of the present model to experimental conditions already tested by earlier researchers has also been examined, however, due to the repetitive nature and abundance of these tests, their details have not been included in this paper. ([8], [18], [19], [20].
The immobility test is the first test conducted after each modification to the model or its execution for a new medium. In this study, the duration of model execution to achieve confirmation of the immobility test at each stage was at least ten years.
Another test examines the effect of removing the Coriolis force and earth's curvature. In this scenario, if a constant force is applied in a specific direction (such as uniform wind flow), the model's output, in the absence of the Coriolis force and earth's curvature, would result in a uniform current aligned with the applied force.

After the model's performance in these two tests yielded positive results, subsequent stages and additional tests, including the effects of wind in different directions, tidal effects, river inflow effects, and density gradient, were examined and analyzed to finalize the developed model. Instead, this chapter presents the results of other laboratorial models that were examined due to the more complex conditions of real mediums and the presence of multiple influencing forces in the actual oceanic system.

The theoretical mediums presented in this study are defined within the longitudinal range of 48.25 °E to 56.75 °E and the latitudinal range of 24.25 °N to 30.25 °N, with a resolution of 0.25 degree in both directions. All laboratorial mediums in this study are configured with 10 layers, and the time step is set to 100 seconds according to C. F. L. stability condition.

3.1. Results of the simulation of the effect of density gradient in a closed laboratorial medium with a concave bottom.

This type of bottom is used to examine the model's response to oceanic basins with a density gradient, as well as the effect of a non-level bottom with a specific and defined curvature (Figure 3).

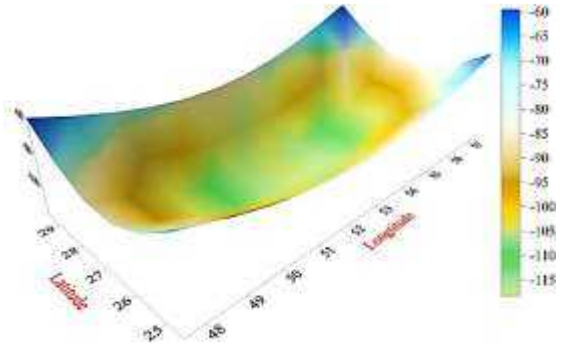

Figure 3- A scheme of the figure and the bottom of the laboratorial medium under study

The maximum depth of this medium is 99.93 m, and the minimum depth is 55.57 m. The surface salinity is 40 psu, with a salinity increased by 0.25 psu per level. The surface temperature is 25 ℃, and the temperature decreased by 0.25 ℃ per level.

Therefore, the studied medium exhibits density gradient across various layers, and in the absence of other forces, it can motivate. This movement is caused by the horizontal gradient in the layers.

When the medium is released from rest, an initial flow toward the center develops. Over time, these vectors rotate to the right, forming a counterclockwise circulation (Figure 4). Similarly, a flow develops in all layers, including the bottom layer.

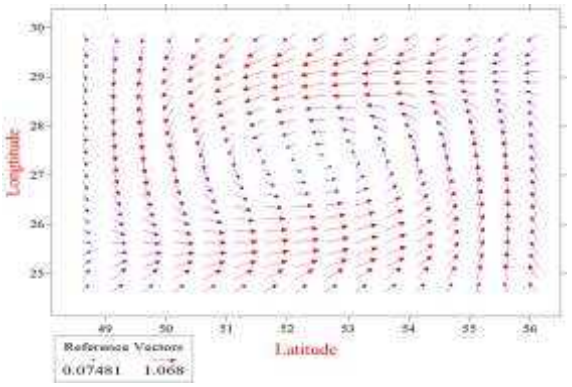

Figure 4- Flow field at the mid-level of the first layer at the end of the fifth day of model execution

The rotation of the current vector is caused by the earth's rotation and the Coriolis force. [21]

According to initial condition, the mid-level of the first layer had a salinity of 40.25 psu and a temperature of 24.75°C. The model results indicate the intrusion of salinity from lower levels into this layer and the diffusion of temperature from this layer to the lower levels (Figure 5 and Figure 6). On the third day of running model, the variations of these parameters reach to semi-steady state (stabilization of currents and water level) and become evident in the model results, continuing until the entire medium reaches uniform temperature and salinity.

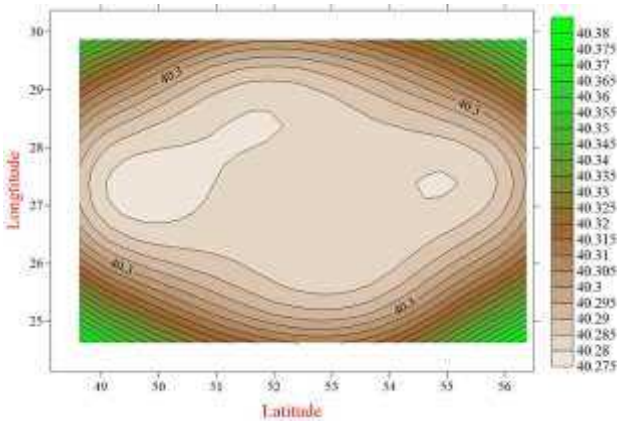

Figure 5- Salinity field at the mid-level of the first layer at the end of fifth day of running the model

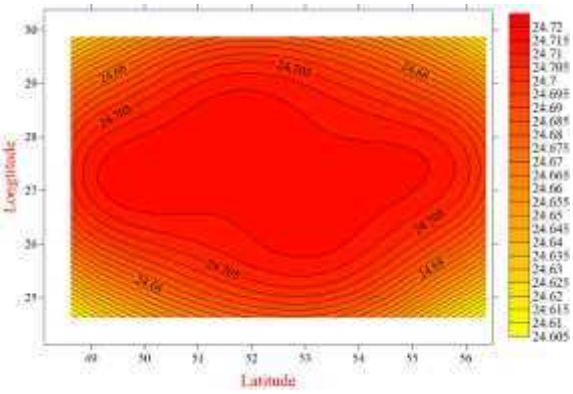

Figure 6- Temperature field at the mid-level of the first layer end of fifth day of running the model

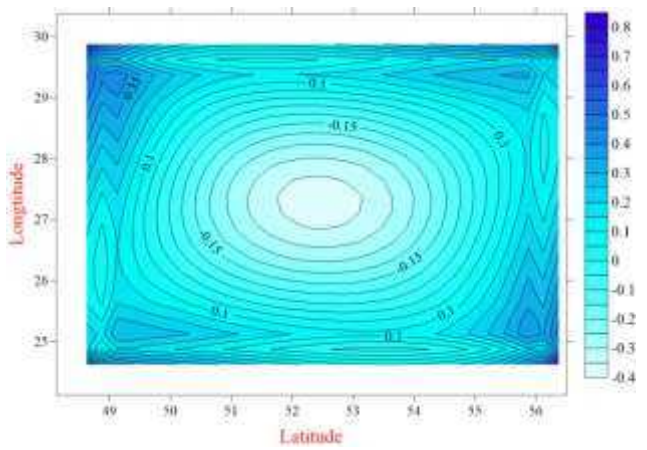

Figure 7- Departure from static equilibrium field at the mid-level of the first layer at the end of fifth day for running the model

The formation of flow in the direction of the density gradient and the counterclockwise rotation of the current vector under the influence of the Coriolis force, as well as the distribution of salinity and temperature, are in accordance with expectations and the principles of ocean physics.

3.2. Tide Simulation Results in a Laboratorial medium with a Level Bottom

As the simplest laboratorial oceanic basin with open boundary, a rectangular cuboid medium with a level bottom and a constant depth of 98 meters, where the eastern boundary is completely open, has been considered.

In this experiment, salinity and temperature are uniform throughout the entire oceanic medium, set at 40 psu and 25 ℃, respectively. Tides are imposed as sea level variations at the open eastern boundary [17].

The model was run for 10 days to examine the response of the medium to tidal forces. The results of the isopleth analysis of the departure from static equilibrium indicate (Figure 8 and Figure 9) that the changes in water level at the eastern open boundary create a current parallel to the coast, which starts moving from the northern boundary of the oceanic domain, resulting in a counterclockwise rotation within the medium. If an observer stands in the direction of the current, the highest water level will be observed on the observer's right-hand side. [21]

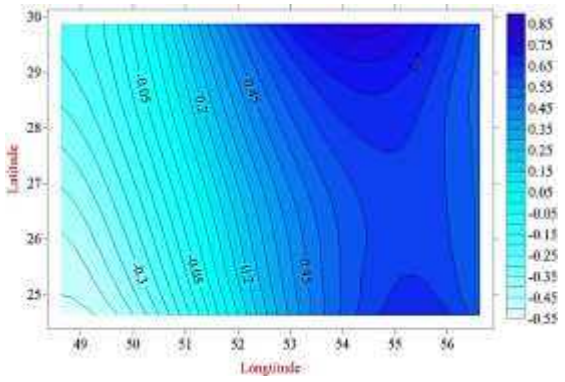

Figure 8- Contour Lines of departure from static equilibrium – mid-level of the first layer- hour zero of the tenth day

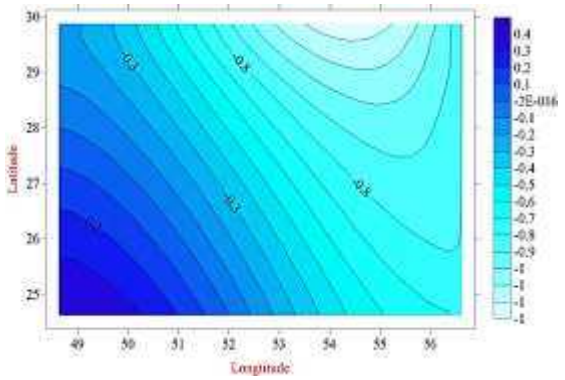

Figure 9- Contour Lines of departure from static equilibrium – mid-level of the first layer- at 12:00 of the tenth day

The presence of amphidromic points is also evident in these figures. The maximum total variation in water elevation relative to static equilibrium in this simulation was approximately 4.8m.

In the analysis of the current fields, a maximum current of $1.33 m/s$ was obtained, which occurred at the open boundary (Figure 10 and Figure 11). The current vectors near the boundaries are parallel to the boundary [21]. Based on contour lines showing the departure from static equilibrium (Figure 8 and Figure 9), if an observer stands in the direction of the flow, the maximum water height will be located to their right and with good accuracy, it can be concluded that the component of the flow normal to the boundary is zero. Therefore, a Kelvin wave could be present in the region.

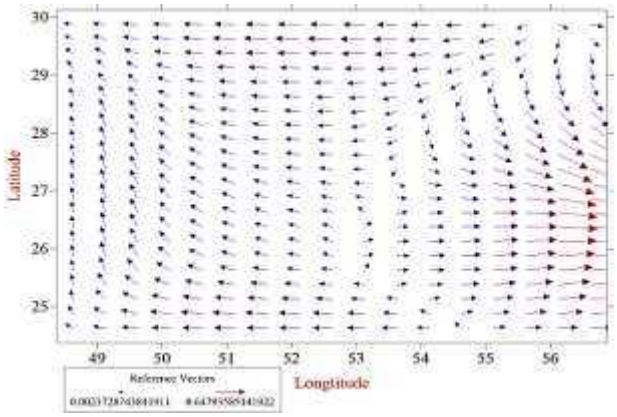

Figure 10- Current field at the mid-layer level, first layer - zero hour of the tenth day

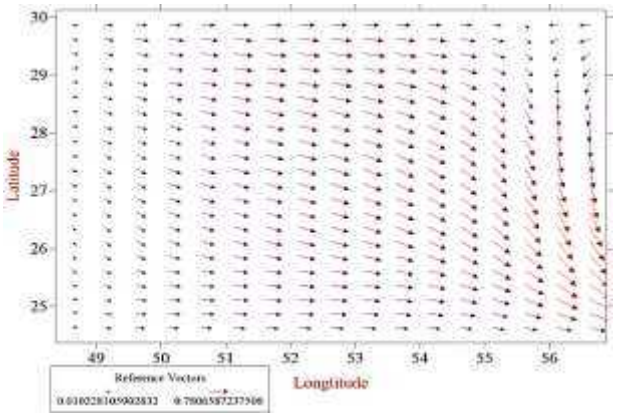

Figure 11- Current field at the mid-layer level, first layer - at 12:00 of the tenth day

3.3. Simulation's results of the effect of wind and density gradient for the laboratorial medium with a level bottom and the Persian Gulf

This closed laboratorial model has a flat bottom, but the shape of the oceanic basin and its boundaries correspond to the Persian Gulf and are used to examine the curvature of the boundaries.

The depth of this oceanic medium is constant at 98 meters. The surface salinity is 40 psu, with an increase of 0.25 psu per level. The surface temperature is 25 ℃, with a decrease of 0.25 ℃ per every level.

Due to the flat seabed, an environmentally uniform increase in salinity and decrease in temperature with depth has been established. This means that the existing density gradient between the layers does not induce motion, and in the absence of other forces, changes in salinity and temperature will occur due to molecular diffusion. Under such conditions, a westerly wind of 10m/s was applied over the medium. At the fourth day, the effects of steady state formation in the current field and departure from static equilibrium were observed. The results of the tenth day of model execution are as follows:

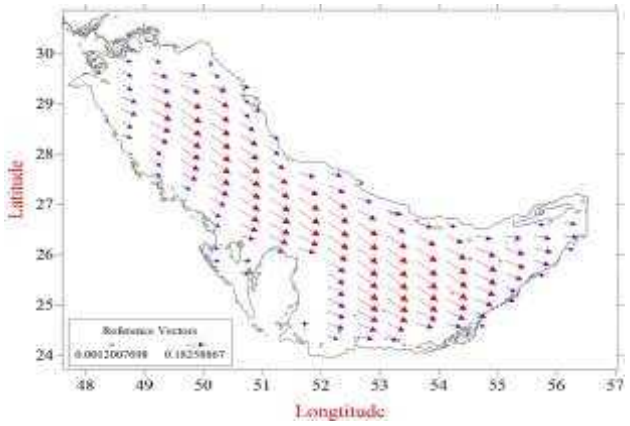

Figure 12- Current field at the mid-level of the first layer

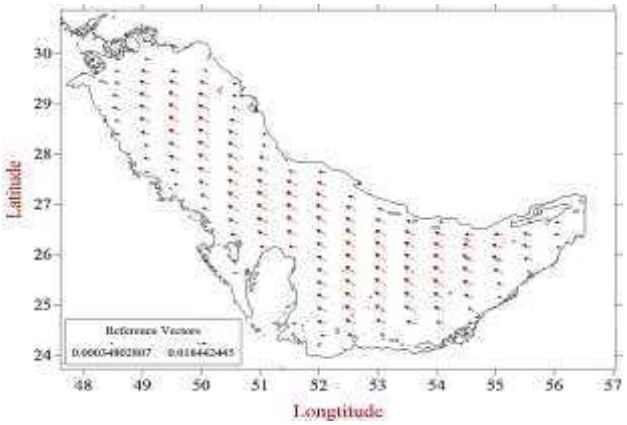

Figure 13- Current field at the mid-level of the tenth layer

It is observed that a current has formed at the surface, with its vector deflected approximately 45 degrees to the right of the downwind direction. This phenomenon occurs under the influence of the Coriolis force [21], and according to Ekman theory, the current vector will rotate with depth, eventually reversing direction at a certain depth, where it will oppose the surface current direction [21]. This result has been observed in this study (Figure 12 and Figure 13). Additionally, the water level is higher at downwind side. The diffusion of salinity and temperature in this experiment follows the principles of ocean physics (Figure 14 to Figure 16), such that water with lower salinity and higher temperature exists in the downstream (east of the laboratorial oceanic medium). However, prolonged wind action could eventually homogenize the medium in terms of both temperature and salinity.

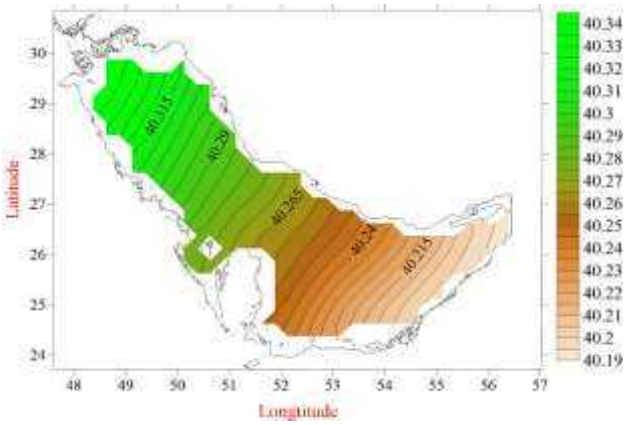

Figure 14- Salinity field at the mid-level of the first layer

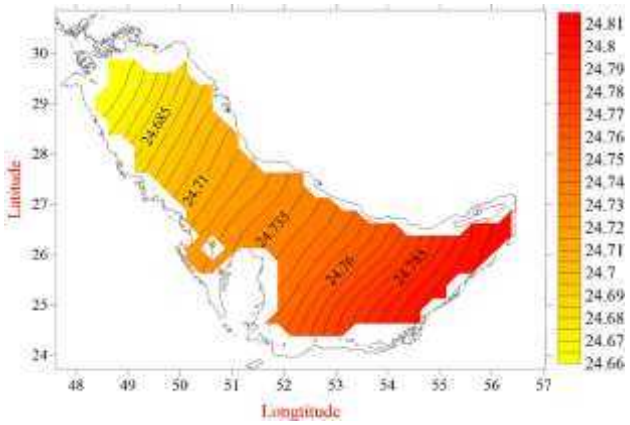

Figure 15- Temperature field at the mid-level of the first layer

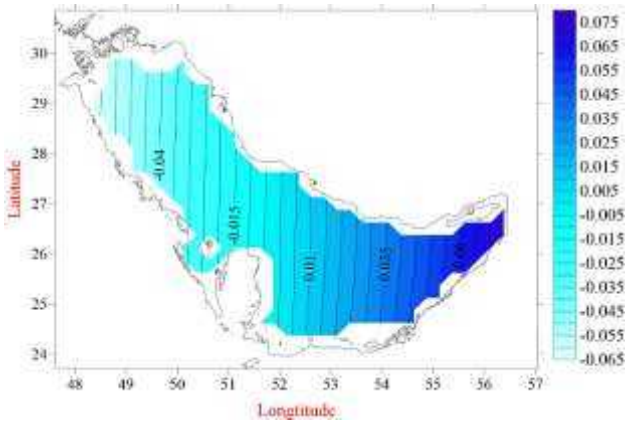

Figure 16- Field of departure from static equilibrium at the mid-level of the first layer

3.4. The results of the simulation of the effect of density difference, tide, river, and wind in a laboratorial medium with a non-level bottom

This theoretical basin is designed to resemble the oceanic medium of the Persian Gulf. Although the bottom slope and environmental conditions of the Hormuz Strait (Eastern open boundary) do not match the bottom slope or the strait of this condition (Eastern open boundary**),** However, general physical and geographical characteristics of the real medium have been assigned to it. Therefore, executing the model in this medium will yield valuable results.

In this experiment, the medium shown in Figure 17 is considered. The maximum depth of this oceanic medium is 97.94 m, and the minimum depth is 56.78 m. At longitude 56.875°E, the oceanic boundary is open from 27.625°N to 28.625°N. The surface salinity is 40 psu, increasing by 0.25 psu at each level. The surface temperature is 25°C, decreasing by 0.25°C at each level downward.

Two rivers, A and M, are assumed to be located at two points in the medium. The impact point of River A is at 29.875°N , 48.625°E (similar to the Arvand-rood River), and the impact point of River M is at 29.125°N, 51.125°E (similar to the Mond River).

The flow velocity at the estuary of River A is assumed to be 0.6 m/s, with a surface temperature of 19.5 °C, bottom temperature of 24 °C, surface salinity of 25 psu, and bottom salinity of 27 psu. Also, the flow velocity at the estuary of River M is assumed to be 0.5654 m/s, with a surface temperature of 19.44 °C, bottom temperature of 25 °C, surface salinity of 22.21 psu, and bottom salinity of 31.35 psu.

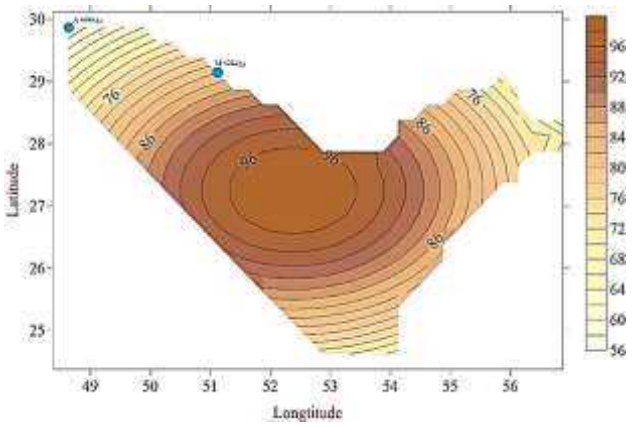

Figure 17- Schematic figure of the medium and the bottom of the laboratorial medium under study

The results of the ten-day model execution are presented in this section. The rivers were activated from the beginning of the model run. From the start of the second day, a westerly wind of 10 m/s was blown over the medium. Beginning on the third day, tides were also added to the forces acting on the system [17]. The current fields at zero and 6 o'clock on the tenth day are as follows:

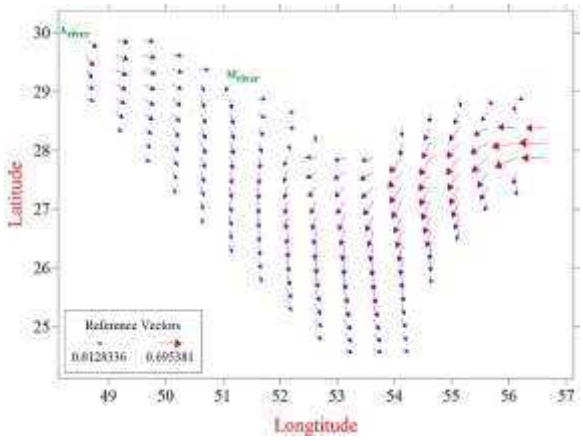

Figure 18- Current Field at the Mid-Level of the First Layer – Day 10, Hour 0

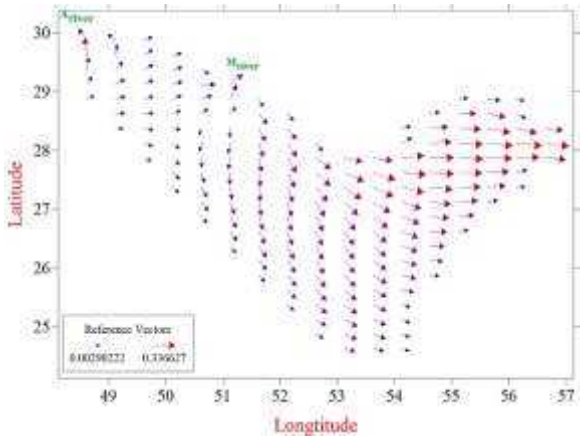

Figure 19- Current Field at the Mid-Level of the First Layer – Day 10, Hour 6

Investigating current fields show that in overall; the effect of tides is dominant. At hours (6:00, 15:00, 18:00), the tidal effect causes ocean water to flow into the M river. During these hours, high tide occurs in that region. At other hours (zero, 12:00 and 24:00), river water is entering the oceanic medium, and at this time, a low tide should have occurred in this area, and this can be better understood from the review of departure from static equilibrium fields. Tide data were taken from Hydrographic Management of National Cartographic Center of the Islamic Republic of Iran, 1983 [17] (Figure 20 to Figure 22).

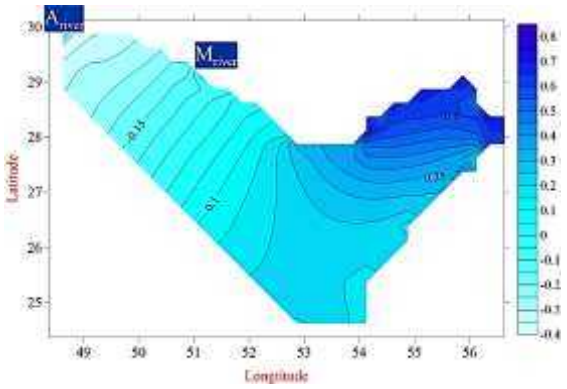

Figure 20- - Contours of departure from static equilibrium in the mid-layer of the first level – Day 10, Hour 0

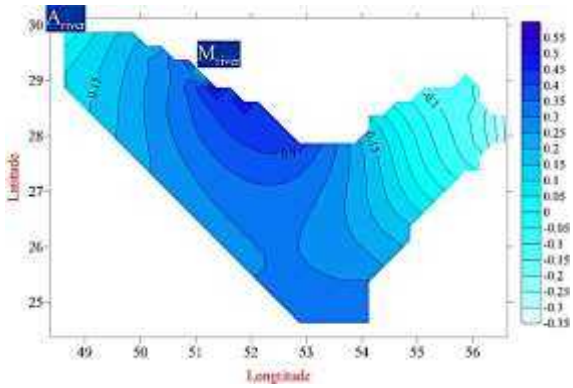

Figure 21 - Contours of departure from static equilibrium in the mid-layer of the first level – Day 10, Hour 3

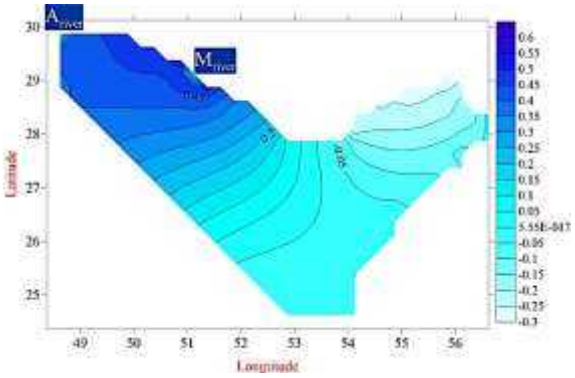

Figure 22- Contours of departure from static equilibrium in the mid-layer of the first level – Day 10, Hour 6

The maximum current speed over these ten days was 1.4 m/s, and the maximum total water level variation relative to static equilibrium during this period was 2.88 meters. An important conclusion is that the tidal current in the northwest of this oceanic medium is always weaker than in the central or eastern parts of the region. Changes in water level at the eastern open boundary generate a coastal-parallel current that originates from the northern boundary of the oceanic domain and induces a counterclockwise circulation within the medium. In that region, if an observer stands in the direction of the current, the highest water level is observed on the observer's right-hand side [21]. Consequently, the component of the current perpendicular to the boundary is effectively zero [21]. These indicators strongly suggest the existence of a Kelvin wave in this region.

The analysis of current fields in this experiment (Figure 18 and Figure 19) indicates that water flows into or out of the basin across the entire strait. This result is consistent with the findings of Hesari et al. (2006) [21] and Zamanian et al. (2022) [23]. It also demonstrates that River A can influence the direction of the circulation.

5. Conclusions

The results of analyzing the departure from static equilibrium in Experiment 3.2 and Experiment 3.4 indicate that tidal circulation in the water basin occurs on a semi-diurnal basis. Furthermore, the model results in Experiment 3.4 show the dominance of the tidal effect over the effects of wind, density gradient, and river input in driving the water circulation in this medium. In other word, tide can strongly influence in this kind of water basin as a body force.

Additionally, the inflow from the open boundary generates a coastal current along the northern boundary, leading to a counterclockwise circulation in the basin. The presence of an amphidromic point is also evident in the results.

These results have also been obtained in experiences implementing this model in other mediums [22].

An attempt has been made to consider laboratorial mediums similar to the geographical and physical

conditions of the Persian Gulf. It is expected that the results of the model implementation can generally show the interaction of this marine medium under the influence of environmental factors. Chao et al. (1992) [24], Reynolds (1993) [23] and Apel (1999) [21] reached similar conclusions regarding the oceanic medium of the Persian Gulf in their studies.

Moreover, the model results are consistent with the principles of ocean physics. This part of the study demonstrates that, even in its simplest configuration, the oceanic numerical model is capable of predicting the physical behavior of coastal and offshore waters. Therefore, it can serve as a suitable foundation for studying the hydrodynamics of coastal and oceanic waters, including the oceanic medium of the Persian Gulf. It is essential that real environmental conditions can be incorporated into the model. Considering the findings of fundamental studies in this field (e.g. [21], [23], [24]) would be highly beneficial. In this way, the groundwork for model improvement is laid. Nevertheless, enhancing the model for full compatibility with the behavior of a real oceanic medium requires further research aimed at determining the momentum, salinity, and temperature diffusion coefficients in oceanic domains.

Acknowledgment (Optional): To conduct this research, the facilities of the National Institute of Oceanography, especially the library of this research institute, were used. I consider it my duty to thank and appreciate the cooperation of the authorities, especially the esteemed director and the esteemed vice president for research of the National Institute of Oceanography.

8. References

1-Zamanian, M. T. (2006), *Project of base oceanic model two layered*, Research Institute of Methodology and Atmosphere Science, Tehran, Iran. [In Persian]

2-Khaleghi Zavare, H., (1992), *Development and application of a non-linear barotropic model for the wind and tide, driven circulation in the Persian Gulf* (Doctoral dissertation, University of the Philippines)

3-Zamanian, M., T., (1994), *Three Dimensional Models for Persian Gulf*, (Doctoral dissertation, University of the Philippines)

4-James, I. D., (1998), *Experiments with a numerical model of coastal currents and tidal mixing fronts*, Continental Shelf Research, Volume 8, Issue 12, Pages 1275-1297.

5-Kämpf, J. & Sadrinasab, M., (2006), *The circulation of the Persian Gulf: a numerical study*, Ocean Science, European Geosciences Union, 2006, 2 (1), pp.27-41, DOI: 10.5194/osd-2-129-2005

6-.Ibrayev, R. A., Özsoy, E., Schrum, C., & Sur, H. İ., (2010), *Seasonal variability of the Caspian Sea three-dimensional circulation, sea level and air-sea interaction*, Ocean Science, Vol. 6, p. 311–329, https://doi.org/10.5194/os-6-311-2010

7-Mehrfar, H., Azad, M. T., Lari, K., & Bidokhti, A. A. A. A. (2020). *A numerical simulation case study of the coastal currents and upwelling in the western Persian Gulf*, Journal of Ocean Engineering and Science, 5(4), 323-332, https://doi.org/10.1016/j.joes.2019.12.005

8-Nesheli Z., H., Zamanian, M., T., & Sadrinasab, M., (2018), *Desigen of Oceanic Model for Caspian Sea*, PHD Thesis, Department of physical oceanography, Faculty of Marine Science and Oceanography, Khorramshahr University of Marine Science and Technology, Iran. 194p. [In Persian]

9-Wu, J., (1982), *Wind-stress coefficients over sea surface from breeze to hurricane*, J. Geophys. Res., 87(C12), 9704–9706, doi:10.1029/JC087iC12p09704.

10-Deldar, H., (2024), *Numerical simulation of lee waves in the Strait of Hormuz using Delft3D model*, Journal of the Earth and Space Physics, 50(2), 451-463. http//doi.org/10.22059/jesphys.2024.363402.1007548, [In Persian]

11-Fallahi M., Zamanian M.T. and Sadrinasab M. 2019. *Design of Five Layers Oceanic Numerical Model for Persian Gulf*. PHD Thesis. Department of physical oceanography, Faculty of Marine Science and Oceanography, Khorramshahr University of Marine Science and Technology, Iran. 183p. [In Persian]

12-Nihoul, J., C., J., (1977), *Three-dimensional model of tides and storm surges in a shallow well-mixed continental sea*, Dynamics Atmosphere Ocean, 2, 29-47.

13-Thorpe, S., A., (2009), *Elements of Physical Oceanography*, Boston, Elsevier, 647 pp.

14-Estoque, M., A., (1963), *A numerical model of the atmospheric boundary layer*, Journal of Geophysical Research, 68(4), 1103-1113, https://doi.org/10.1029/JZ068i004p01103

15-Haltiner, G.J. & Williams, R.T., (1980), Numerical prediction and dynamic meteorology (2nd edition), John Wiley & sons, pp. 496, ISBN-10: 0471059714

16-Kämpf, J., (2009), Advanced Ocean Modelling, Flinders University, School of the Medium, PO Box 2100 Adelaide SA 5001, Australia, 193p.

17-Hydrographic Management of National Cartographic Center of the Islamic Republic of Iran, 1983, Access in: http://iranhydrography.ncc.org.ir/homepage.aspx?site=iranhydrography.ncc.org&tabid=6144&lang=fa-IR, Access Date: August 2018

18-Farjami, H., Zamanian, M., Hesari A., R., E., & Azarmsa, S.A., (2012), Numerical Simulation of Ekman Theory in Five Layers Oceanic Basin, Journal of Marine Science and Technology, 11(1): 41-48. [In Persian]

19-Farjami H. & Zamanian M.T., (2006), *Numerical simulation of wind-driven currents in a hypothetical five-layer ocean basin*, MSc Thesis, Department of Marin Physics, Natural Resources & Marine Sciences, Tarbiat Modares University, Tehran, Iran, p108 [In Persian]

20-Hesari A., R., E., & Zamanian M.T., (2006), *Simulation of currents due to drag and density differences in a hypothetical two-layer basin*, MSc Thesis, Department of Marin Physics, Natural Resources & Marine Sciences, Tarbiat Modares University, Tehran, Iran, [In Persian]

21-Apel, J. R., (1999), Principles of Ocean Physics, San Diego, Academic Press, 634 pp.

22-Zamanian M.T, Sadrinasab M. & Fallahi, M., (2022), Designing a Numerical Model to Study the Effect of Tide and Wind in a Theoretical Basin in Similarity to Persian Gulf, Journal of Marine Science and Technology, 27-38, 21(1), doi:10.22113/jmst.2019.149922.2203, [In Persian]

23-Reynolds, R.M., (1993) *Physical Oceanography of the Gulf, Strait of Hormuz, and the Gulf of Oman—Results from the Mt Mitchell Expedition*, Marine Pollution Bulletin, 27, 35-59, https://www.researchgate.net/publication/223884087 & https://doi.org/10.1016/0025-326X(93)90007-7,

24-Chao, S., Y., Kao, T., W., & Al-Hajri, K., R., (1992*), A numerical investigation of circulation in the Arabian Gulf*, J. Geophysics. Res., 97(C7), 11219–11236, doi:10.1029/92JC00841.

INTERNATIONAL JOURNAL OF
COASTAL, OFFSHORE & ENVIRONMENTAL ENGINEERING IJCOE Vol.10 /No.3 / Summer 2025 (30-43)

Available online at: www. Ijcoe.org

Coupled SWAN-ROMS Numerical Modeling of Nearshore Hydrodynamics and Rip Current Formation Along the Southern Caspian Sea

Mahmood Reza Akbarpour Jannat

Iranian National Institute for Oceanography and Atmospheric Science, No.3, Etemad Zadeh St., Fatemi Ave, P.C: 1411813389, Tehran, Iran, E-mail: akbarpour@inio.ac.ir

ARTICLE INFO

Article History:
Received: ١٥ APR 2025
Accepted: 04 NOV 2025

Keywords:
Rip currents
Caspian Sea
SWAN-ROMS model
Wave-induced currents
Coastal hazards

ABSTRACT

Understanding and modeling coastal currents are crucial for assessing coastal hazards, mitigating human risks, and minimizing structural damage. The southern Caspian Sea, with its diverse geomorphology, variable climatic conditions, and dynamic coastal processes, serves as a key region for the development of various coastal currents. Statistical analyses of drowning incidents in coastal cities indicate that nearshore currents, particularly rip currents, are among the primary contributors to coastal hazards. These currents, which include longshore currents, rip currents, and undertow, are primarily generated by wave breaking in shallow coastal zones. This study aims to identify high-risk coastal areas where specific wave conditions contribute to the formation of strong rip currents, posing significant threats to swimmers and coastal safety. To achieve this, a coupled numerical modeling framework integrating the SWAN (Simulating WAves Nearshore) and ROMS (Regional Ocean Modeling System) models was employed to simulate nearshore current dynamics in four key coastal regions: Nowshahr, Chaboksar, Anzali, and Talesh, located along the southern Caspian Sea. Wind field data were obtained from the ERA5 reanalysis dataset, while boundary conditions were derived from SWAN simulations performed on a mesoscale grid covering the entire Caspian Sea. The results indicate that under prevailing hydrodynamic conditions, longshore currents dominate across all study sites, with rip currents forming in specific localized areas. The orientation of longshore currents is primarily controlled by wind-driven wave propagation patterns, exhibiting an eastward direction in Nowshahr and Chaboksar, while flowing westward in Anzali and Gisum Forest coastal zones. Furthermore, the spatial variability in coastal bathymetry, both alongshore and cross-shore, significantly influences the extent and intensity of these currents, as observed through drifter trajectories. The maximum recorded current velocities range between 0.7 and 1.1 m/s, highlighting the potential hazard posed by these currents in nearshore environments. These findings provide a scientific basis for improving coastal safety measures, informing hazard mitigation strategies, and enhancing numerical modeling frameworks for rip current prediction in the Caspian Sea region.

1. Introduction

The study of hydrodynamic processes along the southern Caspian Sea coastline has long been of scientific and practical significance due to its direct implications for coastal erosion, sediment transport, navigation safety, and the sustainability of coastal ecosystems. In particular, wave-driven nearshore

circulation plays a fundamental role in shaping shoreline morphology and influencing the occurrence of hazardous currents, such as rip currents, which pose substantial risks to swimmers and coastal infrastructure. Despite its critical importance, research on nearshore hydrodynamics in the Caspian Sea remains relatively underdeveloped compared to other enclosed or semi-enclosed basins, such as the Black Sea or the Mediterranean.

For many years, hydrodynamic investigations in the region have predominantly focused on port environments and harbor hydrodynamics, with limited emphasis on open-coast nearshore processes. The Integrated Study of Iranian Seas and Waves (ISWM) (PMO, 2009) provided an extensive analysis of wave conditions in the Caspian Sea, but it largely neglected nearshore current dynamics. In general, past studies have either been regionally constrained or have focused primarily on large-scale circulation and wave characteristics, rather than on the finer-scale nearshore current systems that govern sediment transport and hydrodynamic hazards.

Recent years have seen a growing interest in nearshore hydrodynamics, with several field monitoring campaigns and numerical modeling efforts conducted by research institutions and governmental agencies. Among these, the rip current investigations along the southern Caspian Sea coastline (Akbarpour Jannat et al., 2012, Akbarpour Jannat et al., 2014, Lahijani, H.A.K., 2006, Terziev at al. 2005, Lahijani, H.A.K., 2006, Noraniyan Isfahani, M., 2017, Noraniyan Isfahani, M., 2018) and the Coastal Monitoring Program for the northern shores of Iran (PMO, 2015) have contributed valuable observational data. However, while these studies have provided important insights into nearshore circulation, they remain limited in spatial and temporal coverage and have not fully incorporated high-resolution numerical models capable of capturing the complex interactions between waves and currents.

A notable effort in this direction was the study by Akbarpour Jannat et al., 2012, which represented the first attempt to deploy coastal drifters for rip current tracking in the region. Their work, which combined in situ measurements of current velocity profiles, wave characteristics, and seabed topography with Boussinesq-based numerical modeling (BOSS2D), successfully identified multiple rip current channels extending offshore to depths of approximately 5 meters. However, the reliance on Boussinesq models, while accurate for nearshore wave-current interactions, posed computational challenges, limiting their feasibility for large-scale applications.

Similarly, Akbarpour Jannat et al, 2014 applied a coupled ROMS-SWAN model to investigate nearshore circulation along the southwestern Caspian coastline, incorporating wave spectra derived from ECMWF ERA-Interim wind forcing. Their nested grid simulations provided high-resolution insights into the structure of nearshore currents, confirming the presence of eastward-directed flows and rip current cells along the Kiashahr–Bandar Anzali coastal stretch. These findings were consistent with observational datasets from the Northern Iran Coastal Monitoring Program (PMO, 2015), reinforcing the role of wind-driven circulation in shaping the hydrodynamics of the region.

Beyond numerical modeling efforts, field-based monitoring programs have further contributed to our understanding of nearshore hydrodynamics. A series of observational campaigns along the Nowshahr, Roudsar, Anzali, and Astara coastlines involved current velocity measurements at multiple depths (5 m, 10 m, and 15 m), which were subsequently used to validate numerical models. Comparative analyses between measured current patterns, wind climatology, and numerical simulations confirmed a strong correlation between coastal wind forcing and nearshore circulation dynamics. The prevailing westerly winds were identified as the dominant driver of eastward coastal currents, while statistical assessments indicated that nearshore currents exhibited velocities below 0.1 m/s in 50% of cases, with longshore currents rarely exceeding 0.5 m/s.

Despite these advancements, significant knowledge gaps remain in the understanding of wave-current interactions, particularly in rip current generation, alongshore current variability, and nearshore sediment transport processes. Given the localized nature of rip currents and their dependence on fine-scale bathymetric features, achieving a higher-resolution numerical representation necessitates the use of nested and structured grid systems. However, while unstructured grid models offer enhanced resolution, their computational cost remains prohibitive, limiting their applicability for long-term simulations. To overcome these challenges, this study employs a nested structured grid system, providing an optimized balance between computational efficiency and spatial resolution, representing a novel application for the region.

This study aims to advance the understanding of nearshore hydrodynamics in the southern Caspian Sea by utilizing a coupled SWAN-ROMS modeling framework to simulate nearshore circulation under various wave forcing conditions. By focusing on key transition zones along the Nowshahr, Chaboksar, Anzali, and Talesh coastlines, this research provides a comprehensive assessment of short-term hydrodynamic variations, emphasizing the spatial and temporal evolution of wave-driven currents, rip current formation, and coastal circulation patterns.

The remainder of this paper is structured as follows: Section 2 provides a detailed description of the numerical modeling approach, including grid

configurations, boundary conditions, and external forcing mechanisms. Section 3 presents a comparative analysis of the modeled nearshore circulation with observational drifter buoy data, offering validation and insight into model performance. Section 4 discusses the key hydrodynamic processes governing model outputs and field observations, with a focus on wave-driven coastal dynamics and their implications for nearshore circulation patterns. Finally, Section 5 synthesizes the key findings of this study and outlines recommendations for future research, emphasizing the need for improved coastal hazard mitigation strategies, refinements in numerical modeling techniques, and the development of an observational network for continuous monitoring. This research provides critical insights into the spatial variability of wave-induced currents, highlighting their dependence on coastal morphology, bathymetry, and wind forcing. The findings contribute to improved hazard assessment, coastal risk management, and numerical modeling accuracy, offering a foundation for future studies in the Caspian Sea and other semi-enclosed basins.

2. Numerical Model Configuration

2.1 Computational Grid

Accurate numerical modeling of nearshore hydrodynamics requires a well-defined computational grid that captures the complex interactions between wave forcing, coastal topography, and hydrodynamic circulation. Given the socioeconomic and environmental significance of the southern Caspian Sea coastline, four key study sites were selected to ensure comprehensive spatial coverage and to represent diverse hydrodynamic conditions. These sites include Nowshahr (Hosseini Beach), Chaboksar (Serolat), Anzali (Eastern Shores), and Talesh (Gisoom), each of which experiences distinct nearshore processes, including wave-driven currents, rip currents, and alongshore transport dynamics.

The computational grid system was developed using high-resolution terrain and bathymetric datasets to ensure accurate representation of both land topography and underwater morphology. Land elevation data were obtained from the 30-meter resolution Shuttle Radar Topography Mission (SRTM) dataset, while bathymetric data were sourced from the half-degree resolution General Bathymetric Chart of the Oceans (GEBCO). To improve the accuracy of nearshore depth variations, these datasets were further refined using local hydrographic surveys, ensuring precise bathymetric representation within the wave-breaking and sediment transport zones.

A multi-scale nested grid approach was implemented to achieve an optimal balance between computational efficiency and spatial resolution. To accurately capture the hydrodynamic processes across different spatial scales, two primary grid systems were developed. The first is a large-scale computational grid covering the entire Caspian Sea, which serves as the offshore boundary condition provider for localized simulations. This ensures that energy transfer from deep water to nearshore regions is accurately represented, maintaining physical consistency between different spatial domains. The second consists of high-resolution nested grids tailored for each study site, specifically designed to resolve small-scale nearshore circulation features such as rip currents, wave-induced setup, and alongshore drift. These localized grids enable precise modeling of wave-driven current dynamics and enhance the accuracy of nearshore hydrodynamic predictions.

The Caspian Sea-wide grid was structured as a curvilinear and orthogonal grid, with a horizontal resolution of 2 km × 2 km, covering a total of 604 × 346 computational cells (Figure 1). This grid serves as the offshore forcing domain, allowing energy transfer from deep water to nearshore regions while maintaining physical consistency between different spatial scales.

For localized simulations, four high-resolution nested grids were developed, corresponding to the selected coastal regions. These grids, referred to as N1 (Nowshahr), N2 (Chaboksar), N3 (Anzali), and N4 (Talesh), were designed to ensure numerical stability and accurate representation of coastal hydrodynamics. Each nested grid was developed with a 20 m × 20 m horizontal resolution, ensuring that grid axes remained parallel and perpendicular to the coastline to maintain depth contour consistency and minimize interpolation errors. The key specifications of these nested grids, which are identical for both the SWAN (wave model) and ROMS (hydrodynamic model), are summarized in Table 1.

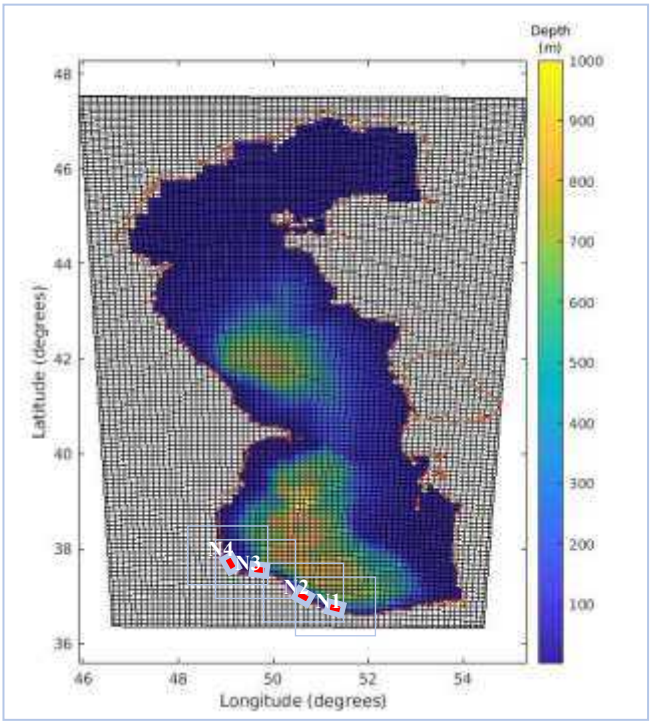

Figure 1 - Computational grid of the wave model in the Caspian Sea with a horizontal resolution of 2 km × 2 km, depicted with a 5:1 cell ratio. The geographical locations of the nested computational grids along the coasts of Nowshahr (N1), Chaboksar (N2), Anzali (N3), and Talesh (N4) are indicated.

Table 1. General specifications of the computational grids for the models in the entire Caspian Sea and the sites of Nowshahr, Chaboksar, Anzali, and Talesh.

Area	*Number of Cells*		*Rotation Angle Relative to True East* (°)	*Horizontal Resolution* (m)	*Maximum and Minimum Depths* (m)		*Wave Breaking Depth with a 5-year Return Period* (m)*
	Perpendicular to Shoreline	*Along Shoreline*					
Caspian Sea	604	346	-	2000	2	1005	--
Nowshahr	178	498	14.6	20	0.5	27	7.22
Chaboksar	248	778	32.6	20	0.5	24	6.7
Anzali	148	368	7	20	0.5	22	7.05
Talesh	118	498	60	20	0.5	۱۳	5.89

* Derived from the monitoring studies of the northern coastal areas of the country, the report on the approximate determination of the wave-breaking zone along the coastline.

2.1.1 Grid Orientation and Spatial Resolution

To optimize computational accuracy, each nested grid was carefully oriented based on local coastline alignment and prevailing wave energy pathways, ensuring a realistic representation of nearshore hydrodynamics. The Nowshahr (N1) grid is rotated 14.6° counterclockwise from true east, consisting of 178 × 498 cells (Figure 2). This orientation aligns with the local wave approach angle, effectively minimizing errors in wave refraction calculations and improving the accuracy of nearshore current simulations. The Chaboksar (N2) grid, with a 32.6° counterclockwise rotation, consists of 248 × 778 cells (Figure 3). Given the steeper bathymetry in this region, the higher grid resolution enables the precise detection of rip current channels and wave-driven circulation patterns, ensuring a more refined simulation of nearshore processes. The Anzali (N3) grid is rotated 7° counterclockwise, comprising 148 × 368 cells (Figure 4). As this region is characterized by a gently sloping seabed, this grid configuration is particularly effective in capturing the broader nearshore circulation patterns typically observed in wave-dominated environments. Lastly, the Talesh (N4) grid is rotated 60°

counterclockwise, consisting of 118 × 498 cells (Figure 5). This significant rotation accounts for coastal curvature and prevailing current directions, which play a crucial role in shaping wave-driven flow structures and sediment transport in this region. These carefully designed grid orientations ensure that the numerical model accurately captures the complex hydrodynamic interactions along the southern Caspian Sea coastline, enhancing the reliability of simulated nearshore circulation and sediment transport patterns.

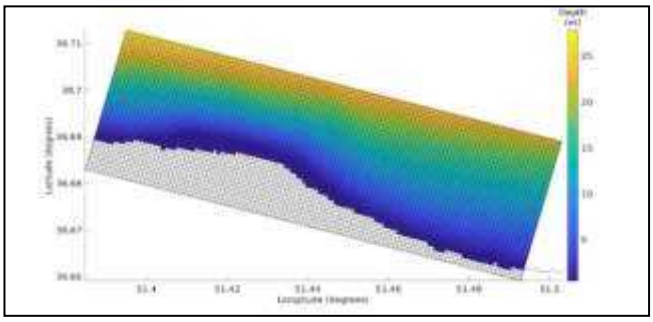

Figure 2 - Computational grid of the model along the Nowshahr coast with a horizontal resolution of 20 meters, depicted with a 4:1 cell ratio.

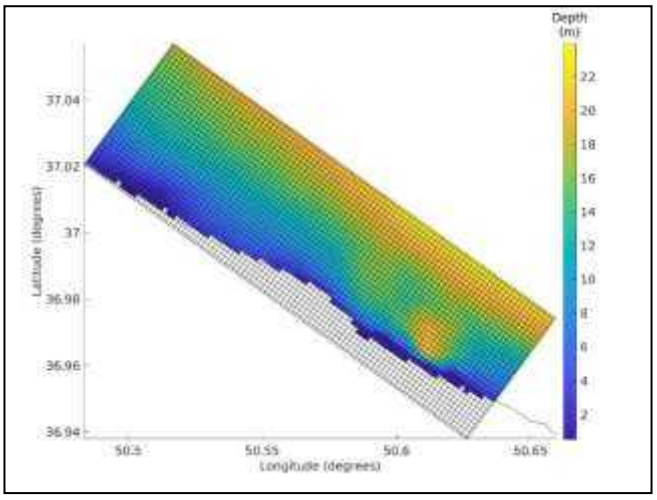

Figure 3 - Computational grid of the model along the Chaboksar coast with a horizontal resolution of 20 meters, depicted with an 8:1 cell ratio.

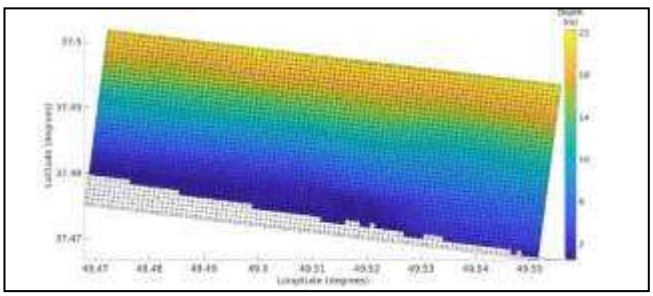

Figure 4 - Computational grid of the model along the Anzali coast with a horizontal resolution of 20 meters, depicted with a 4:1 cell ratio.

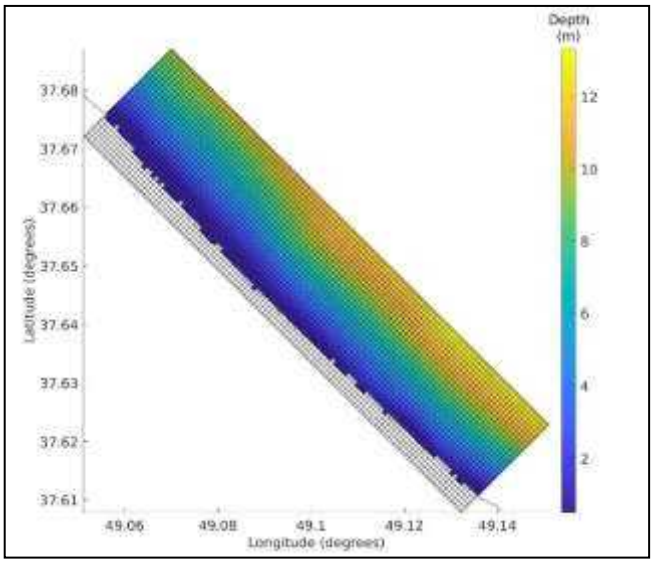

Figure 5 - Computational grid of the model along the Talesh coast with a horizontal resolution of 20 meters, depicted with a 4:1 cell ratio.

2.1.2 Advantages of the Nested Grid Approach

The use of nested grids provides several key advantages for accurately simulating nearshore hydrodynamics, particularly in complex coastal environments such as the southern Caspian Sea. One of the primary benefits is the improved resolution in coastal zones, where the fine-grid resolution (20 m × 20 m) enables the precise simulation of nearshore circulation features, including rip currents, longshore drift, and wave-induced set-up. This high resolution ensures that small-scale hydrodynamic processes critical for coastal hazard assessment and sediment transport modeling are accurately represented.

Another significant advantage is the seamless offshore–nearshore coupling, facilitated by the large-scale Caspian Sea grid, which provides stable boundary conditions for localized high-resolution simulations. This setup ensures a smooth transition of hydrodynamic forcing between deep water and shallow nearshore zones, preserving physical consistency across different spatial scales.

Moreover, the structured nested grid approach offers a computationally efficient alternative to unstructured grid models, which, despite their flexibility, impose significant computational costs. The nested framework maintains high numerical accuracy while significantly reducing computational demand, making large-scale, high-resolution simulations more feasible.

Additionally, the optimized grid orientation plays a crucial role in maintaining numerical stability. Aligning grid axes parallel to depth contours minimizes

numerical diffusion, enhances bathymetric consistency, and ensures that modeled currents and wave transformations remain physically realistic. This approach prevents artificial distortions in simulated wave and current patterns, improving model reliability. Finally, the nested grid framework is highly adaptable for future studies, allowing for easy refinement and expansion. This flexibility makes it particularly suitable for long-term hydrodynamic modeling, enabling researchers to incorporate higher-resolution bathymetric data, refine grid domains, and extend simulations to include sediment transport, climate change impacts, and extreme event forecasting. Given these advantages, the nested grid approach represents a robust and efficient methodology for advancing nearshore hydrodynamic research in the Caspian Sea and other semi-enclosed basins.

2.1.3 Computational Stability and Accuracy Considerations

To ensure numerical stability and accuracy, the grid system was meticulously designed with several key considerations. Bathymetric smoothing was applied by maintaining the slope parameter (r-factor) below 0.2 in the ROMS grids, which helped prevent numerical instabilities arising from abrupt depth variations and steep gradients. This adjustment ensures a more stable simulation environment, reducing errors in the computation of pressure gradients and bottom stress forces.

Additionally, time-step optimization was implemented using a two-level nested time-stepping approach, which allowed for efficient temporal resolution while ensuring that the Courant-Friedrichs-Lewy (CFL) condition was satisfied across all grid scales. This approach was critical in maintaining numerical stability, particularly in areas with high velocity gradients and rapid wave transformations.

Furthermore, wave-current coupling consistency was ensured by fully integrating the SWAN (wave model) and ROMS (hydrodynamic model), allowing synchronized exchanges of wave radiation stresses, bottom shear stress, and turbulent kinetic energy (TKE) between grids. This coupling mechanism was essential for accurately capturing wave-induced circulation patterns, particularly in regions influenced by strong rip currents, longshore transport, and offshore-directed return flows. By incorporating these stability measures, the computational framework effectively enhances the reliability, efficiency, and physical realism of nearshore hydrodynamic simulations, ensuring that the model remains robust under various wave and current conditions.

2.1.4 Expected Contributions of the High-Resolution Grid System

The high-resolution computational grid system developed in this study represents a significant advancement in nearshore hydrodynamic modeling for the Caspian Sea, providing a more refined understanding of wave-driven circulation patterns and sediment transport processes. By employing a multi-scale, nested framework, this study achieves a higher level of precision in simulating rip currents, nearshore circulation, and wave-induced flow structures, which are crucial for hazard prediction, beach safety, and coastal management. The ability to accurately resolve rip current behavior enhances coastal risk assessments, aiding in the development of mitigation strategies to prevent swimmer hazards and structural damage.

Beyond hydrodynamic hazard assessment, the model significantly contributes to the understanding of wave-driven sediment transport dynamics, which is essential for evaluating coastal erosion trends and designing effective engineering solutions. The integration of high-resolution bathymetric data with advanced wave-current interaction modeling allows for a more realistic representation of sediment transport pathways, supporting sustainable coastal development and shoreline protection efforts.

Moreover, the flexibility and computational efficiency of the nested grid approach ensure that this methodology can be adapted and expanded for future hydrodynamic, ecological, and climate impact studies in the region. The model can be further refined to investigate long-term shoreline evolution, storm surge impacts, and climate-driven coastal changes, making it a valuable tool for regional coastal planning and environmental conservation. Through this comprehensive modeling approach, the study provides a strong foundation for future research in semi-enclosed basins such as the Caspian Sea, advancing the field of coastal hydrodynamics and numerical ocean modeling.

The structured multi-scale grid approach adopted in this study ensures a high degree of spatial accuracy, enabling the detailed assessment of hydrodynamic processes along the southern Caspian Sea coastline. The integration of high-resolution SRTM and GEBCO bathymetric datasets, local hydrographic surveys, and advanced grid nesting techniques allows for state-of-the-art numerical modeling of wave-current interactions. These methodological advancements provide a solid foundation for future nearshore hydrodynamic research in semi-enclosed basins such as the Caspian Sea.

2.2 Model Configuration

2.2.1 Flow Model

To increase the stability of the model in each grid, bathymetric data were corrected such that, according to the Backman-Hydogle cell slope criterion [19], the depth ratio between any two adjacent cells does not exceed 0.25. In the vertical direction, each grid is composed of 5 depth layers (sigma) with uniform vertical distribution. The distribution of the grid cell

thickness for bathymetry was determined by selecting vertical stretching functions (Uchiyama et al., 2010) equal to 4 and a transfer function (Shchepetkin et al., 2005) equal to 2. In this way, the Haney criterion [21], which defines the maximum hydrostatic compatibility of vertical stratification, was obtained as less than 5.6. Meeting these criterion values ensures the model's stability.

Considering the longitudinal characteristics of the grids and the number of layers created in the local model, the coupled wave-current model was executed for a one-month period in July 2018, using a Baroclinic time step of 300 and 10 fast Barotropic time steps in each of the grids. The model was implemented using third-order upstream numerical schemes for horizontal propagation and fourth-order for vertical propagation. The Generalized Length Scale (GLS) turbulence model, a generalized two-equation model, was applied for turbulence. The ROMS ocean model supports three types of boundary conditions: closed, open, and periodic for the horizontal boundaries. This model solves the dynamics of the bottom boundary layer processes based on the drag method, which includes linear friction, second-order friction with a constant coefficient, and second-order friction with a logarithmic coefficient.

2.2 Model Configuration

2.2.1 Flow Model

To ensure numerical stability and accuracy, bathymetric data were carefully processed and corrected in each computational grid. This correction was performed in accordance with the Backman-Hydogle cell slope criterion [19], which specifies that the depth ratio between any two adjacent cells should not exceed 0.25. Adhering to this criterion helps prevent numerical instabilities associated with abrupt bathymetric changes, which could otherwise introduce artificial pressure gradients and computational errors.

The vertical discretization of the model was structured using a sigma-coordinate system, where each grid consists of five uniformly distributed vertical layers. The grid cell thickness was determined by selecting vertical stretching functions (Uchiyama et al., 2010) with a parameter value of 4, along with a transfer function (Shchepetkin et al., 2005) value of 2. These parameters were chosen to optimize the vertical resolution, ensuring accurate representation of thermocline structure, bottom boundary layer dynamics, and internal wave propagation. Additionally, the Haney criterion (Haney, R. L., 1991), which defines the maximum hydrostatic compatibility of vertical stratification, was maintained at a value of less than 5.6, further reinforcing model stability by minimizing numerical errors in vertical pressure gradient calculations.

Given the longitudinal characteristics of the grids and the layering structure within the local model, the coupled wave-current simulations were conducted for a one-month period in July 2018. To maintain computational efficiency and accuracy, a baroclinic time step of 300 seconds was used, with 10 fast barotropic time steps executed within each baroclinic step across all grids. The choice of time-stepping strategy ensures that the model accurately captures fast-moving surface gravity waves while maintaining numerical stability for slower baroclinic motions.

For spatial discretization, the model employed high-order numerical schemes to improve accuracy and reduce numerical dissipation. A third-order upstream scheme was applied for horizontal propagation, ensuring precise resolution of advective processes, while a fourth-order scheme was used for vertical propagation, minimizing truncation errors in vertical mixing and stratification processes. To model turbulence closure, the Generalized Length Scale (GLS) turbulence model was implemented. This generalized two-equation approach accounts for mixing length variations, improving the simulation of turbulent kinetic energy (TKE) dissipation rates and subgrid-scale mixing effects, which are crucial for accurate representation of coastal hydrodynamics.

The Regional Ocean Modeling System (ROMS), utilized in this study, supports three types of horizontal boundary conditions: closed, open, and periodic. The appropriate boundary condition type was selected based on the dynamical requirements of each computational domain, ensuring a seamless interaction between offshore forcing and nearshore circulation. Additionally, the bottom boundary layer dynamics were resolved using drag-based formulations, which account for bottom frictional processes critical for wave-current interactions, sediment transport, and bottom stress calculations. Three different formulations were considered for bottom friction: linear friction, second-order friction with a constant coefficient, and second-order friction with a logarithmic coefficient. These formulations help to parameterize seabed roughness effects, improving the accuracy of near-bottom velocity predictions and shear stress computations, which are essential for modeling rip current formation and sediment resuspension.

By incorporating these advanced numerical schemes, turbulence closures, and bottom boundary formulations, the flow model configuration in this study ensures a high degree of accuracy, stability, and physical realism. These methodological refinements contribute to an improved representation of nearshore circulation processes, making the model highly suitable for coastal hazard assessment, sediment transport studies, and future hydrodynamic forecasting applications in the southern Caspian Sea.

2.2.2 Wave Model

The wave modeling component of this study was conducted using a combination of high-resolution wind forcing datasets derived from the ECMWF-ERA Interim global model, which provides spatial resolution of 0.125° and a temporal resolution of 3 hours. This dataset offers reliable global atmospheric reanalysis and forecasting products, ensuring an accurate representation of wind forcing as a key driver of wave generation and transformation in the Caspian Sea.

To simulate wave growth, energy dissipation, and bottom interactions, well-established parameterizations were applied within the spectral wave model. The KOMEN formulation (Akbarpour Jannat et al, 2012) was used to model wave energy growth due to wind input, capturing the influence of wind stress on wave amplitude and spectral evolution. Additionally, KOMEN's approach was employed to parameterize wave energy dissipation due to whitecapping, a critical process affecting wave energy decay and spectral peak attenuation in coastal environments.

For the representation of bottom friction effects, the MADSEN formulation (Akbarpour Jannat et al, 2014) was implemented. This method provides an improved estimation of wave energy dissipation over the continental shelf and shallow-water regions, where bottom roughness and frictional drag significantly influence wave transformation, energy dissipation, and sediment transport dynamics. By integrating these well-established physical formulations, the wave model effectively captures the key processes governing wave propagation, dissipation, and bottom interactions, ensuring a high level of accuracy and physical realism in nearshore wave dynamics simulations.

This comprehensive wave modeling approach provides a robust foundation for understanding wave-induced hydrodynamics, which is essential for coastal hazard assessment, rip current modeling, and shoreline stability studies in the southern Caspian Sea.

2.3 Forcing Mechanisms

The Caspian Sea, as the world's largest enclosed inland body of water, exhibits unique hydrodynamic characteristics, particularly in terms of forcing mechanisms that drive its wave and current systems. Unlike open ocean environments, the Caspian Sea lacks significant tidal fluctuations, resulting in a hydrodynamic regime primarily governed by wind forcing and atmospheric interactions. Due to its vast surface area of approximately 371,000 square kilometers, the sea is highly responsive to synoptic-scale wind patterns, which play a dominant role in wave generation, current formation, and water mass movement.

In coastal waters, the primary mechanism driving nearshore circulation is the interaction between incoming waves and the swash zone. As waves propagate toward the shoreline and break in the surf zone, they generate wave-driven currents, which contribute to longshore transport, rip current formation, and cross-shore exchange processes. The momentum transfer associated with wave breaking is a key driver of coastal circulation, leading to the development of rip channels, wave setup, and alongshore drift.

Additionally, wind-driven currents outside the breaking zone significantly influence coastal circulation, particularly through their role in the undertow current cycle. In this process, wind stress over the water surface generates large-scale surface currents, which, upon reaching the nearshore zone, interact with return flows beneath the wave-breaking layer, resulting in the development of undertow currents. These currents contribute to sediment resuspension, cross-shore mixing, and nearshore water mass exchange, playing a crucial role in coastal morphodynamics.

In this study, the coupled hydrodynamic-wave model explicitly accounts for these key forcing mechanisms by incorporating wind forcing for wave generation and wave-induced forcing for coastal current formation. This approach ensures that both atmospheric-driven large-scale circulation and wave-driven nearshore hydrodynamics are accurately represented, providing a comprehensive understanding of the dominant forcing processes that govern coastal dynamics in the southern Caspian Sea.

2.4 Initial and Boundary Conditions

Accurate initial and boundary conditions are essential for ensuring the physical realism and numerical stability of hydrodynamic and wave simulations. In this study, the initial and boundary values for velocity components (u and v), water level, temperature, and salinity were extracted from the Caspian Sea circulation model (Akbarpour Jannat et al, 2014), which provides a detailed representation of large-scale oceanographic processes within the basin. The initial conditions were derived from the HYCOM (Hybrid Coordinate Ocean Model) data bank, a widely used global oceanographic dataset that offers high-resolution representations of temperature, salinity, and current structures.

For wave modeling, the initial and boundary conditions for wave characteristics at the local grid boundaries were obtained from the SWAN wave model, which was run over the entire Caspian Sea basin (Akbarpour Jannat et al, 2014). By nesting local wave simulations within the larger-scale SWAN model, the approach ensures that energy transfer, spectral wave evolution, and offshore forcing conditions are accurately represented within the high-resolution nearshore grids. The model was forced using wind data from the ECMWF-ERA Interim global reanalysis/forecasting model, which provides a spatial resolution of 0.125° and a temporal resolution of 3 hours. These data include horizontal wind components at a height of 10

meters above the water surface, ensuring an accurate representation of wind-driven wave generation and atmospheric forcing.

Since there are no significant riverine inputs within the domain of the local grids, the predicted nearshore flow patterns primarily consist of wave-driven currents. Despite the extension of the model domain to depths beyond the wave-breaking zone, wind-driven currents were not explicitly incorporated into the local-scale circulation modeling due to their minimal impact on nearshore hydrodynamics compared to wave-induced forcing. By adopting this approach, the model effectively captures the dominant hydrodynamic mechanisms governing coastal circulation, sediment transport, and rip current dynamics in the southern Caspian Sea.

2.5 Calibration

To ensure the accuracy and reliability of the numerical simulations, the model was calibrated and validated using observational datasets from multiple sources. The calibration process involved adjusting the wave and current model coefficients to achieve the best agreement between simulated results and measured field data. For this purpose, data from tracking buoys, wave buoys operated by the Ports and Maritime Organization, and the Acoustic Doppler Current Profiler (ADCP) deployed by the National Institute of Oceanography and Atmospheric Sciences were utilized. The observational datasets, recorded in 2011, provided critical insights into wave height, period, and current velocity, enabling a robust statistical evaluation of model performance.

A comparative analysis of statistical wave characteristics was conducted at both deep and shallow water points along the southern Caspian Sea shoreline, with results summarized in Table 2. This assessment allowed for the refinement of key wave and current model parameters, ensuring that the numerical model accurately reproduced real-world hydrodynamic conditions. By integrating high-quality observational data into the calibration process, the study enhances the credibility and predictive capability of the coupled wave-current model, making it a valuable tool for coastal hydrodynamic research, hazard assessment, and marine engineering applications in the southern Caspian Sea.

Table (2): Statistical Parameters of Waves Based on Mean Bias Error (MBE), Root Mean Square Error (RMSE), Scatter Index (SI), Correlation Coefficient (CC), and Agreement Index (AA), at the Wave Buoy Station of the Ports and Maritime Organization (Deep Water) and at the ADCP Wave Buoy Station of the National Institute of Oceanography and Atmospheric Sciences (Shallow Water).

	M1		M3	
	H_s (m)	T_p (s)	H_s (m)	T_p (s)
MBE	-0/05	0/8	0/02	0/03
RMSE	0/23	1/09	0/1	1/42
SI	0/47	0/24	0/27	0/25
CC	0/76	0/51	0/81	0/67
IA	0/87	0/65	0/82	0/8

Based on Figure 6, the comparison between measured flow velocity at Bandar Anzali and the corresponding numerical model outputs provides a critical assessment of model accuracy. The time series analysis demonstrates how well the simulated results align with the ADCP field measurements recorded at a depth of 3 meters from the surface. Meanwhile, the simulated velocity data corresponds to the fourteenth vertical layer in the model, ensuring a direct comparison of near-surface current dynamics.

The validation results indicate a strong correlation between measured and simulated flow velocities, confirming the model's ability to capture nearshore circulation dynamics in the region. Minor discrepancies observed between the two datasets may be attributed to spatial variability in current patterns, uncertainties in bathymetric data, and subgrid-scale turbulence effects that are not fully resolved in the model. However, the overall agreement supports the robustness of the hydrodynamic model in reproducing wave-driven currents and wind-induced flows along the southern Caspian Sea coastline. This validation strengthens the model's applicability for coastal hazard assessment, rip current prediction, and sediment transport studies, providing a reliable framework for future hydrodynamic forecasting in the region.

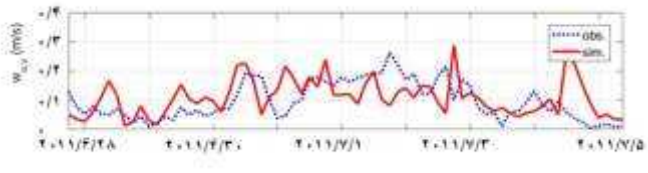

Figure (6): Time series of horizontal flow velocity measured and simulated at Bandar Anzali. The ADCP data corresponds to a depth of 3 meters from the surface, while the simulated data corresponds to the fourteenth layer (from the surface).

3. Results and Discussion

Coastal currents influenced by wave forcing along the coasts of Nowshahr, Chaboksar, Anzali, and Talesh

were investigated using coupled ROMS-SWAN models for a one-month period in July 2018. The results were extracted from the model at one-hour time intervals to ensure high temporal resolution. Using the modeled data, the current vectors and the vorticity derived from horizontal currents were calculated and plotted for times corresponding to the measurements from the drifter trackers, allowing for direct comparison between simulated and observed patterns.

The wave-driven current averaged at depth for the Nowshahr coast is shown in Figure (7). The coastal flow pattern in this region indicates the presence of a dominant easterly alongshore current, which is primarily driven by wave-induced forces and modulated by local bathymetric variations. The velocity of these currents exhibits spatial variability, with stronger flows observed in the western sector compared to the eastern region. This gradient in current intensity could be attributed to variations in coastal morphology, wave energy dissipation, and local sediment transport dynamics.

Notably, multiple cells of rotational currents are evident, indicative of rip current activity. These rip currents, formed due to wave breaking and nearshore bathymetric features, play a critical role in nearshore circulation by redistributing sediment and energy. In the eastern section of the domain, the spacing between rip current channels is approximately 700 meters, and their influence extends offshore to a depth of about 2 meters. This suggests the presence of rhythmic topographic features, such as sandbars, which regulate the formation and spacing of rip currents.

The vorticity field (Figure 8) derived from horizontal currents further supports these observations. The dominant flow regime remains coastal, characterized by persistent alongshore currents, yet several localized zones of elevated vorticity correspond to the rip currents identified in the velocity field. The intensity and penetration depth of these rip currents appear to vary along the coast, with a noticeable increase in offshore penetration in the central part of the study area. This enhancement is likely linked to the geomorphological characteristics of the coastline, including variations in seabed slope and nearshore bathymetry, which can channelize wave energy and enhance the offshore-directed return flow.

These findings highlight the complex interactions between wave forcing, coastal morphology, and nearshore circulation processes, emphasizing the importance of high-resolution numerical modeling in assessing hydrodynamic behavior in dynamic coastal environments.

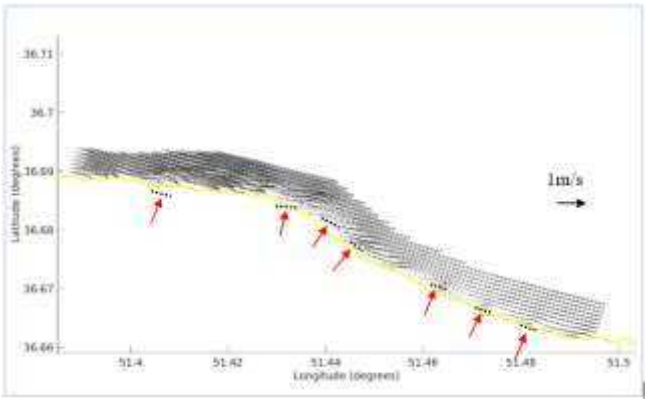

Figure (7): Coastal currents resulting from the modeling at the Nowshahr coast, confined to a depth of 6 meters up to the shoreline.

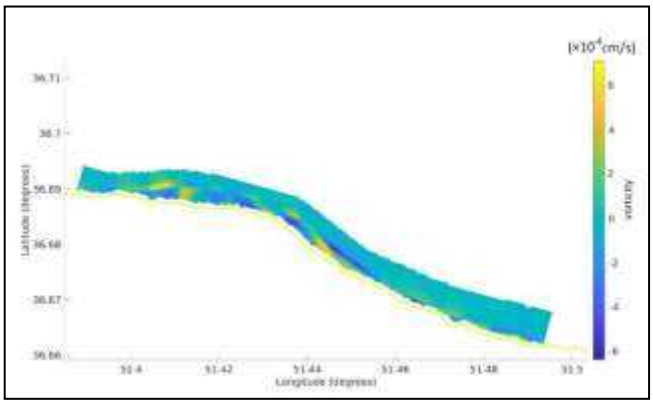

Figure (8): Vorticity field resulting from the modeling at the Nowshahr coast, confined to a depth of 6 meters up to the shoreline.

At the Chaboksar coast (Figure 9), the coastal slope is steeper than in the Nowshahr region, leading to a more confined nearshore zone and narrower coastal currents. This steep slope influences the wave transformation and energy dissipation, resulting in a more concentrated and intensified nearshore flow. Similar to the Nowshahr region, the coastal current pattern exhibits a dominant onshore component and an eastward-alongshore flow, primarily driven by wave forcing and local bathymetric constraints. However, in contrast to Nowshahr, the variation in the onshore current velocity remains relatively uniform across the region, indicating that the steep bathymetry may play a role in stabilizing the nearshore flow field.

Rip currents are clearly visible along almost the entire coastline, marked by distinct vortices embedded within the broader coastal current system. These rip currents exhibit greater offshore penetration than those observed at Nowshahr, extending to depths of 5–6 meters. This increased offshore reach suggests that stronger wave breaking and nearshore circulation processes are at play, likely facilitated by the steeper slope and channelized return flows. The rip currents are particularly pronounced in the western section, where their intensity surpasses that of those in the eastern region. This asymmetry in rip current strength may be

attributed to regional variations in incident wave energy, bottom roughness, and shoreline morphology.
Several rotational cells, spaced between 700 and 1000 meters apart, are identified along the coastline. These rotational features are indicative of rip current dynamics and their associated vorticity structures. The study of the vorticity field (Figure 10) further corroborates these findings, revealing that the western region is characterized by stronger and more persistent rip currents, as indicated by the higher vorticity values. In contrast, the eastern section displays weaker, more diffuse rip current signatures.
In the central part of the study area, the vortices appear more consolidated and well-defined, suggesting that localized geomorphological factors, such as submerged sandbars or rocky outcrops, may be contributing to the spatial organization of these currents. Despite the dominance of stronger rip currents in the western section, weaker rip currents are still present throughout the region, underscoring the variability and complexity of nearshore hydrodynamics along the Chaboksar coast.
These results highlight the critical role of bathymetry in shaping rip current dynamics and emphasize the need for high-resolution hydrodynamic modeling to improve our understanding of nearshore circulation patterns in steep-slope coastal environments.

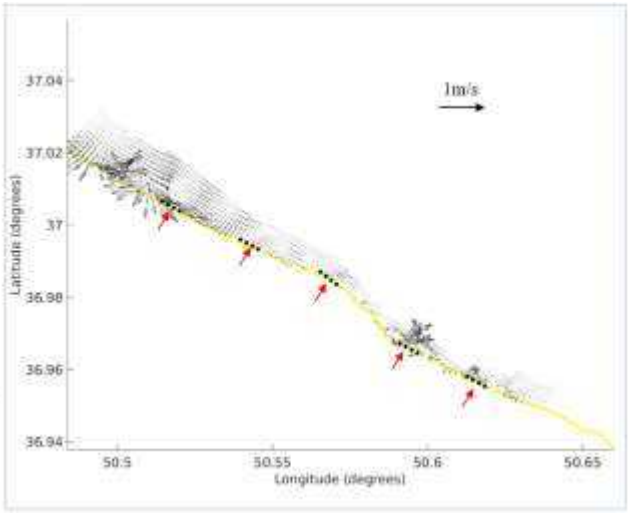

Figure (9) Coastal currents resulting from modeling at the Chaboksar coast, limited to depths of 8 meters from the shoreline.

At the Anzali coast, the shoreline currents exhibit relatively weak intensity at the selected simulation time (Figure 11). The gentle coastal slope plays a significant role in shaping the nearshore circulation, resulting in a broader, more diffused current band. Unlike regions with steeper bathymetry, where currents are more concentrated and energetic, the gradual slope at Anzali facilitates the dissipation of wave energy over a wider area, leading to a more uniform and less intense coastal flow.

While offshore currents have developed, there is limited evidence linking them to well-defined rip currents. Only two rip currents are distinctly visible, and their influence on offshore transport appears to be weak compared to other study areas. The offshore-directed currents extend to a depth of approximately 8 meters, suggesting that while some rip current activity is present, it lacks the pronounced intensity observed in regions with steeper slopes, such as Chaboksar. This subdued rip current activity may be attributed to weaker wave forcing, reduced wave breaking intensity, or a more uniform seabed profile that lacks the morphological features necessary to generate strong rip channels.

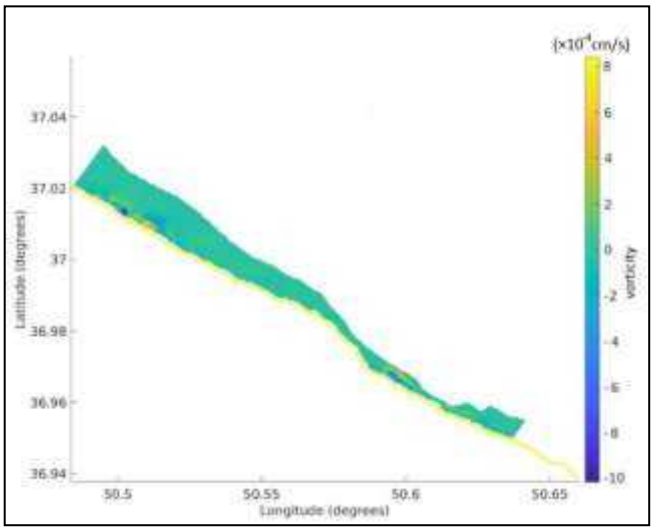

Figure (10) Vorticity field resulting from modeling at the Chaboksar coast, limited to depths of 8 meters from the shoreline.

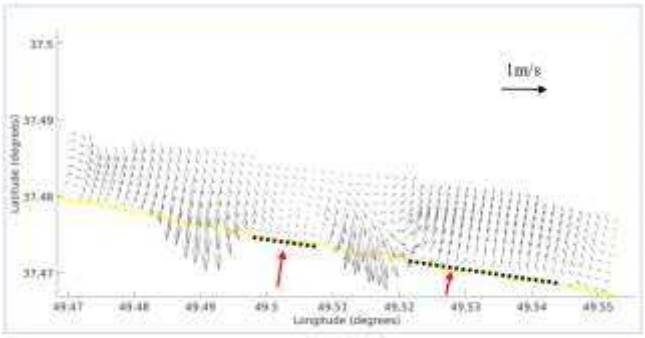

Figure (11) Coastal currents simulated at the Anzali coast, limited to a depth of 8 meters from the shoreline.

The vorticity field (Figure 12) further supports these findings. The analysis indicates that rip currents in the eastern part of the area exhibit stronger vorticity signatures than those in the western region. This spatial variation suggests that local geomorphological factors or variations in wave energy distribution may be influencing the development of rip currents. The weaker rip activity in the western section could be due to the presence of alongshore sediment transport

processes that redistribute wave energy, preventing the formation of well-defined rip channels.

Overall, the results for the Anzali coast highlight the influence of coastal slope on nearshore hydrodynamics. The broader current band and weaker rip currents observed in this region underscore the importance of local bathymetry in modulating wave-driven circulation patterns. These findings provide valuable insights into the spatial variability of nearshore currents along the Caspian coastline and emphasize the necessity of detailed hydrodynamic modeling for improved coastal hazard assessment and management.

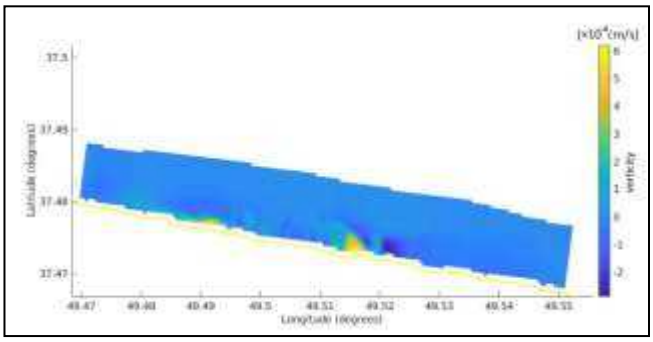

Figure (12) Vorticity field simulated at the Anzali coast, limited to a depth of 8 meters from the shoreline.

Based on Figures 13 and 14, which depict coastal currents and the vorticity field at the Talash coast, the hydrodynamic characteristics of this region are closely linked to the gently sloping seabed and extended wave-breaking zone.

The broader current band observed in Figure 13 confirms that wave breaking occurs farther offshore, leading to a gradual transition between wave-induced and offshore-directed flows. This is characteristic of regions with low-gradient bathymetry, where wave energy dissipation is more evenly distributed across a wider area. The dominant onshore current directed westward suggests that wave-induced setup plays a major role in driving coastal circulation, with coastal morphology acting as a secondary influence.

A distinctive feature of the Talash nearshore circulation is the presence of cyclonic upwelling currents, consistently observed along the entire coastline. Figure 14 (vorticity field) reinforces this observation, highlighting spatial variations in current intensity. The relatively uniform bathymetry supports the formation of broad, persistent upwelling currents, contrasting with localized rip currents that typically emerge in regions with pronounced topographic irregularities. The penetration depth of these upwelling currents, extending 3–4 meters offshore, suggests their potential role in nutrient transport and sediment redistribution, influencing coastal productivity and seabed stability.

The western sector of the study area exhibits stronger current intensities, as indicated by higher vorticity values in Figure 14. This intensification may result from regional variations in wave energy dissipation, localized wind-driven circulation patterns, or subtle bathymetric differences that enhance flow acceleration. The eastern section, in contrast, shows weaker upwelling activity, suggesting a more diffuse flow regime with less concentrated current structures.

Overall, the hydrodynamic regime of the Talash coast is characterized by a broad, low-energy nearshore current system, with persistent upwelling rather than strong rip current formation. These findings highlight the critical role of coastal slope and wave forcing in shaping nearshore circulation and underscore the importance of morphological considerations in assessing coastal hydrodynamics. Future studies incorporating high-resolution field measurements and three-dimensional flow analysis would provide further insights into the mechanisms governing upwelling and sediment transport in gently sloping coastal environments.

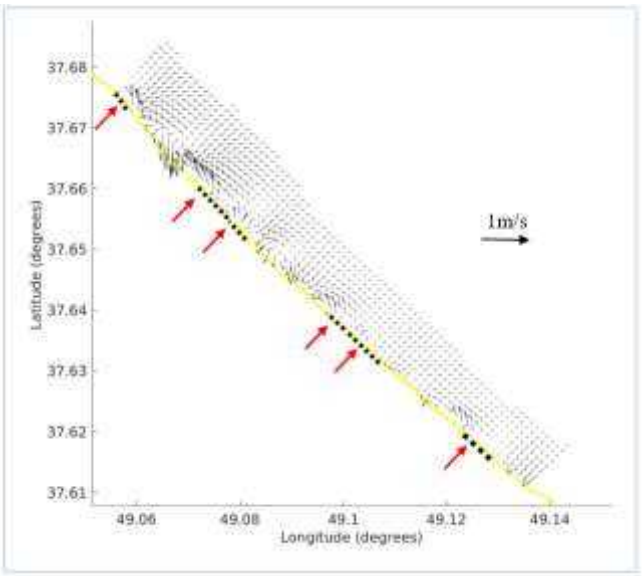

Figure (13) Coastal currents obtained from modeling at the Talash coast, limited to a depth of 8 meters to the shoreline.

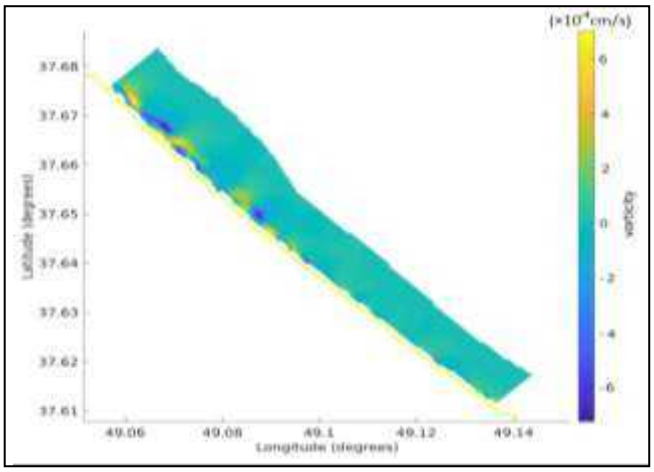

Figure (14) Vorticity field obtained from modeling at the Talash coast, limited to a depth of 8 meters to the shoreline.

4. Conclusion

This study utilized coupled SWAN-ROMS numerical modeling to analyze wave-driven nearshore currents along the southern Caspian Sea, focusing on four coastal regions: Nowshahr, Chaboksar, Anzali, and Talesh. The results demonstrated that wave-induced circulation is a dominant hydrodynamic feature throughout these coasts, significantly influenced by coastal morphology, bathymetric characteristics, and wave forcing. The interaction between wave energy dissipation, shoreline slope, and nearshore bathymetry plays a crucial role in shaping current intensity and distribution patterns.

A key finding of this study is the spatial variability in current intensity, which decreases from east to west along the study domain. This trend is primarily governed by differences in coastal slope and the width of the wave-breaking zone. In regions with steeper bathymetry, such as Chaboksar, the nearshore current system is more concentrated, generating stronger alongshore and rip currents. Conversely, in areas with gentler slopes, such as Anzali and Talesh, wave breaking occurs farther from the shoreline, leading to broader, more diffused current bands with weaker intensities. The extent of offshore-directed currents also varies accordingly, with steeper regions exhibiting deeper penetration of rip currents, while in gently sloping regions, the return flows are more gradual and widespread.

Rip currents were observed as a significant hydrodynamic feature in the study area, with their presence particularly pronounced along the Nowshahr and Chaboksar coasts. These currents exhibited well-defined circulation cells, penetrating offshore up to 5–6 meters in depth, with spacing between rip channels ranging from 700 to 1000 meters. The variation in rip current intensity and distribution is closely linked to local bathymetric variations and wave forcing mechanisms. In contrast, the Anzali and Talesh coasts exhibited fewer and weaker rip currents due to their more uniform seabed morphology, which limits the formation of strong, concentrated return flows.

Current velocities reached up to 1 m/s in certain sections, emphasizing their potential implications for sediment transport, beach morphology, and coastal erosion processes. These findings highlight the necessity for high-resolution bathymetric datasets to enhance the accuracy of hydrodynamic modeling and improve the identification of high-risk zones for rip current hazards. Given the dynamic and regionally variable nature of nearshore circulation, periodic updates to bathymetric surveys are essential to capture evolving seabed features that influence current formation.

Moreover, the results underscore the need for establishing a dedicated observation network for waves and shallow water currents across the southern Caspian Sea. The absence of continuous in situ measurements poses a challenge for accurately validating numerical models and improving the predictive capability of hydrodynamic simulations. Implementing a real-time monitoring system with drifter deployments, ADCP measurements, and wave buoys would provide critical data to refine model accuracy and enhance coastal hazard assessments.

From a practical perspective, the insights from this study have direct implications for coastal zone management, maritime safety, and beachgoer risk mitigation. The identification of strong rip currents in certain areas necessitates the implementation of targeted public safety measures, such as warning systems, designated safe swimming zones, and enhanced coastal surveillance. Additionally, the influence of nearshore currents on sediment transport processes highlights the need for integrated coastal engineering strategies to mitigate erosion and shoreline instability.

Overall, this research provides a comprehensive understanding of wave-driven nearshore circulation in the southern Caspian Sea, emphasizing the interplay between bathymetry, wave forcing, and current dynamics. The findings serve as a foundation for future studies focusing on coastal hydrodynamics, wave-current interactions, and hazard mitigation strategies in similar semi-enclosed basins. Further research incorporating high-resolution field measurements and data assimilation techniques is recommended to enhance the predictive accuracy of numerical models and support sustainable coastal management efforts in the region.

5. Acknowledgements

This research is part of a project funded by the Iranian National Science and Technology Foundation (INSF) under the Vice Presidency for Science and Technology, titled:

"Hazard Zonation of Rip Currents and Associated Mortality Risks along the Iranian Caspian Coastline (Gilan and Mazandaran Provinces: Talesh, Anzali, Chaboksar, and Nowshahr)."

References

Akbarpour Jannat, M.R., V. Chegini, H.A.K. Lahijani, M. Noranian Esfahani, and J. Azizpour, (2012). Field Measurement and Numerical Modeling of Rip Currents in the Southern Caspian Sea Waters, Phase One - Pilot Project. Report, National Institute of Oceanography.

Akbarpour Jannat, M.R. and M. Noranian Esfahani, (2014). Modeling of Coastal Currents, Part One:

Caspian Sea. Report, National Institute of Oceanography.

Haney, R. L. (1991). On the pressure gradient force over steep topography in sigma coordinate ocean models. Journal of physical Oceanography, 21(4), 610-619.

Lahijani, H.A.K., (2006). Understanding the Effects of Rip Currents in the Iranian Coasts of the Caspian Sea. National Institute of Oceanography and Atmospheric Sciences.

Lahijani, H.A.K., (2006). Understanding Features Caused by Rip Currents on the Iranian Coasts of the Caspian Sea. National Institute for Oceanography and Atmospheric Science.

Terziev, F., A. Kosarev, and A. Aliev, (1992). Hydrometeorology and hydrochemistry of the seas. The Caspian Sea, (1): p. 360.

Noraniyan Isfahani, M., M. R. Akbarpour Jannat, and B. Banijamali, (2017). Evaluation of the ROMS-SWAN Integrated Model in Simulating Currents of the Southern Caspian Sea. Oceanography, 8(32).

Noranian Esfahani, M., Akbarpour Jannat, M. R., Banijamali, B., & Siadatmousavi, S. M. (2018). The impact of ERA-Interim winds on wave generation model performance in the Southern Caspian Sea region. Meteorology and Atmospheric Physics.

Ports and Maritime Organization (2015). Monitoring Studies of the Northern Coasts of the Country, Report on the Monitoring and Simulation Studies of the Northern Coasts. Ports and Maritime Organization.

Ports and Maritime Organization (2009). Modeling of Waves in the Seas of Iran, Volume 1: Caspian Sea. Ports and Maritime Organization.

Shchepetkin, A. F., & McWilliams, J. C. (2005). The regional oceanic modeling system (ROMS): a split-explicit, free-surface, topography-following-coordinate oceanic model. Ocean modelling, 9(4), 347-404.

Uchiyama, Y., McWilliams, J. C., & Shchepetkin, A. F. (2010). Wave–current interaction in an oceanic circulation model with a vortex-force formalism: Application to the surf zone. Ocean Modelling, 34(1-2), 16-35.

INTERNATIONAL JOURNAL OF
COASTAL & OFFSHORE ENGINEERING IJCOE Vol.10/No. 3/ Summer 2025 (44-52)

Available online at: www. Ijcoe.org

Investigation of the motions and added resistance of dhow vessel in regular head waves using CFD method

Abouzar Ebrahimi[1*], Reza Dorostkar[2], Abuzar Abazari[3]

[1] Assistant Professor, Chabahar Maritime University; Ab_ebrahimi@cmu.ac.ir*
[2] Marine Engineering Department, Sharif University of Technology; rezadorostkar.bnd@gmail.com
3 Associate Professor, Chabahar Maritime University; Abazari@cmu.ac.ir

ARTICLE INFO

Article History:
Received: 07 MAY 2025
Accepted: 19 NOV 2025

Keywords:
Dhow Vessel
CFD
Added Resistance
Regular Waves

ABSTRACT

Dhow vessels are among the earliest traditional vessels employed for fishing and transporting goods in some countries around the Indian Ocean and Persian Gulf for many years. So far, no research has been done on the hydrodynamics and resistance of these vessels, and the body form of these vessels has been designed in a totally classical and experimental way. One of the most critical issues in the hydrodynamic design and safety of vessels is the added resistance to waves. In this research, the effect of different waves on the hydrodynamic resistance of a dhow vessel has been numerically investigated. The numerical method used in this research is computational fluid dynamics, and StarCCM software was used for this purpose. KCS model results were used to validate CFD results, and finally, the added resistance of the dhow vessel in waves with different lengths and 3 wave heights was investigated. Results show that at short and long wavelengths, the added resistance is lower than at moderate wavelengths. Also, for all three wave heights, the maximum added resistance occurred at a wavelength ratio of 1.8.

1. Introduction

The word dhow or 'Lenj' in Persian, is used for various types of traditional sailing vessels with one or more masts with sails found in the Indian Ocean, Red Sea, Persian Gulf and the Oman Sea [1]. Nowadays, diesel engines and propellers are employed for the propulsion of dhows instead of sails. In Iran, Dhow vessels are also used for cargo transport and fishing. Often, dhows sail in areas with significant waves and the propulsion system cannot provide the thrust force necessary, so the waves overcome the vessel and ultimately cause it to break and sink. Consequently, it is necessary to evaluate the added resistance and motion of this vessel in waves. In the present research, the added resistance and motion of the dhow in the Persian Gulf waves have been investigated using a numerical method.

There has been no comprehensive study on the added resistance and motions of dhow vessels in the waves. Moreover, added resistance is important to commercial ships, including oil tankers and container ships, and there has been a lot of research on this topic. In the study by Storm-Tejsen et al [2] the added resistance in waves was studied experimentally for a vessel with a 60 series hull form. Pinkster [3] and Faltinsen [4] used the three-dimensional potential theory method to calculate the resistance in short waves on a floating structure and then compared the results with experimental results.

Moctar et al. [5] numerically calculated the added resistance of a 14,000 TEU containership and a medium size cruise ship in long and short waves of different frequencies. Sadat-Hosseini et al. [6] calculated the motions and added resistance of KVLCC2 model in short and long head waves by means of URANS and validated it with experimental data. Yu et al. [7] studied the added resistance and motions of the KVLCC tanker model under the impact of 14 regular waves have been investigated using experimental and computational methods. Ebrahimi et al. [8] studied the resistance of catamaran vessel using CFD method and investigated the effect of interference of demi-hull waves on total resistance.

In the study by Park et al. [9], the added resistance of a large tanker was estimated experimentally and numerically in an oblique sea with an angle of 0 to 180 degrees. The model tests were carried out in the SSPA

seakeeping basin. The results showed that the computational results were in good agreement with the experimental results.

Shivachev et al. [10] studied the added resistance and motion responses of KRISO container ship (KCS) at six different trim angles experimentally and numerically using CFD. Ship motions and added resistance were measured for several wavelength conditions considering short and long wave ranges with a wave slope of 1 to 60. Experimental and numerical results for pitch motions and added resistance were compared with CFD results and showed reasonable agreement with experimental data for ships in head waves.

In the study of Diaz et al. [11], they investigated experimentally and numerically a small fishing vessel. First, they tested a model in the towing tank, and their experimental and numerical results showed a good agreement. Using experimental and numerical results, they proposed a modified bow form that reduces vessel resistance by 10 percent.

In the study of Seif et al. [12], they numerically investigated the flow around the hull of a 500-tonne Dhow. In this research, they used ANSYS Fluent software to model the flow and calculate vessel resistance at different speeds.

2. Main Characteristics of Dhow Vessel

In this paper, we studied a model scale of a fishing dhow vessel with 130 tones displacement. The body plan view and 3D CAD view of this vessel are shown in Figures 1 and 2, respectively. Also, the main dimensions of the full scale and model of dhow vessel are presented in Table 1. The COG of a full scale vessel is located about 10 meters from aft perpendicular and 2 meters above the keel.

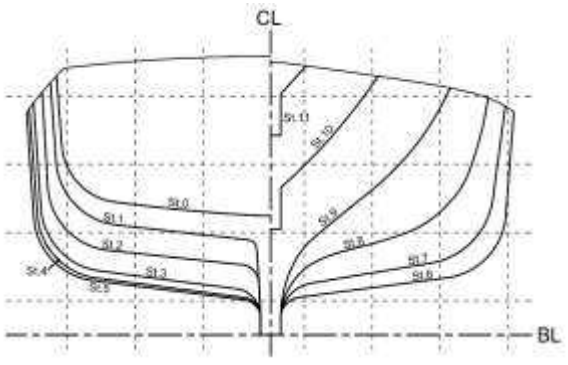

Figure 1. Body plan view

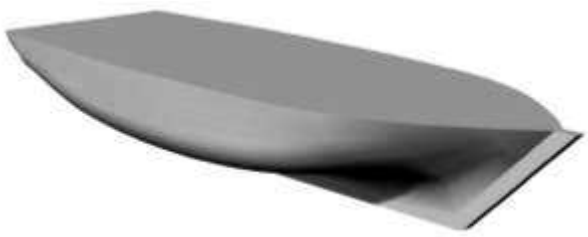

Figure 2. 3D CAD of dhow vessel

Table 1. Main dimensions of dhow vessel

	Value	
Characteristic	Full Scale	Model
Length (m)	21.1	0.95
Breath (m)	7.1	0.32
Height (m)	3.3	0.14
Draft (m)	2.2	0.1
Design Speed (m/s)	5.14	1.1

3. Numerical method

Nowadays, numerical methods are widely used to study the hydrodynamics of vessels. The reason for this is the low cost and availability of this method compared to the experimental method. Computational fluid dynamics is one of the most widely used numerical methods, which uses finite volume methods (FVM) to discretize the governing equations.

The equations to be solved in CFD method are the incompressible Navier–Stokes equations. The references for this method are Versteeg and Malalasekera [13] and Moukalled et al. [14]. To simulate turbulent flow, three general methods can be employed; Reynolds-Averaged Navier-Stokes Equations (RANSE), direct numerical simulation (DNS) and large eddy simulation (LES). Among these three methods, the RANSE method has a lower computation cost and has good accuracy. A RANSE method was used in the present study. Numerical models have been carried out in a three-dimensional, unsteady, turbulent flow mode. Navier-Stokes equations have been expressed as follows:

$$\rho\left(\frac{\partial \vec{u}}{\partial t}+(\vec{u}.\nabla)\vec{u}\right)=\rho g-\nabla p+\mu\nabla^2\vec{u} \qquad (1)$$

In these equations, $\vec{u}$, g, p and μ are the velocity vector, gravitational acceleration, pressure and viscosity of the fluid, respectively. The flow around the ship hull is always turbulent and the main characteristic of these flows is the fluctuating flow field. Instead of directly modeling these equations, they can be simplified by the Reynolds averaging method, which is called RANS equations. Time-averaged equations are obtained in the following form:

$$\frac{\partial}{\partial x_i}(\rho u_i u_j)=-\frac{\partial p}{\partial x_i}+\frac{\partial}{\partial x_j}(-\rho\overline{u_i' u_j'})+\frac{\partial}{\partial x_j}\left[\mu\left(\frac{\partial u_i}{\partial x_j}+\frac{\partial u_j}{\partial x_i}(\frac{2}{3}\delta_{ij}\frac{\partial u_l}{\partial x_l}\right)\right]$$

In the above equations, the term $-\rho\overline{u_i' u_j'}$ shows turbulence effects and is called Reynolds stresses. Turbulence models are used to solve the equations

using Reynolds stresses according to known flow parameters [10].

Solution domain

Choosing the appropriate computational domain can lead to a reduction in solution time and ensure that the results are accurate. In this research, according to previous works, the dimensions mentioned Figure 3 have been selected for the solution domain.

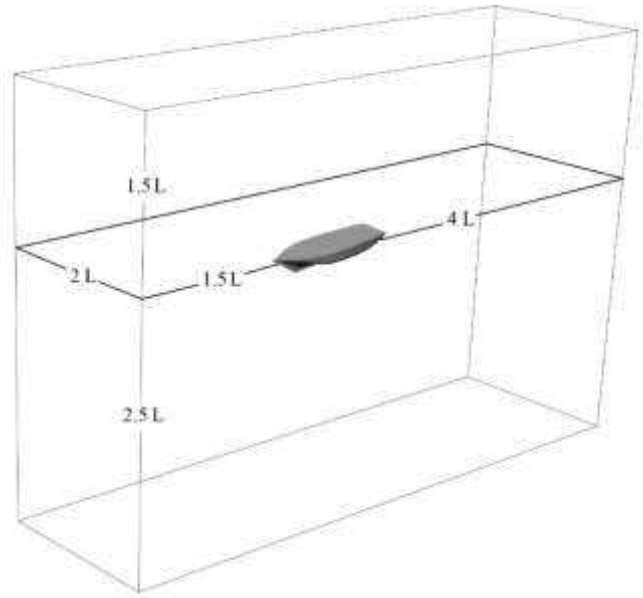

Figure 3. Computational domain dimensions

SST model with standard coefficients was chosen for the turbulence model. Table 2 shows the boundary conditions applied to the virtual towing tank and ship geometry. DFBI Morphing (dynamic fluid body interaction) was used to specify the ship's motion. Also, Volume of Fluid (VOF) flat waves were used to model the free surface.

Table 2. Boundary conditions

Boundary	Boundary Type
Dhow - Deck	Wall
Dhow - Hull	Wall
Tank - Bottom	Wall
Tank - Inlet	Velocity Inlet
Tank - Outlet	Pressure Outlet
Tank - Port Side	Symmetry plane
Tank - Starboard Side	Symmetry plane
Tank - Top	Velocity Inlet

3.1 Mesh generation

As a part of all numerical methods based on equation discretization, mesh generation is one of the most important steps. Even though, with the development of computers, there are fewer mesh size limitations than in the past, reducing computing costs has always been one of the main objective of researchers. In this study, with reference to previous experiences, a trimmed cell mesh with 2.7 million cells was used for simulation of the vessel.

Also, Considering the two DOF of the vessel in waves, that is pitch and heave, to improve the simulation of ship motions, the overset mesh has been used for modeling the motion of the dhow vessel. In this method, the domain is composed of two parts, the overset region and the background, where the overset region slides over the background region. The details of this grid is shown in Figure 4.

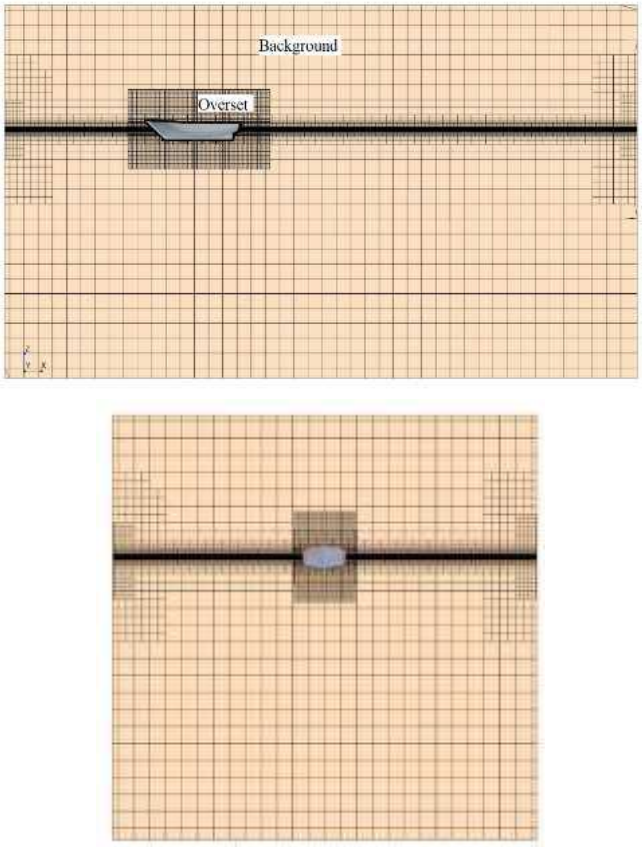

Figure 4. Mesh details of domain

3.2 Validation

After choosing the optimal grid and applying solver settings, it is required to validate the numerical results. To validate the present study results, KRISO container ship (KCS) resistance data was used. This ship is used in many numerical solution researches as a workbench to verify the results. SIMMAN workshop [15] presented an experimental data of this model and its resistance and motions under different wave conditions. Main geometric particulars of KCS model are given in Table 3.

Table 3. Main particulars of KCS ship model [15]

LBP (m)	6.0702
BWL(m)	0.8498

T (m)	0.2850
C_B	0.65
$\nabla\ (m^3)$	0.9571
U (m/s)	2.017

Figures 5 and 6 show the 3D CAD geometry and generated mesh for the KCS model.

Figure 6. CAD view of KCS container ship model

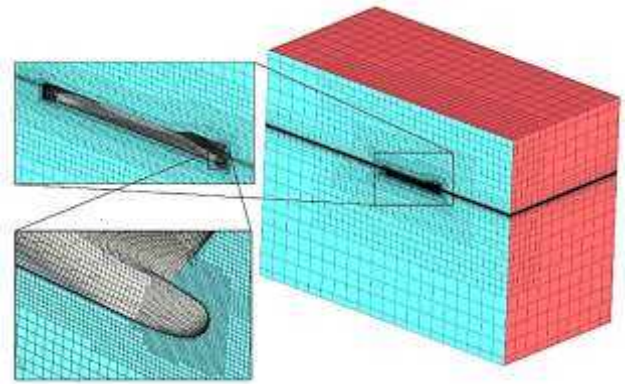

Figure 5. Details of mesh generated for KCS model

In Figure 7 the total resistance coefficient of KCS model in the present study is compared with experimental results of [15] in head waves with wave length (λ) of 11.84 m, wave height of 0.196 m and λ/LBP=1.95.

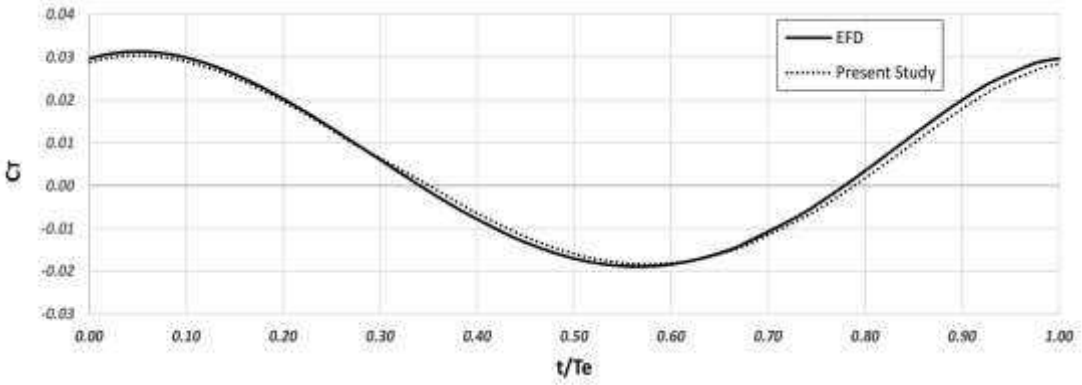

Figure 7. Validation of total resistance coefficient (C_T) for KCS ship

As shown in the above figure, the present study results are in reasonable agreement with experimental results. Therefore, we can use these mesh and solver settings to obtain the added resistance of the dhow vessel in different waves.

4. Added Resistance in Waves

The speed that a ship can achieve in calm water depends on its total resistance, propeller efficiency and engine power. In rough sea conditions, resistance may change due to forces imposed by waves and wind; and the resulting change in propeller load usually reduces propeller efficiency. Consequently, the ship's speed at a given engine power is usually reduced by these effects. This involuntary reduction of speed is often no more than two or three knots, but may result in significant financial losses for merchant ships.

A ship moving in regular waves will have oscillating resistance. In head waves, the mean value of resistance will be higher than calm water and the difference may be attributed to waves. The total resistance (RT) of the ship in waves can be written as:

$$R_T = R_c + R_{aw} \quad (3)$$

Where Rc is the ship resistance in calm water and Raw is the wave added resistance.

In the present study, the movement of the dhow vessel has been investigated in several different regular waves. The characteristics of these waves are presented in the

Table 4. Lw/L is ratio of wave length to dhow model length.

Table 4. Characteristics of waves

Wave No.	Wave height (cm), H	Lw/L
1	3	0.65
2	3	0.8
3	3	1.2
4	3	1.643
5	3	1.8
6	3	2
7	3	2.5
8	5	0.65
9	5	0.8
10	5	1.2
11	5	1.643
12	5	1.8
13	5	2
14	5	2.5
15	10	0.65
16	10	0.8
17	10	1.2
18	10	1.643
19	10	1.8
20	10	2
21	10	2.5

All numerical analysis was carried out in design speed of dhow vessel and all waves encounter the vessel in head sea state.

5. Numerical Results

In the following figures, the surface waves generated around the bow and stern of the dhow hull and the interference of these waves with regular head waves are displayed, at 2 wavelengths.

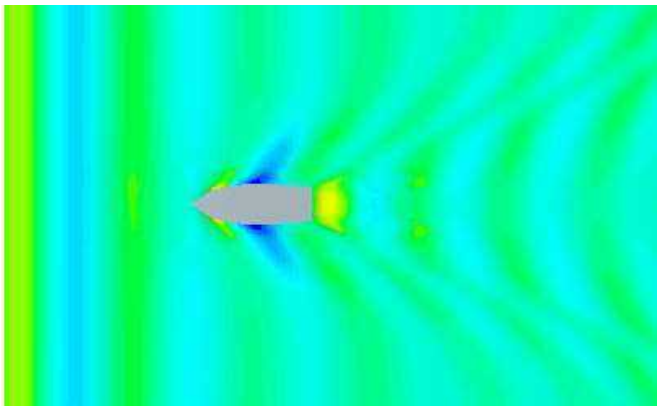

(a)

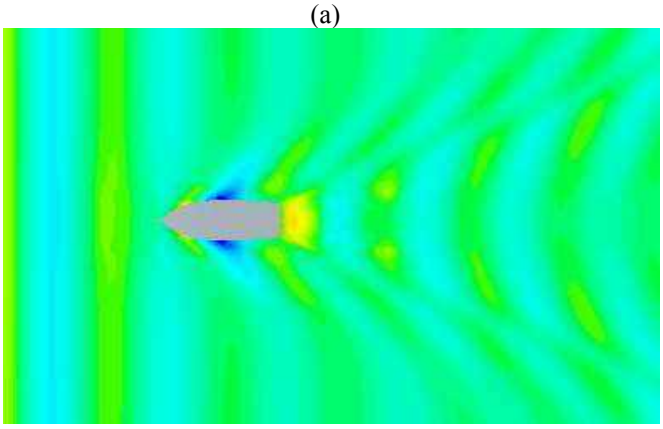

(b)

Figure 8. Waves elevation around ship for wave of H=3 cm; (a): Lw/L=0.65, (b): Lw/L=1.2

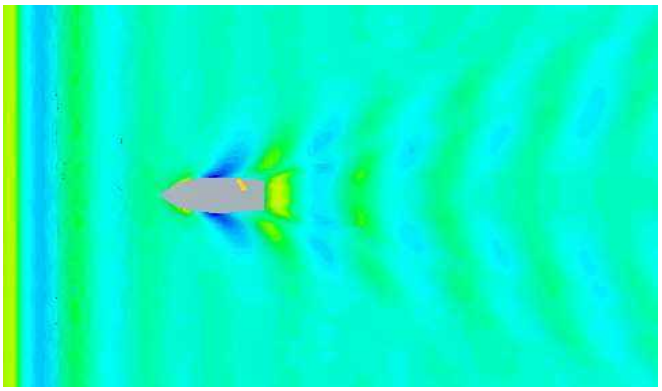

(a)

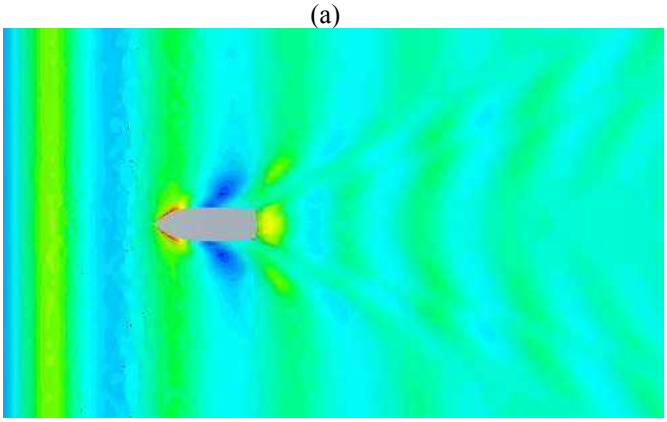

(b)

Figure 9. Waves elevation around ship for wave of H=5 cm; (a): Lw/L=0.65, (b): Lw/L=1.2

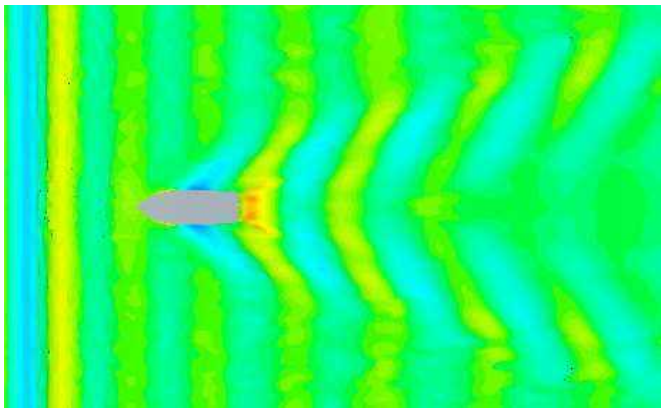

(a)

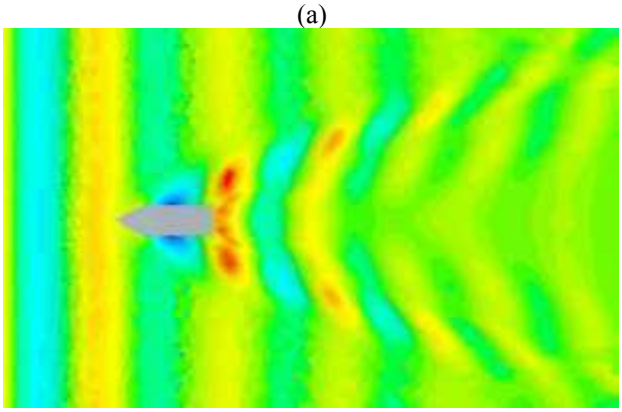

(b)

Figure 10. Waves elevation around ship for wave of H=10 cm; (a): Lw/L=0.65, (b): Lw/L=1.2

As can be seen in the figures, in higher waves, in some cases, the wave breaks on the vessel deck. Also, the interference between the sea waves and the hull generated waves is clearly evident, particularly at the aft of the vessel.

As the numerical modeling is done in an unsteady state, for checking the convergence of the numerical results, the time history of total resistance should be evaluated over time. After checking the resistance, it was observed that after about 35 seconds, the resistance reached a steady state and the solution could be stopped. The time history of total resistance for some waves is shown in the figures below. Also, the mean value of resistance in waves and calm water resistance is shown in figures.

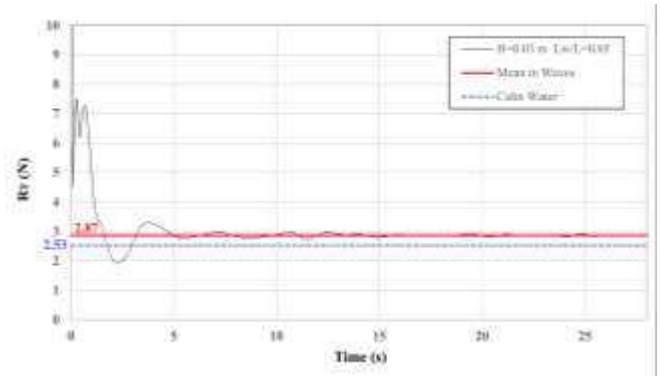

(a)

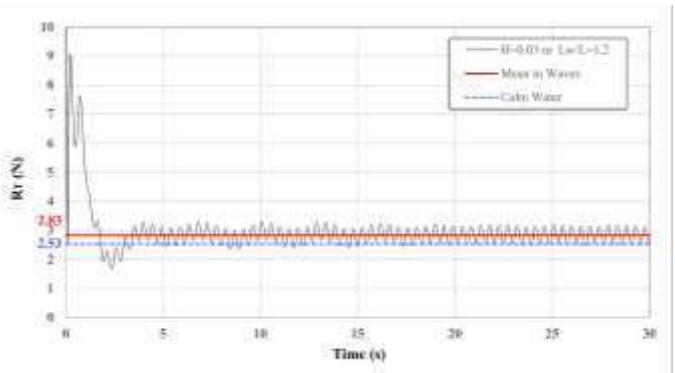

(b)

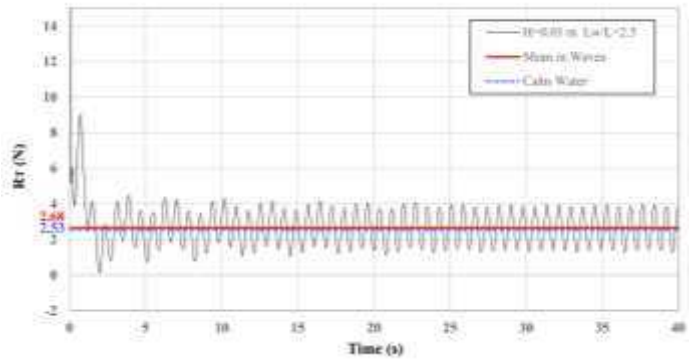

(c)

Figure 11. Comparison of ship total resistance in calm water and wave of H=3 cm; (a): Lw/L=0.65, (b): Lw/L=1.2, (c): Lw/L=2.5

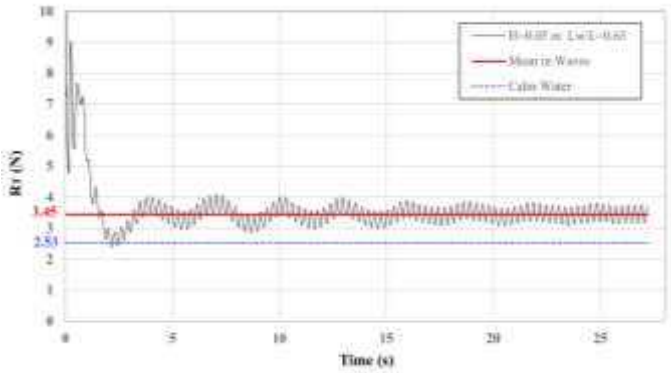

(a)

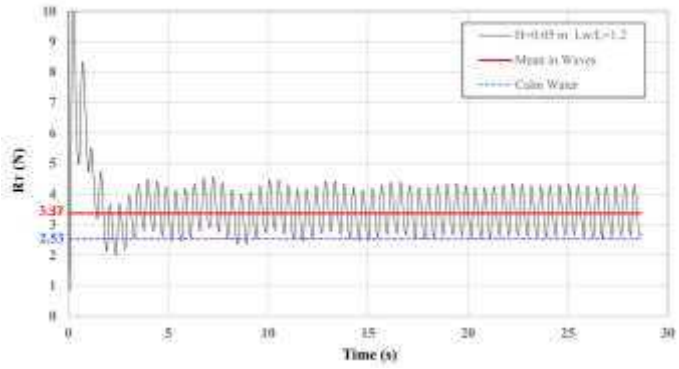

(b)

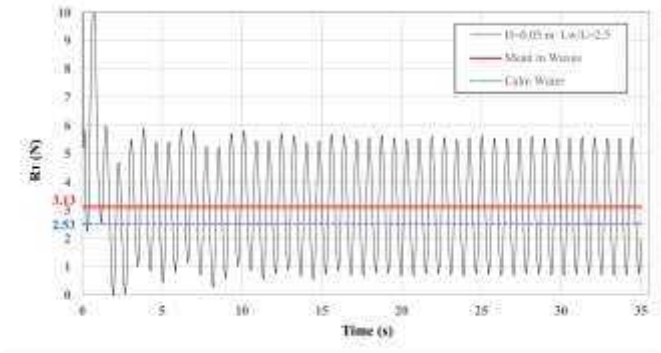

(c)

Figure 12. Comparison of ship total resistance in calm water and wave of H=5 cm; (a): Lw/L=0.65, (b): Lw/L=1.2, (c): Lw/L=2.5

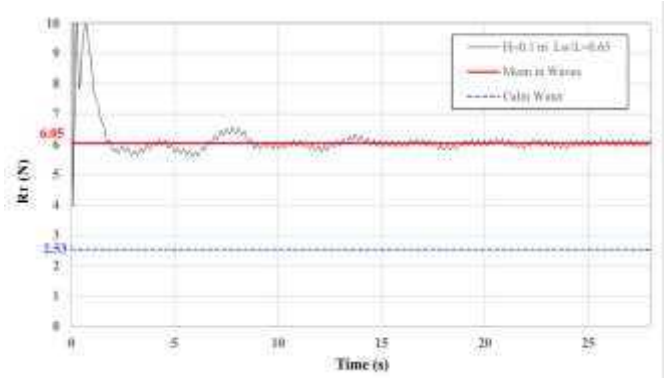

(a)

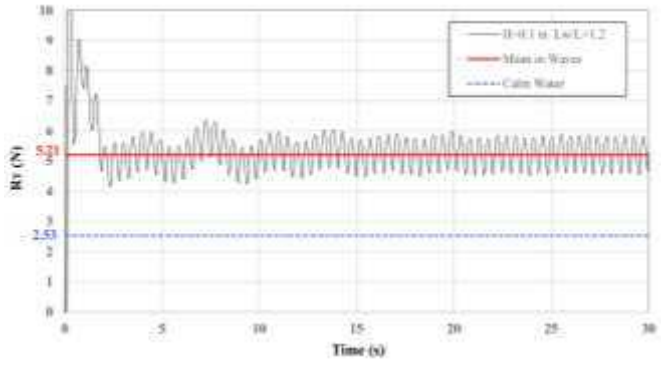

(b)

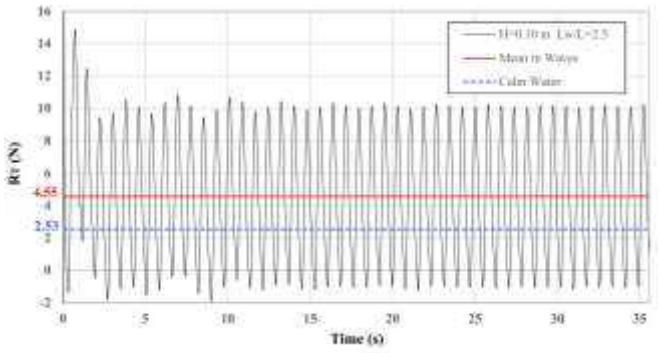

(c)

Figure 13. Comparison of ship total resistance in calm water and wave of H=10 cm; (a): Lw/L=0.65, (b): Lw/L=1.2, (c): Lw/L=2.5

As can be seen, at short wave lengths, vessel resistance fluctuations are much less than at long wave lengths. At short wave lengths, vessel resistance is always greater than calm water. The longer the wave length, the greater the maximum resistance, and the minimum resistance is less than in calm water.

To better examine the effect of waves on the resistance of vessel, the wave added resistance value for all waves is shown in the figure below.

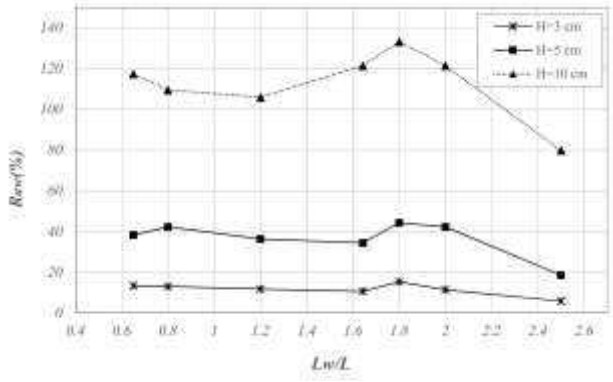

Figure 14. Added resistance of dhow vessel in all wavelengths

As can be seen, at short and long wavelengths, the added resistance is lower than at mean wavelengths (Lw/L between 1.6 and 2). For all three wave heights, the maximum added resistance occurred at a wavelength ratio of 1.8. The maximum added resistance of dhow vessel in wave heights of 10, 5 and 3 cm is 133 %, 44 % and 17 % respectively.

Heave is one of the most significant motions of a vessel in waves. This motion has a considerable effect on the added resistance of the vessel. Because this can result in an increase in the frictional and pressure resistance of the vessel. In the following, variations in the heave motion of the vessel at all 3 wave heights (for 3 different wavelengths) are shown.

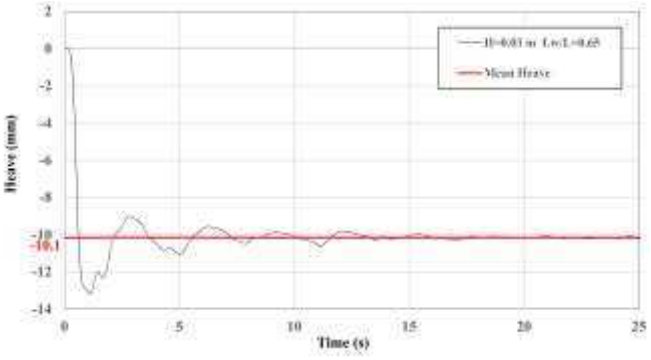

(a)

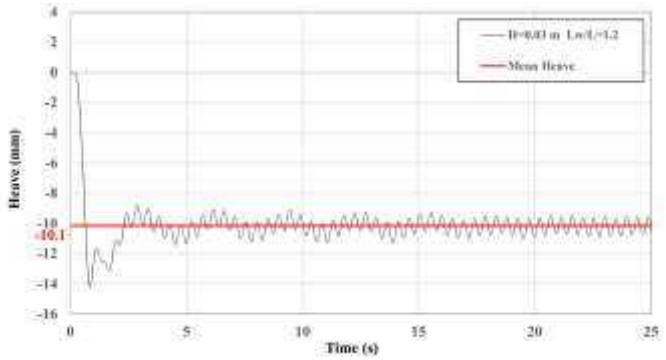

(b)

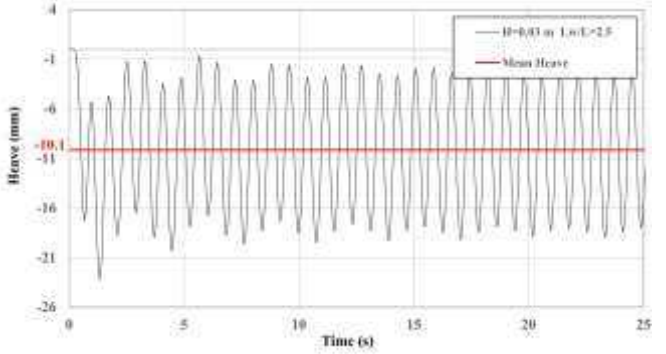

(c)

Figure 15. Heave motion of dhow vessel in wave of H=3 cm; (a): Lw/L=0.65, (b): Lw/L=1.2, (c): Lw/L=2.5

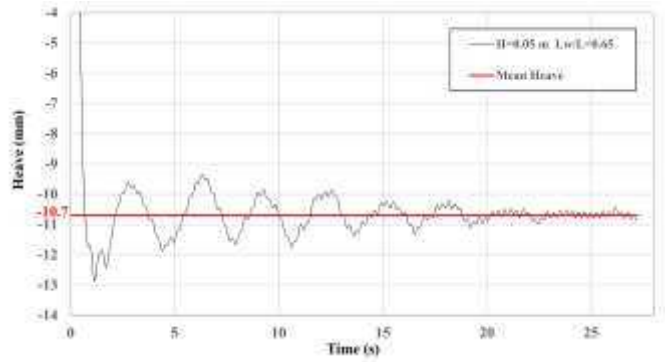

(a)

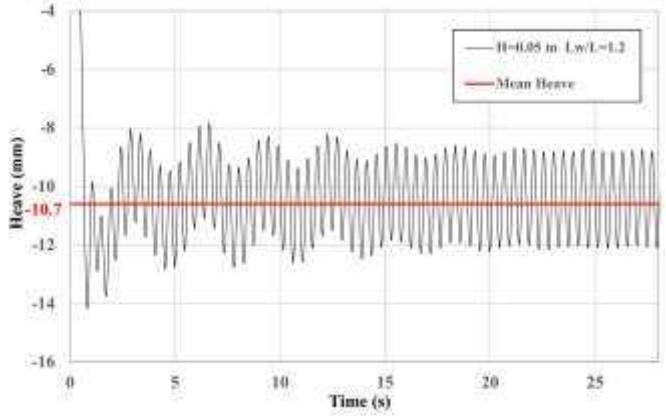

(b)

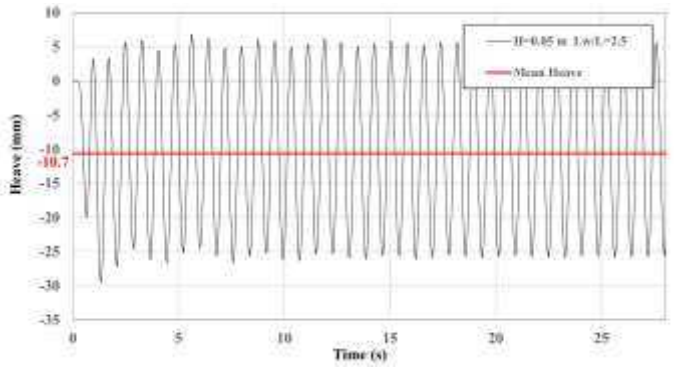

(c)

Figure 16. Heave motion of dhow vessel in wave of H=5 cm; (a): Lw/L=0.65, (b): Lw/L=1.2, (c): Lw/L=2.5

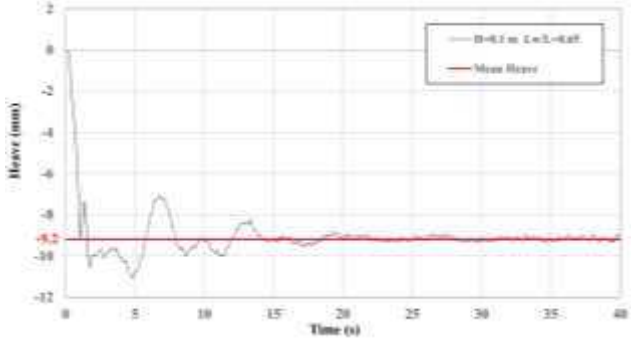

(a)

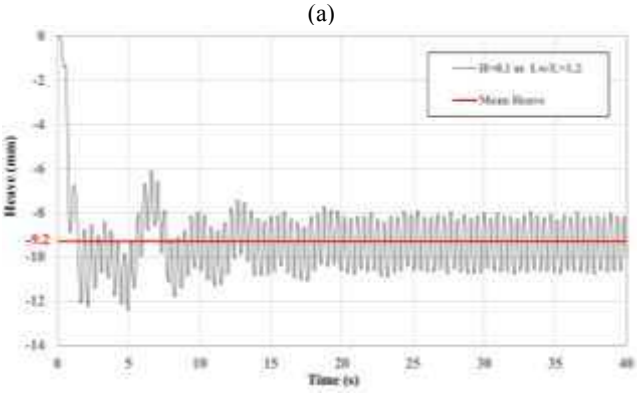

(b)

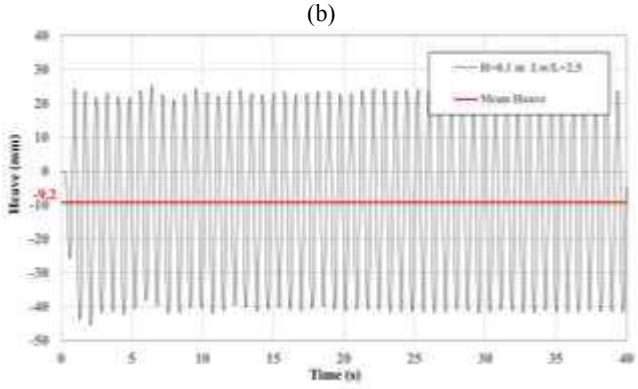

(c)

Figure 17. Heave motion of dhow vessel in wave of H=10 cm; (a): Lw/L=0.65, (b): Lw/L=1.2, (c): Lw/L=2.5

A study of the vessel's heave motion at different wavelengths and wave heights reveals the following:

- In all waves, the vessel suffers sinkage (increased draft) when encountering waves, which increases the

vessel's resistance, where for all waves, the mean heave is approximately 1 centimeter.
- Each wave height produces approximately the same mean heave at all wave lengths.
- The amplitude of heave motion is increasing with the increment in wave height and wavelength.
For further clarification of the effect of waves on vessel heave, the maximum heave of the vessel at different wave heights and wavelengths is shown in the Figure 18.

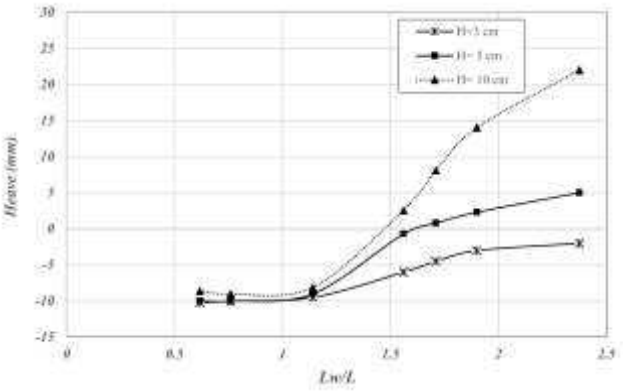

Figure 18. Maximum heave of dhow vessel at different wave conditions

As can be seen in the figure, the maximum heave of the vessel increases with increasing wave height.

6. Conclusions

This study was carried out in order to examine the effect of regular head waves on the added resistance of a dhow vessel. The vessel was numerically simulated at three different wave heights and several different wavelengths for each wave height, and the following results were obtained:
- As a result of encountering waves, the vessel suffers sinkage (increased draft), which increases its resistance, with a mean heave of approximately one centimeter for all waves.
- The mean heave produced by every wave length is approximately the same regardless of the wave height.
- In general, the amplitude of heave motion increases as wave height and wavelength increase.
When the height of the waves increases, the maximum heave of the vessel increases as well.

7. References

[1] Vosmer, T., 1997. Indigenous fishing craft of Oman. *International Journal of Nautical Archaeology*. 26(3): p. 217-235.

[2] Strom-Tejsen, J., 1973. Added resistance in waves. *Trans SNAME,* 81: p. 109-143.

[3] Pinkster, J., 1979. Mean and low frequency wave drifting forces on floating structures. *Ocean Engineering*, 6(6): p. 593-615.

[4] Faltinsen, O.M,1980. Prediction of resistance and propulsion of a ship in a seaway. *13th Symposium on Naval Hydrodynamics,* Tokyo.

[5] Moctar, O.e., et al., 2016. Numerical and Experimental Analysis of Added Resistance of Ships in Waves. *Journal of Offshore Mechanics and Arctic Engineering,* 139.(۱)

[6] Sadat-Hosseini, H., et al., 2013. CFD verification and validation of added resistance and motions of KVLCC2 with fixed and free surge in short and long head waves. *Ocean Engineering*, 59: p. 240-273.

[7] Yu, J.-W., et al., 2017. Effect of ship motions on added resistance in regular head waves of KVLCC2. *Ocean Engineering*, 146: p. 375-387.

[8] Ebrahimi, A., M. Rad, and A. Hajilouy , 2014. Experimental and Numerical Studies on Resistance of a Catamaran Vessel with Non-Parallel Demihulls. *Scientia Iranica*, 21(3): p. 600-608.

[9] Park, D.-M., et al., 2019. Experimental and numerical studies on added resistance of ship in oblique sea conditions. *Ocean Engineering*, 186: p. 106070.

[10] Shivachev, E., et al., 2020. Impact of trim on added resistance of KRISO container ship (KCS) in head waves: An experimental and numerical study. *Ocean Engineering*, 211: p. 107594.

[11] Díaz-Ojeda, H.R., F .Pérez-Arribas, and S.R. Turnock, 2023. The influence of dihedral bulbous bows on the resistance of small fishing vessels: A numerical study. *Ocean Engineering,* 281: p. 114661.

[12] Seif, M.S. S.H. Sadat Hosseini, 2004. Numerical Solution of Viscous Flow around Dhow Vessel. 6th *Iranian Marine Industries Conference*, Tehran (In Persian).

[13] Malalasekera, W., H. Versteeg, 2007. An introduction to computational fluid dynamics. *Pearson education limited.*

[14] Moukalled, F., et al., 2016. The finite volume method. *Springer.*

[15] Workshop on Verification and Validation of Ship Manoeuvring Simulation Methods, 2008. http://www.simman2008.dk./

INTERNATIONAL JOURNAL OF
COASTAL, OFFSHORE & ENVIRONMENTAL ENGINEERING IJCOE Vol.10/No. 3/ Summer 2025 (53-61)

Available online at: www. Ijcoe.org

Evaluation of Ultra Border Analyzes of Researches Conducted In The Persian Gulf Sea Basin

Mehri Fallahi[1], Masoud Sadrinasab[2*]

[1,] PhD Physical Oceanography, Khorramshahr University of Marine Science and Technology, Khorramshahr and Instructor of Physics Lab, Department of Agricultural Machinery Engineering, University of Tehran, Tehran, Iran,mehri_fallahi@ut.ac.ir

*[*2,] Associate Professor, Department of Environment Engineering, School of Graduate Environment, university of Tehran , Tehran, Iran.* masoud.sadri@ut.ac.ir

ARTICLE INFO

Article History:
Received: 22 MAY 2025
Accepted : 19 NOV 2025

Keywords:
Iran
Persian Gulf
Scopus
Evaluation
Marine sources

ABSTRACT

Given the significance of the Persian Gulf marine basin, research efforts must emphasize the protection and sustainable use of marine resources. Despite the unique importance and strategic position of the Persian Gulf in the region, and the numerous studies conducted across various scientific, economic, and social fields, the effectiveness of these investigations has never been evaluated. In fact, no quantitative or qualitative assessment has been carried out regarding these research efforts. Accordingly, the management of research activities across various scientific fields in this region becomes particularly important. Therefore, in this study, using data from the Scopus database, a quantitative perspective on the research conducted in the Persian Gulf is provided, along with an overview of the research topics over a defined period. With a particular focus on the themes related to marine science and engineering, conclusions will be drawn. A quantitative analysis of the research documentation reveals that Iran, followed by the United States, has produced the highest number of research outputs to date. Among Iranian research institutions, the University of Tehran and Amirkabir University of Technology rank at the top with the highest number of scientific publications. In this study, researchers' interest in biological sciences and geology is also evident. The Persian Gulf, due to its connection to open waters, can be a source of sustainable energy and new perspectives for research. However, only a small percentage of studies have been conducted in this area and in the field of engineering. A comparison of citation counts for the conducted studies also reveals a lack of attention to research in the fields of marine science and engineering, as well as computer science. The analysis of the results indicates that effective management in research planning can lead to more informed decision-making and more efficient outcomes.

1. Introduction

Oceans, containing over 97 percent of the Earth's water, cover approximately 71 percent of the planet's surface. As the largest ecosystem on Earth, the ocean plays a critical role in environmental sustainability. It regulates the planet's climate and weather systems. Oceans are the cradle of life and serve as key players in oxygen production and atmospheric carbon dioxide absorption, while also providing habitat for a vast array of living organisms. The utilization of oceans and seas holds immense global importance today in areas such as transportation, trade, food and pharmaceutical resources, mineral extraction, freshwater supply, tourism, and national security.

A vast expanse of Iran's territory—stretching over 5,700 kilometers—is bordered by the waters of the Caspian Sea, the Persian Gulf, and the Sea of Oman. The Persian Gulf is considered a strait extending from the Makran (Oman) Sea, sharing maritime boundaries with Iran, Saudi Arabia, Kuwait, Qatar, the United Arab Emirates, Bahrain, Oman, and Iraq (Figure 1).

The geographical location of the Persian Gulf is situated between 24° to 30°30′ north latitude and 48° to 56°25′ east longitude (see Figure 1). Today, the

boundaries of this gulf extend from the Strait of Hormuz in the east to the Arvandrud in Khuzestan, Iran, in the west.

The primary renown of the Persian Gulf is due to the immense oil and gas resources found in its sedimentary basins. However, this water body also holds special significance in geological, sedimentological, oceanographic, and many other scientific studies [1]. In light of this importance, conducting research in various fields and managing these studies is of strategic importance.

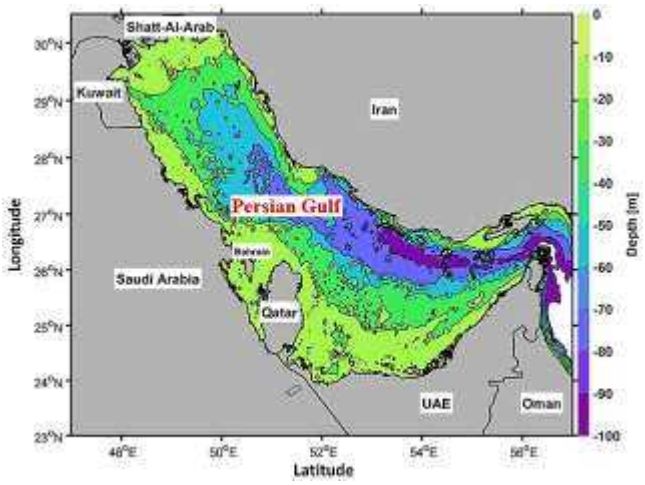

Figure 1- Geographical location of the Persian Gulf

The earliest investigations into the oceanographic characteristics of the Persian Gulf can be traced back to Iranian scholars, who conducted studies in the ancient the Persian Gulf. These studies were eventually compiled into a book known as Rahnâmik, Rahnâmag, or Rahnâmaj during the Sassanid era. With the advent of modern oceanography, the Persian Gulf has also become one of the principal focuses of oceanographers. Among the earliest studies in this field is the research conducted by James Murray in the 1880s [1].

Marine research cruises in Iran do not have a long-established history; however, perhaps the most longstanding institution in this regard is the Iranian Fisheries Research Institute. Among this institute's objectives are the examination of fish stocks, experimental fishing and the testing of equipment and catch ratios, the development of fishing models, training, developmental programs for the fisheries industries, statistical programs, and assisting in the management of fishery resource exploitation [1].

After fisheries, the Hydrography Department of the National Cartography Organization has been actively engaged in mapping activities aimed at preparing hydrographic maps and nautical charts for this sea. Although other organizations and institutions—such as the Ports and Maritime Organization, coastal universities, and the research division of the Ministry of Energy—also conduct marine cruises in the country, these cruises are generally small-scale, local, and carried out with limited and specific objectives [1].

The Marine Geology Department of the Geological and Mineral Exploration Organization was officially established in 1372, and this department, by conducting marine surveys and equipping itself with the necessary tools, has carried out marine cruises to produce geological maps and atlases of Iran's coasts in its coastal waters [1].

One of the first organizations to conduct extensive and relatively comprehensive marine surveys in the Persian Gulf in collaboration with other countries was the Environmental Organization. These surveys were generally carried out to assess the latest physical, chemical, and biological conditions, as well as pollution and the ecosystem of the Persian Gulf and the Sea of Oman. In the years 1991 and 2001, regional marine surveys in the Persian Gulf and the Sea of Oman were conducted for the first time by the ROPME[1] member countries (Saudi Arabia, United Arab Emirates, Kuwait, Qatar, Bahrain, Oman, and the Islamic Republic of Iran) under the management of Iran (Environmental Protection Organization). Prior to these extensive surveys, similar research cruises were carried out in collaboration with experts from non-ROPME member countries (Sediments and Water of the Persian Gulf 1956). In this context, the research cruise "Mont Michel" was conducted in 1991 by American experts, and the research cruise "Omita Camaro" was carried out by Japanese experts in 1993 in this region [1].

The National Institute of Oceanography and Atmospheric Sciences has also conducted several research cruises in the northern and southern waters of the country. Many of these cruises have been confined to the coastal areas of the Persian Gulf or have been carried out with specific, limited objectives in certain fields. Notably, the Persian Gulf and Gulf of Oman Oceanographic Studies (PGGOOS) project—aimed at measuring the oceanographic and environmental characteristics of the Persian Gulf, the Strait of Hormuz, and the Sea of Oman—was conducted with comprehensive objectives over various seasons during an 18-month period starting in November 2012 [1].

In addition to these targeted and organized studies, numerous research investigations in various branches of marine sciences have been carried out by scholars at universities and research centers, with findings being published as articles in journals or presented at conferences both domestically and internationally.

Some of these studies are conducted in the form of review studies. These studies lack a specific structure. Each researcher plans it based on a specific goal. Some of these studies are discussed below.

[1] The Regional Organization for the Protection of the Marine Environment (ROPME) - https://ropme.org/

Mirkheshti et al. (2017), in a review study, examined the risks associated with offshore wind energy in the Persian Gulf. The study aimed to identify the relevant risks of offshore wind energy projects to determine which variables, through qualitative analysis by applying the impact and probability of each risk, have the greatest effect on the project [2].

In 2021, **Soleimani** conducted a Review on energy and renewable energy policies in Iran. Results showed that renewable energy technologies currently do not have a significant and adequate role in the energy supply of Iran [3].

Zhang et al. (2021) presented a review study on marine resources and economic development. The aim of this study was to analyze the current status of marine resources and achieve sustainable utilization of marine resources. It was found that, compared to the current state of research on land resources and economic development, there is significant lag both in theoretical development and in methodological innovation in marine resources and economic development. [4]

Wang et al. (2022) conducted a review study aimed at developing approaches for high-quality marine development and effective ocean governance. They concluded that research on the marine economy mainly centers on marine industries, with the marine circular economy representing the latest research frontier. Marine resources were identified as the foundation of the marine economy, and the implementation of a natural resource ownership system in marine domains was deemed necessary for more efficient resource utilization. [5]

Ocean literacy (OL) refers to the ability of citizens to understand and explain the concepts and phenomena related to the oceans, and leads them to positive behavioral change for the protection and sustainability of the oceans. **Cavas et al. (2023)** examined the research trends and content analysis of ocean literacy studies conducted between 2017 and 2021. They carefully selected seventy-nine articles from forty academic journals on ocean literacy indexed in WoS and Scopus, using predefined criteria. The findings of this study can contribute to the advancement of ocean literacy research, support informed investigations, and provide citizen input for policy development related to ocean literacy. [6]

Tavakoli et al. (2023) provided a review on the progress and research directions of ocean engineering over the past 50 years. They concluded that research has been conducted in six major research divisions (I) Ocean Hydrodynamics, (II) Risk Assessment and Safety, (III) Ocean Climate and Geophysics: Data and Models, (IV) Control and Automation in the Ocean, (V) Structural Engineering and Manufacturing for the Ocean, and (VI) Ocean Renewable Energy. They concluded that machine learning methods have attracted significant attention from researchers. They also identified the subfields of research within these areas and examined the continuity and quality of these studies. [7]

Halpin et al. (2004) presented an overview of interactions among oceanography, marine ecosystems, climatic and human disruptions along the eastern margins of the Pacific Ocean. They present an overview of the oceanographic processes that dominate the coastlines, and give examples of ecosystems and the effects that oceanography, human activities and their interaction have on the communities. [8]

Saleh and Ershadifar in 2024 investigated Decreasing Dissolved Oxygen in the Persian Gulf and the Gulf of Oman: Impacts and Strategies for Mitigation in a review study. They concluded, the Oxygen Minimum Zone (OMZ) in the Arabian Sea and the Gulf of Oman has intensified over the past few decades. Marine organisms of the near-bottom layer or surface sediments are most affected by the expansion and intensification of hypoxic and suboxic conditions. They proposed three categories of management actions to halt or reduce the effects of oxygen depletion in the Persian Gulf and the Sea of Oman: a) ecosystem-based mitigation measures for environmental restoration and protection, b) adaptation-based measures to restore and protect marine organisms and fisheries, c) implementation of monitoring programs and analysis of the information obtained. [9]

It can be seen that review studies can provide an overall perspective on a given topic. Review studies can enable the validation of the methods used and help identify research gaps related to the study topic. They can also determine the most effective approach to achieving results with minimal cost.

Despite the unique significance of the Persian Gulf environment in global oceanography and the country's reliance on this strategic waterway, a comprehensive depiction of the environmental characteristics of the Persian Gulf and the Sea of Oman, particularly the northern half belonging to the Islamic Republic of Iran, has yet to be provided [1]. Moreover, the effectiveness of these studies in various economic, social, and industrial sectors of the country has never been evaluated, and no quantitative or qualitative assessment of the research has been conducted. Therefore, managing research across various domains, including marine sciences, technical and engineering fields, military, economic, social sectors, and tourism, gains particular importance.

The present study provides a quantitative overview of the research conducted in the Persian Gulf over a defined period of time. While offering a general perspective, it places particular emphasis on marine studies. **The aim of this study** is to present a broad picture of the research conducted during this time frame and to highlight the existing gaps in the topics of studies carried out within this important geographic region.

2. Method and Theoretical Framework

Research topics in various fields, including oceanography, can be fundamental, applied, or developmental. The outcome of research enhances decision-making in various economic, military, or social domains, which consequently leads to improved decision-making in marine and atmospheric matters at different domestic and regional levels. Furthermore, the development and expansion of research will provide effective solutions for better utilization of marine resources and making products more economical. Therefore, in this study, regardless of the type of research, a quantitative comparison of the research efforts is presented.

For this purpose, data from the Scopus database has been used. This database is the largest repository of articles, books, and scientific journals. In this database, one can access relevant research in reputable publications, as well as utilize the analytical tools available within the platform.

A quantitative study was conducted in three stages within this database:

1- A search was performed without restrictions on the Article title, Abstract, and Keywords using the terms "Persian" and "Gulf." From the period 1856 to 2024, 10,910 results were obtained.

2- A search was conducted in the Article title using the terms "Persian" and "Gulf" and "Arabian Sea." From the period 1856 to 2024, 3,541 results were obtained.

3- A more targeted search was performed within the results from stage (2), focusing on fields such as energy, engineering, or research related to researchers and countries.

These results include all research titles in various formats within this marine environment. The use of mathematical tools within this system allows for categorizing these studies, enabling different analyses and comparisons, which lead to valuable conclusions.

3. Results and Discussion

The Chart showing the number of documents from stage1, by year, within the time range of 1856 to 2024 is provided in Chart 1.

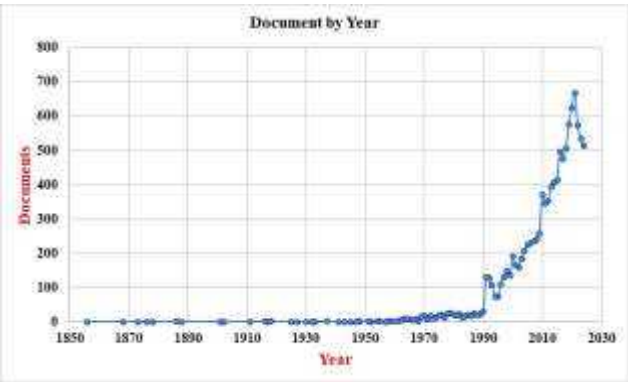

Chart 1- Chart showing the number of documents by year (Stage 1 Search)

This chart shows a growing trend in research from 1990 to 2021, with 667 results in 2021 representing the peak. After 2021, a decline in the number of studies has occurred, highlighting the need to investigate the reasons for this decrease and its impact on economic and social planning.

The number of research documents according to the research centers affiliated with the researchers is shown in Chart 2**Error! Reference source not found.** for the 15 centers with the highest number of documents.

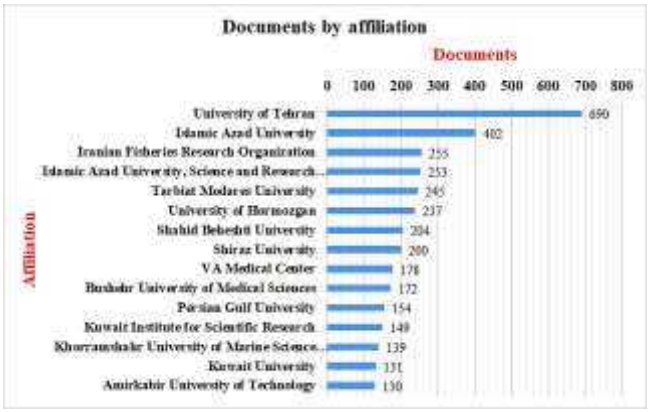

Chart 2- Comparison of research document counts for academic and research institutions (Stage 1 search)

Chart 2**Error! Reference source not found.** shows t hat the University of Tehran (Iran) is significantly leading research in the Persian Gulf domain. Investigating the reasons behind this difference, reviewing the outcomes of these studies, and discussing the application of these findings in industrial, economic, and tourism sectors is a relevant topic for further discussion.

compares the number of research documents for the top 10 researchers with the highest number of publications.

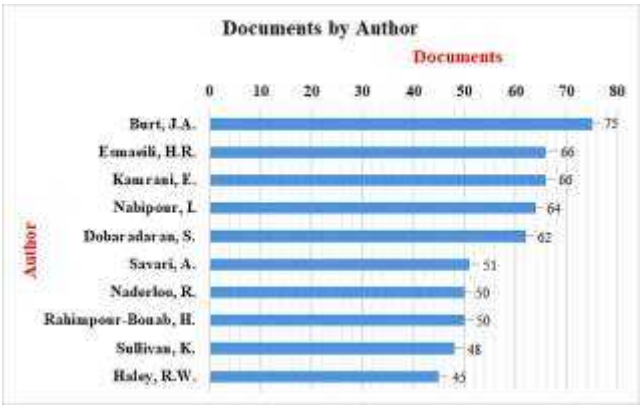

Chart 3- Comparison of research document counts for the top ten researchers (Stage 1 search)

Examining the perspectives of these researchers regarding the Persian Gulf marine area will yield valuable insights. It will not only highlight research gaps but also provide useful findings for management planning by reviewing the results of these studies.

John A. Burt, with 75 publications, leads this chart. He is a marine biologist at New York University Abu

Dhabi (NYUAD). This researcher uses the Persian Gulf, the hottest sea in the world, as a "natural laboratory." His studies focus on the responses of marine organisms to the unique environmental conditions of this water basin. He explores how marine organisms adapt and also provides insights into the potential impacts of future climate changes on the sea. He conducts research on corals, coral symbionts, reef fish, mangroves, and seagrasses in tropical ecosystems. Burt and his colleagues use science to support local policies, management, and conservation actions related to these areas.

The comparison of the number of research publications by country or territory regarding the Persian Gulf also provides valuable insights into the significance of the Persian Gulf (Chart 4).

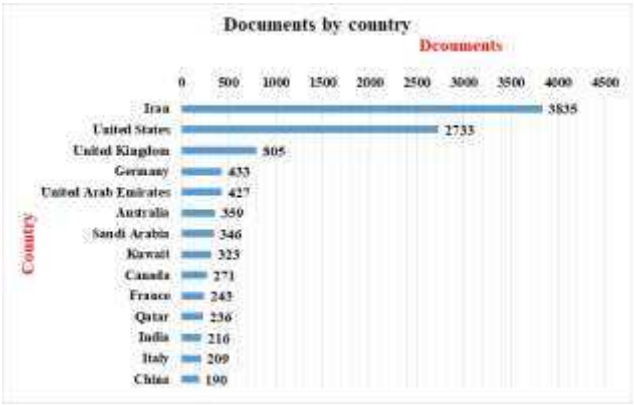

Chart 4- Number of Research Documents by Country (Stage 1 Search)

Chart 4 indicates the special attention given by the United States and the United Kingdom to the Persian Gulf. Examining the viewpoints of researchers from these countries in economic, military, and management programs is valuable.

The type of research and the study area are also other aspects of the current review, shown in Chart 5

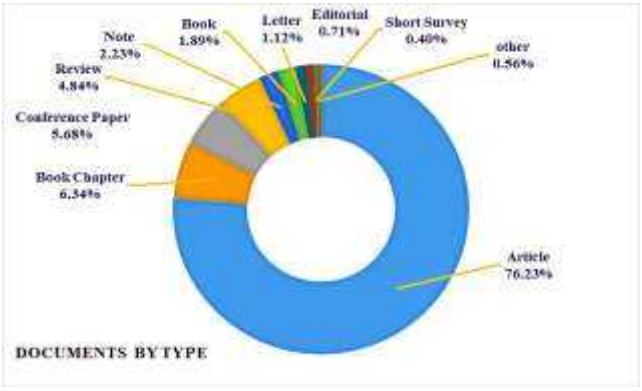

Chart 5- Research Documents by type (Stage 1 Search)

A large portion of the documents are articles, indicating that the research titles can form a wide range. Examining the impact of these studies on industry, the economy, and social life can be a subject of discussion.

A quantitative comparison of research areas presents the interests of the researchers.

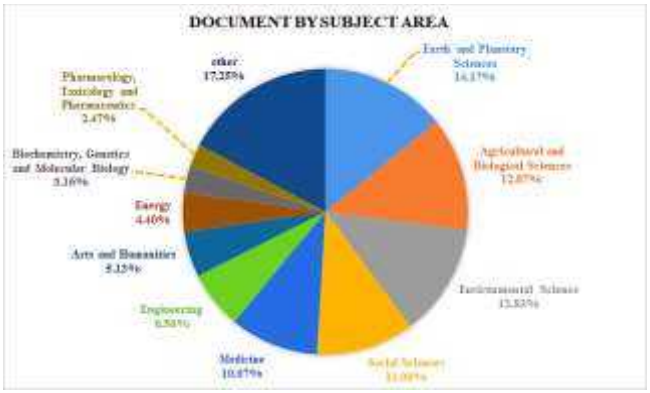

Chart 6- Comparison of research document by subject area (Stage 1 search).

Chart 6 indicates that considerable research attention has been directed toward Earth and space sciences, followed by agricultural and biological sciences. However, despite the Persian Gulf being an oceanic basin and a significant energy resource, related scientific research remains substantially underrepresented.

The following key findings can be highlighted:

- A noticeable decline in the number of publications since 2021
- Iran's leading position in terms of the number of publications
- The University of Tehran (Iran)ranking highest among Iranian universities in publication count
- Significant research interest in the Persian Gulf region by the United States and the United Kingdom
- The prominent focus and contributions of John A. Burt, a marine biologist at New York University Abu Dhabi (NYUAD), to research on the marine domain of the Persian Gulf

For a more detailed analysis, the second search stage, focused on "*Article title*", was examined, followed by a third stage involving a closer inspection of the results from the second stage.

The search in the "*Article title*" section revealed 3541 research titles. In this type of search, the title of the paper provides a concise summary of its content. Every word is carefully selected to convey the maximum amount of information in the smallest possible package, enabling optimal "findability" in article databases, journals, and internet search engines.

In the results, changes in the number of research documents over the years under review can be observed (Chart 7):

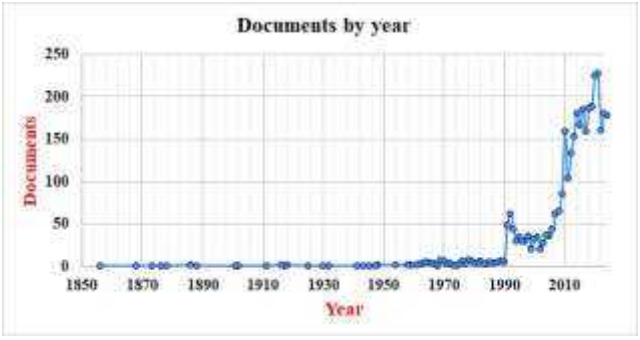

Chart 7- Number of research documents by year (stage 2 search)

At this stage, the research focus on the water basin of the Persian Gulf from 1990 to 2021 shows an upward trend, with a decline in the number of documents after 2021, as indicated by this chart. Additionally, the highest number of documents, 228 research titles, is recorded in 2021.

The following chart shows the number of documents by country for the 15 countries with the highest number of documents.

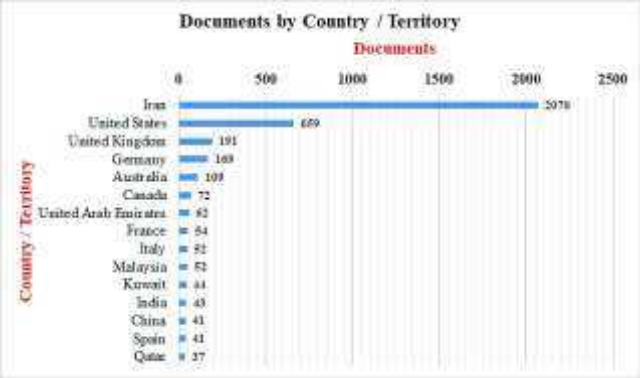

Chart 8- Number of research documents per country (stage 2 search)

This chart highlights the significance of the Persian Gulf region for various countries. Iran has shown the greatest attention to this marine area, followed by the United States and the United Kingdom, as seen in stage 1.

Chart 9- Comparing documents based on the study area of the United States (Search Stage 3)

In a more detailed analysis (Chart 9), among the 659 documents from the United States, social sciences titles accounted for 19.9%, showing the highest interest, while economic and financial titles, with 1.9%, showed the least interest (Chart 9).

Among the 3541 documents obtained, a comparison of research centers affiliated with the researchers for the top 15 centers with the most data can also provide valuable insights (Chart 10).

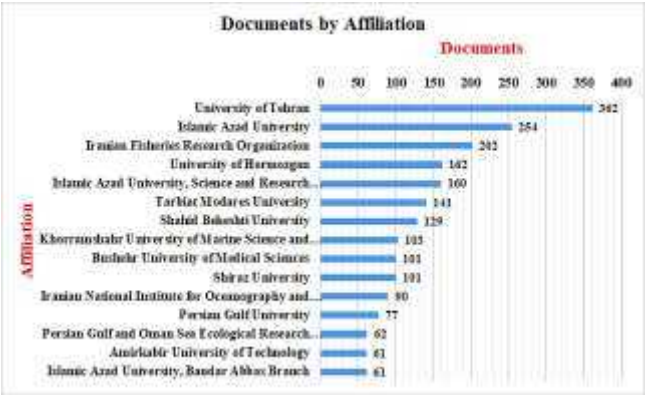

Chart 10- Comparison of the number of research documents for each research institution (Stage 2 of the search).

Examining the researchers' interests can help identify the areas of focus as well as potential research gaps. Therefore, a more detailed comparison of the number of documents by researchers has been made (Chart 11), where the number of documents by the top 15 researchers (with the most documents) is compared.

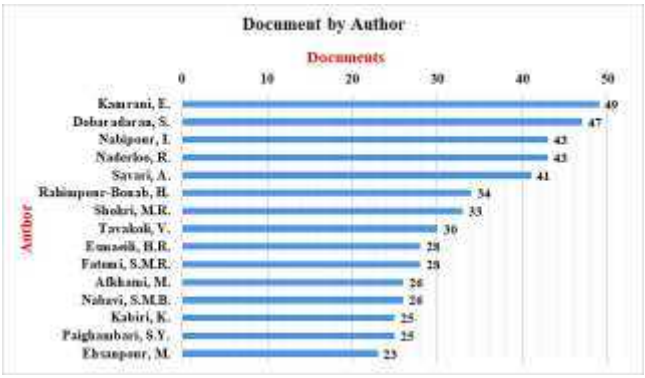

Chart 11- Comparison of the number of documents for the 15 researchers with the most publications (Stage 2 of the search).

In this comparison, Kamrani, a researcher at Hormozgan University (Iran), is at the top with 49 research results, focusing on fisheries and aquaculture. Kabiri, a researcher at the National Institute of Oceanography and Atmospheric Science, works in the field of remote sensing. Other researchers in this chart have conducted studies in the areas of biological sciences and geology. It appears that various disciplines within basic sciences, engineering, and energy topics are of relatively low interest. Therefore, a thematic analysis of the research documents could be valuable (Chart 12).

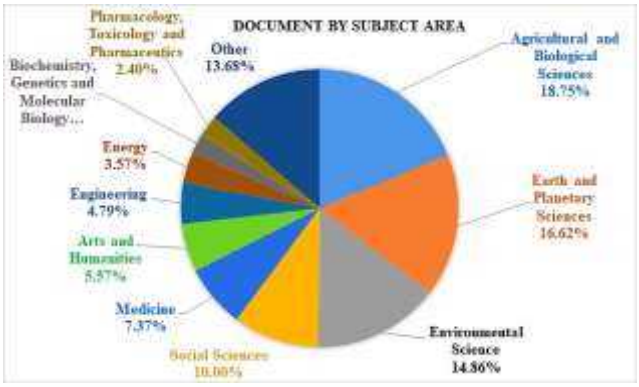

Chart 12- Comparison of documents based on subject area (Stage 2 of the Search)

Disregarding the "Other" category (13.7%), which includes fields such as computer science, psychology, materials science, physics and astronomy, chemistry, and mathematics, this chart shows that the highest attention from researchers (18.7%) is directed toward agriculture and biological sciences. This can be considered natural due to the biodiversity of organisms in the islands and waters of the region. Following that, earth and planetary sciences attract the attention of researchers (16.6%).

In this field, the evolution of the Earth and planets is addressed, from the Earth's interior to the atmosphere, along with their physical and chemical processes. Given that the Persian Gulf is a vital water basin, economic hub, and strategic area, and considering that water is a renewable energy source, the relatively small share of documents related to energy (3.6%) and engineering sciences (4.8%) warrants further investigation.

The "Other" category in this Chart 12 encompasses fields such as computer science, psychology, material science, physics and astronomy, chemistry, mathematics, and others, each contributing a negligible share individually. On the other hand, fluid dynamics is a significant topic in the fields of physics and even engineering. Therefore, the lack of interest among researchers from the physics and engineering disciplines in this area warrants further investigation.

In search 2, out of the 3541 research documents, 199 are related to the energy sector, which accounts for 3.6%. Among these, the University of Tehran (Iran) holds the largest share with 42 documents (Chart 13).

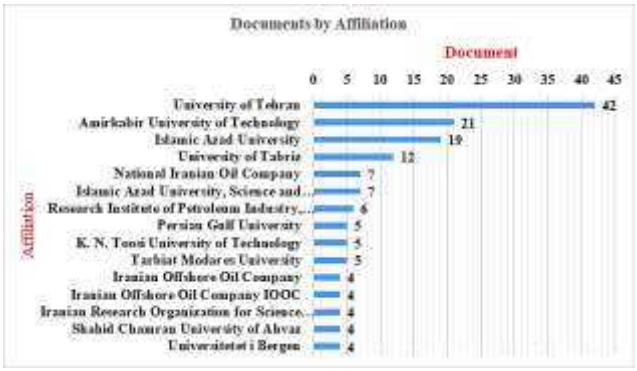

Chart 13- Comparison of the number of research documents on energy for each research center (Stage 3 of the search)

In these 199 documents, energy in the Persian Gulf region has been examined in various ways. A more detailed review of the titles reveals that 15 documents are related to numerical modeling, 10 documents to wave energy, and 3 documents to wind energy.

It is also observed that out of the 3541 research documents, 267 are related to the field of engineering, accounting for 4.8%. In this regard, the University of Tehran (Iran)ranks first, slightly ahead of Amirkabir University and Khajeh Nasir Toosi University (Iran), (Chart 14).

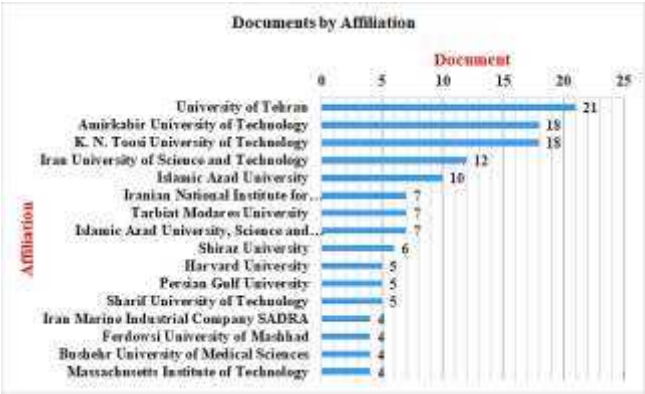

Chart 14- Comparison of the number of research documents on engineering topics for each research institution (Stage 3 of the search).

Given the geographical, climatic, and social conditions of the Persian Gulf basin, there are various topics for research, and different engineering disciplines can address them, which has already occurred. The compiled statistics do not show a particular focus on a specific subject within the field of engineering.

Despite the fact that the waters of the Persian Gulf have the potential to be a source of renewable energy, only a small percentage of research has been conducted in this area.

Another important perspective is the result of examining and comparing the number of citations by researchers to a specific topic or research title. The result of this comparison highlights the research areas that attract the most attention. The top ten research titles with the highest number of citations are as follows:

1. Microplastics in different tissues of fish and prawn from the Musa Estuary, the Persian Gulf, 2018, with 506 citations.
2. Health of UK servicemen who served in the Persian Gulf War, 1999, with 490 citations.
3. War syndromes and their evaluation: from the US Civil War to the Persian Gulf War, 1996, with 336 citations
4. Submarine lithification of Holocene carbonate sediments in the Persian Gulf, 1969, with 306 citations.
5. Shoreline reconstructions for the Persian Gulf since the last glacial maximum, 1996, with 303 citations.
6. Mortality among US veterans of the Persian Gulf War, 1996, with 296 citations.
7. Investigating a probable relationship between microplastics and potentially toxic elements in fish muscles from northeast of the Persian Gulf, 2018, with 290 citations.
8. Microplastics contamination in molluscs from the northern part of the Persian Gulf, 2018, with 276 citations.
9.I solation and characterization of crude-oil-degrading bacteria from the Persian Gulf and the Caspian Sea, 2012, with 243 citations.
10. The circulation of the Persian Gulf: a numerical study, 2006, with 241 citations.

The comparison shows that biological research has received the highest number of citations, while numerical and physical studies have received the fewest citations. Additionally, research in the fields of industry, engineering, and computer science has not played a role in this comparison.

Therefore, given the role of industry and basic sciences in advancing the scientific level of the country, and to align the country's progress with global advancements, more attention must be given to research in the fields of marine science and engineering, particularly in computer science (both hardware and software) within the Persian Gulf marine basin. This, in turn, requires specific planning and investment.

In this way, various topics can be viewed in an overview, research titles can be examined and analyzed, and research gaps in different research areas can be identified.

4. Conclusions

This study aims to provide a comprehensive and quantitative overview of the research conducted in the oceanic domain of the Persian Gulf over the period from 1856 to 2024. The most significant outcome of this study is the identification of gaps in research topics. To achieve this, the characteristics of 10,910 research papers registered in the Scopus database were examined.

Chart 1 and Chart 7 demonstrate that the highest level of research attention to the Persian Gulf region occurred in 2021, followed by a declining trend in subsequent years.

Among the Persian Gulf littoral countries, Iran has shown the greatest attention to issues related to this region, followed by the United States with the highest number of research publications in this field (Chart 4 and Chart 8).

Likewise, among academic and research institutions, the University of Tehran (Iran) ranks highest in terms of the number of research publications (Chart 2 and Chart 10).

Researchers' interests can also reveal important insights; as shown in Chart 3, John A. Burt, a marine biologist at New York University Abu Dhabi (NYUAD), has produced the highest number of research publications. A more detailed analysis of the titles (Chart 11) shows that Kamrani, a researcher at the University of Hormozgan specializing in fisheries and aquatic organisms, has produced the highest number of publications. An analysis of the research specializations in Chart 11 indicates that the Persian Gulf has primarily attracted the attention of experts in biological and geological sciences.

This study indicates that various disciplines within the basic sciences, such as ocean physics and chemistry, as well as engineering, have received relatively limited attention. In the second search, a total of 3,541 documents were identified, of which 267 were related to engineering and 199 to the energy sector. A more detailed analysis of the 199 energy-related titles revealed that 15 focused on numerical modeling, 10 on wave energy, and 3 on wind energy.

Despite the fact that the waters of the Persian Gulf could serve as a renewable energy source, a small percentage of research has been conducted in this area. On the other hand, a comparison of citation counts reveals a lack of attention to research in marine sciences and engineering, as well as computer science. The reasons for the low level of interest in these areas can be attributed to the need for research outcomes, research facilities, and specialized human resources.

Given the importance of the Persian Gulf marine basin, research must emphasize the protection and sustainable use of marine resources. Therefore, in addition to quantitative assessments, content analysis of articles and research documents can be considered one of the most essential actions.

Focusing research planning within a centralized institution or organization can create opportunities for the broader application of research outcomes. Additionally, establishing an internal, multidisciplinary database in the field of marine sciences can facilitate researchers' access to various research data and information, as well as analytical tools and criteria. This database can significantly contribute to guiding research priorities, advancing studies, and achieving educational goals. The use of a centralized database can lead to more informed decision-making and more efficient outcomes.

In this regard, in addition to training specialized personnel, focusing research planning within a centralized institution or organization, and facilitating researchers' access to data, research information, and analytical tools, will play a vital role in guiding research priorities and advancing studies toward practical and applicable outcomes.

Acknowledgment (Optional)

8. References

1- Chegini, V., Alizandeh, H., Mehdinya, A., & Saleh, A, (2019), *Research project report "Persian Gulf and Gulf of Oman Oceanographic Studies (PGGOOS*) , Iranian National Institute, publication number 01-101-398, [In Persian]

2- Mirkheshti, S. A. H., & Feshari, M. (2017). *Qualitative and Quantitative Analysis of Off-Shore Wind Energy Project's Risks*, Journal of Energy, 2017(1), 4205083, https://doi.org/10.1155/2017/4205083

3- Solaymani S., (2021), *A review on energy and renewable energy policies in Iran*, Sustainability, 13(13):7328.

4- Zhang H & Chen S., (2022 May), Overview *of research on marine resources and economic development*, Marine Economics and Management, 4;5(1):69-83. DOI: 10.1108/MAEM-11-2021-0012

5- Wang S., Li, W. & Xing, L., (2022, August), *A review on marine economics and management: How to exploit the ocean well*, Water. 26;14(17):2626, https://doi.org/10.3390/w14172626

6- Cavas, B., Acık, S., Koc, S. & Kolac, M. , (2023 Oct), *Research trends and content analysis of ocean literacy studies between 2017 and 2021*, Frontiers in Marine Science, 2;10:1200181, DOI: 10.3389/fmars.2023.1200181

7- Tavakoli, S., Khojasteh, D., Haghani, M. & Hirdaris, S. (2023 Mar 15), *A review on the progress and research directions of ocean engineering,* Ocean Engineering, 272:113617, DOI: 10.1016/j.oceaneng.2023.113617

8- Halpin, P.M., Strub, P.T., Peterson, W.T. & Baumgartner T.R., (2004 Sep), *An overview of interactions among oceanography, marine ecosystems, climatic and human disruptions along the eastern margins of the Pacific Ocean*, Revista Chilena de Historia Natural. 1;77(3), DOI: 10.4067/S0716-078X2004000300002

9- Saleh A, Ershadifar H. Decreasing Dissolved Oxygen in the Persian Gulf and the Gulf of Oman: Impacts and Strategies for Mitigation – A Comprehensive Review. Journal of Oceanography 2024; 14 (56) :47-62 URL: http://joc.inio.ac.ir/article-1-1781-fa.html [In Persian]